MODELING OF AUTOGENOUS DEFORMATION IN CEMENTITIOUS MATERIALS, RESTRAINING EFFECT FROM AGGREGATE, AND MOISTURE WARPING IN SLABS ON GRADE

by

Ya Wei

A dissertation submitted in partial fulfillment
of the requirements for the degree of
Doctor of Philosophy
(Civil Engineering)
in The University of Michigan
2008

Doctoral Committee:

Professor Will Hansen, Chair
Professor Jwo Pan
Associate Professor Gustavo J. Parra-Montesinos
Assistant Professor Elin A. Jensen

This thesis is dedicated to my beloved son DongDong.

ACKNOWLEDGEMENTS

I wish to thank the many individuals who assisted me in the completion of this dissertation. First, special thanks to my advisor, Prof. Will Hansen, for providing support, encouragements, and suggestions during this research. His knowledge and dedication have made this work possible. I also wish to thank my committee members Prof. Jwo Pan, Prof. Gustavo J. Parra-Montesinos, and Prof. Elin A. Jensen for spending time reviewing my work and providing comments.

I would also like to express my appreciation to the faculty and staff of the Department of Civil and Environmental Engineering at the University of Michigan. The professors, technicians, and office staff have offered me endless support throughout my study here. Thank you to Phil Mohr, Yanfei Peng, and Youngjae Kang for their friendship and support. Finally, thank you to my family who are always supportive and patient.

TABLE OF CONTENTS

LIST OF FIGURES

Chapter 4

Chapter 5

Chapter 6

Chapter 7

LIST OF TABLES

CHAPTER 1

INTRODUCTION

1.1 PROBLEM STATEMENT

Concrete infrastructures undergo complex chemical and physical changes from cement hydration and exposure to the environments. These changes will affect the desired service life or durability of the hydraulic-cement concrete. In recent years, the durability problem of infrastructures has become a major concern since many of them are in serious need of repair, retrofitting, or replacement. There is increasing pressure to ensure that new constructions remain serviceable condition for long periods with only minimum maintenance.

There are many factors affecting the durability of the cementitious materials and the importance of these factors is varying with circumstances. Shrinkage is one of the major causes for cracking in bridge decks, pavements, indoor floors and other structures. Concrete develops volumetric changes due to the thermal and moisture related deformations which can be detrimental when substantial stresses occur in restrained structural elements, particularly at early ages while the concrete has a low tensile strength.

The particular aspects of degradation related to shrinkage cracking include chemical and microbiological degradation of concrete, corrosion of reinforcing and prestressing steels, sulfate attack, alkali-silica reaction, and deterioration associated with certain aggregates that leads to spalling of concrete pavements. The impacts of pre-mature cracking in concrete pavement can be significant. Poor structural condition due to cracking affects the ride quality and safety of motorists. Each year, more than 13,000 people die on the nation’s highways because of poor road conditions, according to the

U.S. Department of transportation's National Highway Traffic Safety Administration.

The increasing focus on shrinkage-cracking-related durability problem requires a better understanding of the material properties to be able to adjust the concrete to the level of attack it must resist. Concrete is a porous material, in addition to affecting the mechanical properties such as strength, modulus, and toughness of concrete, the porous microstructure is the main source of shrinkage. Cement hydration leads to the formation of the vapor-filled porosity upon the percolation of the solid phase. The paste phase undergoes internal pore drying known as self-desiccation due to the consumption of moisture from pore structures for further hydration. Unlike drying that may occur from the outside of the specimen inward, self-desiccation occurs uniformly throughout the concrete microstructure and results in autogenous shrinkage which is the major source of cracking if external (adjunct structures) or internal (aggregate or anhydrous cement particles) restraints exist.

Though the phenomenon of autogenous shrinkage and its influence on structure behavior have long been recognized, the mechanism behind is not fully understood yet and no standard test method has been accepted by the scientific community. Numerous researchers have investigated, toward better understanding the underlying process of autogenous shrinkage, the influence factors which include:

- Cement chemical compositions and physical properties
- Water/cementitious ratio (*w/cm*)
- Supplementary cementitious materials (SCM)
- Exposure temperature

As a contribution, this work focuses on the investigations using a new methodology for determining autogenous shrinkage and its relationship with the hydration products through thermogravimetric analysis (TGA) for paste systems with different cement types, *w/cm*, and ground granulated blast-furnace slag (GGBFS) contents.

Quantifying the autogenous shrinkage of cementitious systems, especially given the increasing and widespread utilization of high-performance concrete containing supplementary cementitious materials, becomes important in order to understand and control premature cracking in concrete structures. However, lack of data on this property

due to testing challenges has hampered the development of sound prediction models for this property.

Another contribution of this work is to develop prediction models for both cement paste and concrete autogenous shrinkage by incorporating a shrinkage-stress equilibrium model developed by Pickett with a time-domain model developed by Freiesleben-Hansen and Pedersen. The predicted autogenous shrinkage can be used in assessing the risk of early-age cracking in concrete.

In addition to the uniform autogenous shrinkage, understanding self-desiccation related properties helps explaining other types of the structural behaviors such as warping of slabs on grade. It is generally believed that slab warping uplift in Jointed Plain Concrete Pavement (JPCP) is caused by the external drying shrinkage that develops moisture gradients mostly within the top region of a slab cross section [Ytterberg 1987, Suprenant 2002, Nasvik 2002]. However, both field investigation and finite element (FE) analysis show that external drying combined with a negative temperature gradient is not sufficient to cause the extensive joint uplift found in the field [Hansen and Wei 2008]. Work presented here will explain this phenomenon through self-desiccation and autogenous shrinkage.

In the past decades, new techniques have been introduced to reduce the potential for cracking through: modifying the characteristics of the binder system; using expansive additives; using shrinkage reducing chemical admixtures; using internal curing through water saturated porous inclusions. However, not many studies have been carried out and covered the whole range of experimental investigations on the effect of internal curing on the development of autogenous shrinkage, restrained stresses, moisture warping, and drying shrinkage. These aspects will be addressed in this research.

1.2 OBJECTIVES AND SCOPE OF THIS RESEARCH

The aim of this research is, through fundamental studies, to build a basic understanding of the shrinkage mechanism from the hydration products point of view; to propose prediction models; and to explore the causes of the extensive warping found in JPCPs. This will potentially contribute to the assessment of the durability problems in

concrete infrastructures such as bridge decks, pavements, and indoor floors. The research focuses on achieving the following objectives:

- Assess the development of autogenous shrinkage in different systems by means of experimental measurements.
- Characterize the hydration products and quantify the relationship between the autogenous shrinkage and the hydration products for the paste systems with and without GGBFS.
- Develop models for the prediction of paste autogenous shrinkage based on cement hydration and microstructural characteristics.
- Develop a new methodology for predicting concrete autogenous shrinkage based on an elastic-based composite model (Pickett's model).
- Explain the extensive warping problem found in JPCPs.
- Evaluate the effectiveness of internal curing using pre-soaked lightweight fine aggregate (LWFA) on reducing autogenous shrinkage, self-induced stress, moisture warping, and drying shrinkage development.
- Propose new test methods for quantifying autogenous shrinkage development and moisture warping of concrete slabs.

To efficiently achieve these objectives, the experimental investigation is limited to the following variables:

- Ordinary portland cement (for paste and concrete) and white cement (for paste)
- Water/cementitious ratios of 0.35; 0.4; and 0.45
- Use of GGBFS as supplementary materials with content of 0%, 30% and 50% by mass of the total cementitious materials at *w/cm*=0.35

1.3 RESEARCH STRATEGY

The purpose of this research is to advance the knowledge on understanding the underlying mechanism of autogenous shrinkage and the extensive warping found in JPCPs. This will allow engineers to develop performance-based specifications to mitigate pre-mature shrinkage cracking. The outcome of this fundamental research on autogenous

shrinkage and self-desiccation will advance the application of binder optimization in JPCPs. Based on this concept, the research focus on these three aspects:

- Experimental studies of the influences of *w/cm* ratio, GGBFS contents, cement types and curing age on the development of autogenous shrinkage and the hydration products. The correlation between these two properties is made in the hydrating cement pastes.
- Develop models for quantifying autogenous shrinkage of cement paste and concrete with wide range of *w/cm* ratios and aggregate contents.
- Improve understanding of the interaction between concrete pavement or indoor floor and its environment through experimental testing and numerical simulations.

Regarding the experimental plan, this study focuses on a new methodology for determining the initiation and progression of pozzolanic reactions through autogenous deformation measurements and thermogravimetric analysis on hydrating cement paste. In addition, warping of a concrete beam simulating the complex field moisture conditions is assessed using a well-designed equipment. Linking the material and structural level testing is a step forward while utilizing new testing methods with improved ability to characterize autogenous deformation and moisture warping.

Regarding the predictions and simulations, the F-H model is found to be able to accurately predict effects of *w/cm* ratio, curing age, and GGBFS content on autogenous shrinkage. This provides a basis for concrete shrinkage predictions using the newly developed methodology. Numerical simulation of the hygral effects (i.e. moisture gradient and moisture warping uplift) in concrete slabs on grade explains why combined drying at the slab top and exposure to water at the slab bottom causes larger slab uplift than drying shrinkage gradient alone.

Figure 1.1 illustrates the flow chart of the thesis structure.

1.4 THESIS OUTLINE

The results of this research are presented in following chapters.

Chapter 2 reviews the properties of hydrating cementitious materials, the existing mechanisms of autogenous shrinkage, and the changes in the hydration products and the microstructure.

In Chapter 3, the experimental work conducted in this research is presented in detail. It covers the determination of autogenous shrinkage of paste and concrete, thermogravimetric analysis of paste systems, and mechanical properties testing such as restrained stresses, strength, and modulus. Information on materials and mixture proportioning are provided.

Chapter 4 presents the experimental results of autogenous shrinkage and thermogravimetric analysis on paste systems with the main purpose of developing a methodology for assessing how these properties are influenced by supplementary cementitious materials such as GGBFS, *w/cm* and cement types. The results show that autogenous shrinkage is a result of porous hydration products (PHP) and the associated pore drying within these porous hydration products.

The measured or predicted autogenous shrinkage of paste systems is then used as an input to composite shrinkage model in Chapter 5 in order to model concrete shrinkage as a function of *w/cm* and time for mixtures with various aggregate contents. This could be beneficial as it would not require stringent test conditions and elaborate apparatus to assess concrete autogenous shrinkage.

The investigations in Chapter 4 and 5 lay a foundation for understanding the particular aspects of pre-mature cracking associated with extensive warping found in JPCP slabs. In Chapter 6, both experimental study and numerical simulation prove that moisture warping is directly related to the self-desiccation and the consequent pore discontinuity. A new warping theory is given.

Chapter 7 evaluates the effect of internal curing using pre-soaked lightweight fine aggregate on mitigating autogenous shrinkage, self-induced stress, moisture warping, and drying shrinkage development.

Chapter 8 summaries the primary conclusions of this thesis and provides suggestions for possible extension to the research performed in this study.

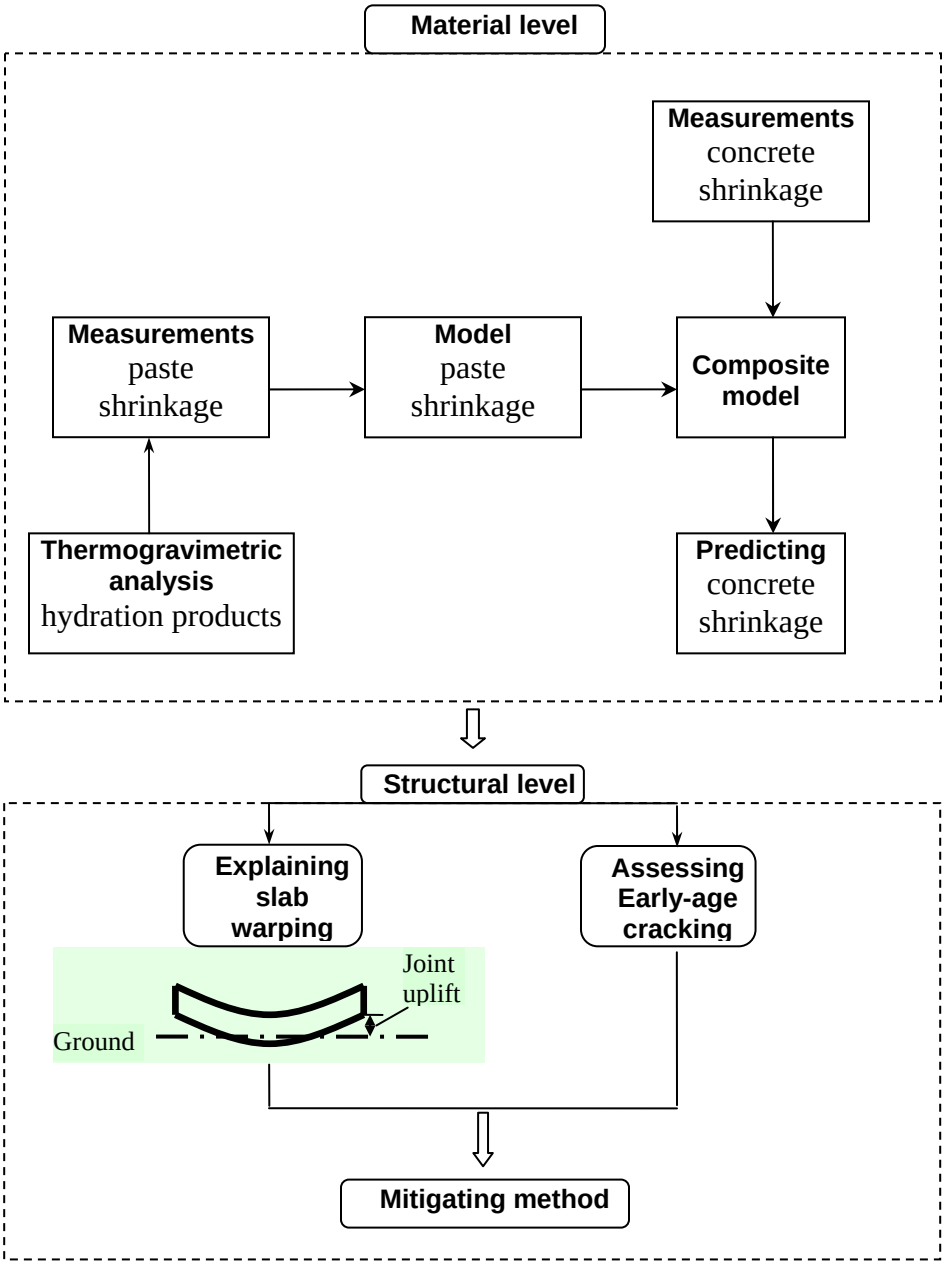

Figure 1.1 Flow diagram of this thesis

CHAPTER 2

CHARACTERISTICS OF HYDRATING CEMENT PASTE: LITERATURE REVIEW

2.1 INTRODUCTION

In this chapter, cement hydration, microstructure formation, and the existing mechanism of autogenous shrinkage are reviewed along with the structural-level response to shrinkage deformation of a slab on grade. In addition, hydration and pozzolanic reactions of ground granulated blast-furnace slag (GGBFS) are discussed because of the increasing and widespread utilization of this material in high-performance concrete containing supplementary cementitious materials (SCM).

2.2 HYDRATION PROCESS

2.2.1 Hydration Reactions

The major minerals in portland cement are tricalcium silicate (C_3S), dicalcium silicate (C_2S), tricalcium aluminate (C_3A), and tetracalcium aluminoferrite (C_4AF). These components react with water and build up cementitious gel. Gypsum $CaSO_4 \cdot 2H_2O$ ($C\bar{S}H_2$) is added to cement powder to control the reaction and avoid immediate stiffening of paste which is known as flash set [Neville 1981]. And thus, cement hydration is a complex set of reactions rather than a single reaction [Mindess and Young 1981, Odler 1998].

The hydration reactions can be divided into three stages as shown in **Figure 2.1** [Locher et al. 1976, Jennings et al. 1981]:

1. Dormant stage: a very short period when cement grains are in contact with water and start to react. It is mainly the active reaction of C_3A with gypsum and water to form ettringite which is typically seen as slender needles (**Figure 2.2**). In this stage, the cement paste remains plastic and it only lasts for a few hours dependent on the curing temperature, chemical composition and fineness of cement.

2. Setting stage: In this stage, C_3S and C_2S react actively with water and form amorphous calcium silicate hydrate (C-S-H) and crystalline calcium hydroxide (CH). The hydration product of C-S-H, with several morphological forms [Lachowski and Diamond 1983], is in the form of long fibers [Locher et al. 1976] in this stage and is responsible for the first contacts between cement grains [Ye 2003], as illustrated in **Figure 2.1**. The final set occurs before the maximum rate of hydration which is at the end of this stage. Secondary hydration of C_3A occurs in this stage forming ettringite that is later converted into monosulphate.

3. Hardening stage: The small disk or sphere-like C-S-H continues to be formed, which is mainly from C_2S reaction [Locher et al. 1976, Van Breugel 1991]. However, the hydration process slows down due to the formation of a dense layer from hydration products around the reacting particles. In this stage the rate of heat liberation slows down gradually as well.

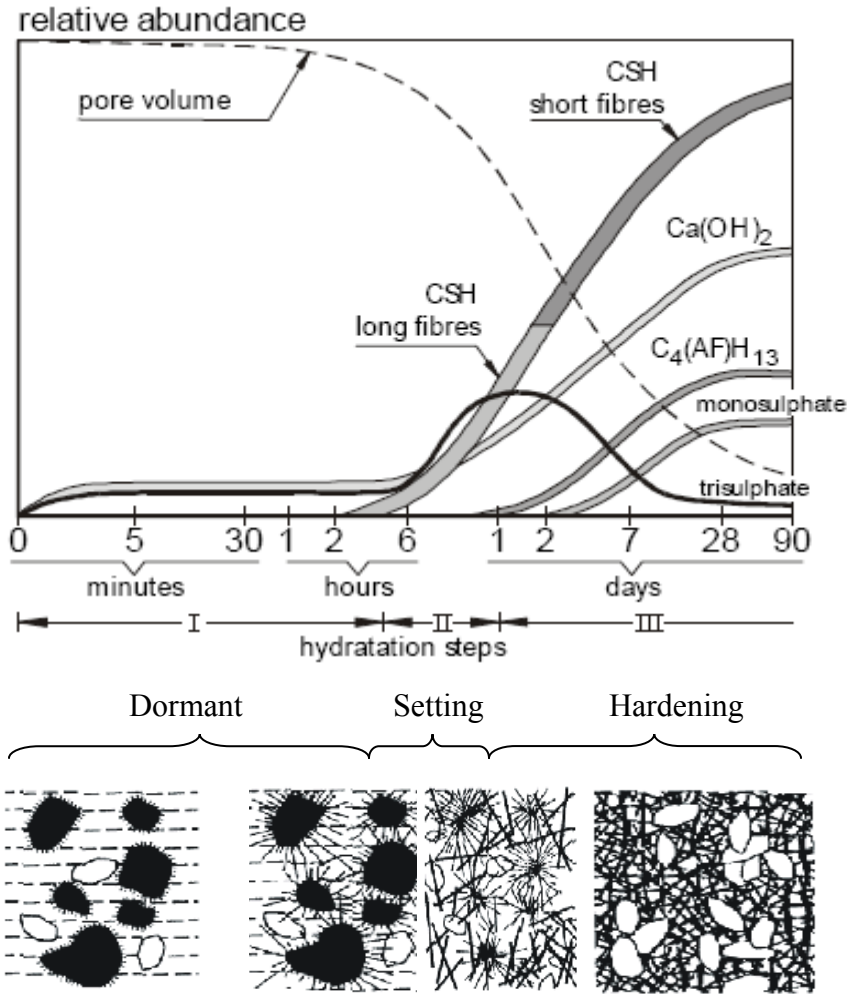

Figure 2.1 Development of hydration stages and hydration products [Locher et al. 1976]

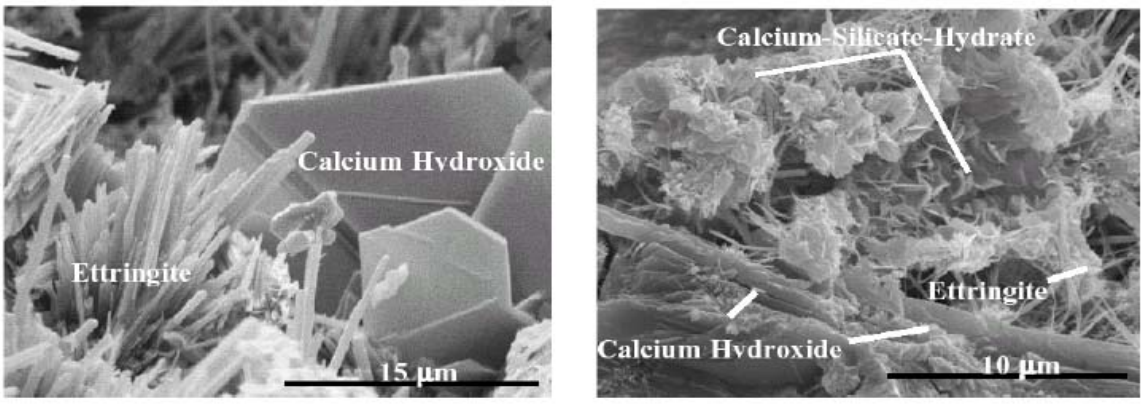

Figure 2.2 Morphology of the plate-like CH and fine bundles of C-S-H, and ettringite needles [Stutzman 2001]

2.2.2 Development of Pore Structure

With cement hydration, the solid phase (hydration products) and pore structure develop. The formation of pore structure mainly depends on degree of hydration and *w/cm* ratios. It is generally agreed that there are mainly three types of pores [Powers 1959, Mindess and Young 1981]: gel pores, capillary pores, and air voids, though Jennings [2004] has proposed a new classification of pore size based on the studies on mechanisms of reversible shrinkage. As part of C-S-H gel, gel pores are very small with diameter of about 0.5 nm to 10 nm. Capillary pores are meso-macro pores between the gel pores and air voids, with diameter ranging from 10 nm to 10 μm. Larger than the capillary pores are the air voids.

Capillary pores are considered to be responsible for the water and gas transport within cement paste [Mindess and Young 1981]. They are formed during cement hydration where water in the pores is removed for providing reactant for further hydration. Thus, the capillary pores depend on the degree of hydration as well as the *w/cm* ratios. Capillary pores increase with the initial *w/cm* both in the pore volume and pore size. However, capillary pore volume and size decrease as the hydration progresses and as hydration products start filling the pores. Conversely, as more hydrated gel is formed the associated gel pore volume increases. However, the capillary pore volume decreases more rapidly than gel pore volume increases, because only a portion of the gel which fills the capillary spaces is porous. Thus the total capillary and gel pore volume of the cement paste decreases with continuing hydration. There is a pore structure depercolation threshold when all the pores are closed off and thus changes the transport properties in cement paste.

2.2.3 Shrinkage due to Chemical Reactions

Chemical reactions are generally accompanied by volume changes. The major mechanisms of volume change (shrinkage or swelling) due to chemical reactions in hydrating cement have been nicely summarized by Wittmann [1982], Kovler and Zhutovsky [2006] as chemical shrinkage; thermal shrinkage; crystallization swelling; carbonation shrinkage; phase transition shrinkage; and dehydration shrinkage. Chemical

shrinkage is discussed in this work as it is the principle cause for volume change and closely tied to autogenous shrinkage.

Chemical shrinkage is the volume reduction typically on the order of 6-7 ml/100g of cement reacted [Powers and Brownyard 1948] due to the fact that the volume of the reaction products is smaller than the volume of the original reactants (water and cement). Chemical shrinkage increases with the progression of the hydration process and the net value is the increase of the pore volume in the hardening paste as shown in **Figure 2.3**.

The chemical shrinkage occurs at the expense of the water. For the three hydration stages, **Figure 2.3** demonstrates the volumetric proportion of a paste with *w/cm*=0.475 in a sealed condition. It was assumed that the paste has initial volumes of 60 ml of water and 40 ml of cement. At 100% degree of hydration, the 40 ml of cement produces 61.6 ml of solid hydration products, which is the solid part of the cement gel. The volume of the total reaction products including the solid products, gel water and capillary water is 92.6 ml, which is 7.4 ml less than the initial volume of 100 ml. This 7.4 ml of the capillary pores are empty and represents the total chemical shrinkage.

Chemical shrinkage is more like a molecular-level volume change and creates the underlying driving force to the occurrence of macroscopic bulk deformation known as autogenous shrinkage. Chemical shrinkage is identical to autogenous shrinkage as long as the paste is liquid. Around the time of setting, however, a solid skeleton is formed allowing empty pores to form, and the resulting bulk deformation (termed as autogenous shrinkage) becomes much smaller than the underlying chemical shrinkage.

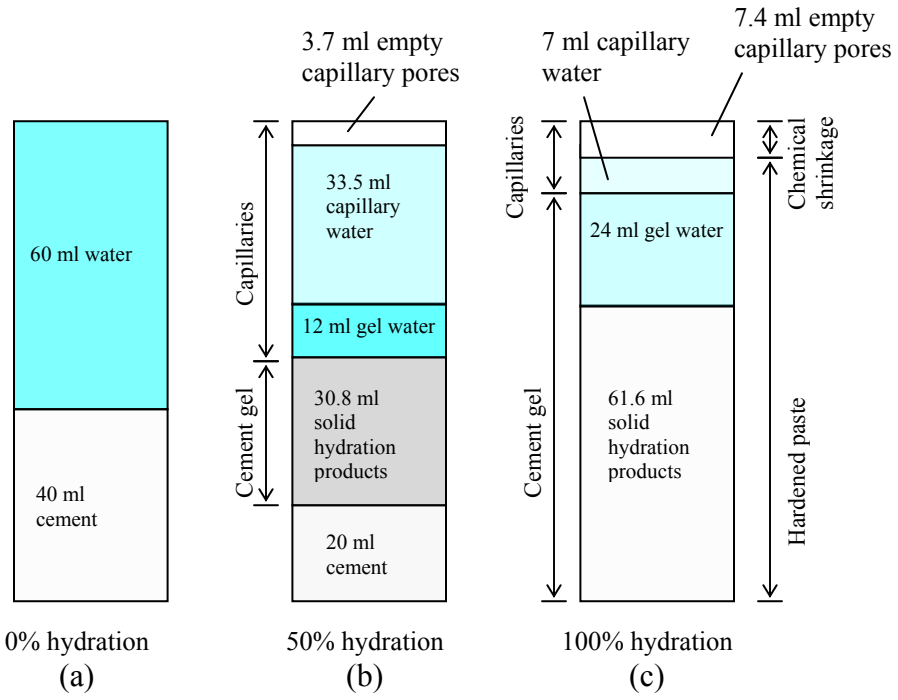

Figure 2.3 Schematic illustration of the volumetric changes of sealed cement paste for *w/cm*=0.475 at different stages of hydration [Kovler and Zhutovsky 2006]

2.3 AUTOGENOUS DEFORMATION

2.3.1 Definitions

Autogenous shrinkage was not a concern until concrete is made at much higher strength and lower water/cementitious ratios, field cracking and durability problems have been observed in these modern high performance concretes. Though much research has been devoted to this complex problem, the mechanisms leading to autogenous shrinkage are still far from being fully understood. There is general agreement about the existence of a relationship between autogenous shrinkage and relative humidity changes in the capillary pores of the hardening cement paste [L'Hermite 1960, Wittmann 1968, Powers 1968].

The following terminologies related to autogenous shrinkage are adopted from Jensen and Hansen [2001]. Other definitions about autogenous shrinkage can be found in [JCI 1999].

Autogenous deformation:

The bulk deformation of a closed, isothermal, cementitious material system not subjected to external forces.

Autogenous relative humidity change:

The change of internal relative humidity in a closed, isothermal, cementitious material system not subjected to external forces.

Self-desiccation:

Autogenous relative humidity change of a cementitious material system after setting, caused by chemical shrinkage.

Self-desiccation shrinkage:

Autogenous deformation of a cementitious material system after setting, caused by chemical shrinkage.

Note that "*closed*" means no exchange of water occurs between the cementitious material and the surroundings; "*isothermal*" requires that the temperature is kept constant.

For autogenous shrinkage, changes in tension in capillary water, disjoining pressure, and surface tension of the solid gel particles are the principal mechanisms that have been suggested.

2.3.2 Mechanisms of Autogenous Shrinkage

Capillary Tension

Capillary pores are formed during cement hydration that water in the pores is removed for providing reactant for further hydration. This will cause a reduction of the relative humidity of the capillary pores, known as self-desiccation. **Figure 2.4** illustrates the calculated reduction of pore humidity with the increase of degree of hydration [Koenders 1997]. The reduction of pore humidity is sensitive to *w/cm*. The humidity drop is very slow in a high *w/cm* system and the pore structure will probably remain filled with capillary water for a long period of time. However, the self-desiccation is pronounced in a low *w/cm* cement paste. For *w/cm*=0.3, the pore humidity drops to78% at 50% degree of hydration. Thermodynamic analysis by Jensen [1995] showed that the pore humidity could not drop below 75% from self-desiccation alone.

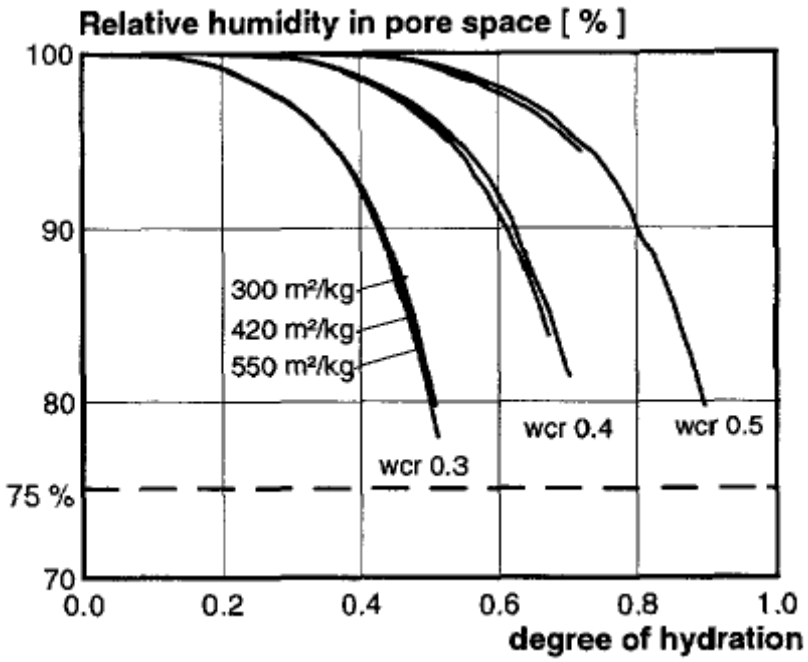

Figure 2.4 Calculated pore humidity versus degree of hydration for three different cement finenesses and *w/cm* of the cement paste [Koenders 1997]

With the reduction of pore humidity, meniscus and surface tension of the liquid forms in capillary pores to maintain the equilibrium between the liquid and the vapor over the liquid. And thus, the capillary pressure develops, which is the vapor pressure minus water pressure. This capillary pressure will cause water in capillaries under depression (under tensile stress) and has to be balanced by compressive stress of the surrounding solid. This compressive stress will result in volume decrease in cement paste as demonstrated in **Figure 2.5**. Because this compressive stress is originally induced by the reduction of internal relative humidity, any drying process either from external drying or internal drying (self-desiccation) will cause shrinkage in cement paste.

Laplace equation gives the relationship between capillary pressure or capillary tension and surface tension:

$$P_{cap} = -\frac{2\gamma}{r} \qquad \text{Eq. 2.1}$$

where,

P_{cap} = capillary tension (MPa)

γ = surface tension of the liquid

r = the radius of menisci curvature

Further hydration decreases the relative humidity resulting reduction of the curvature radius of the meniscus. According to Laplace equation, the relationship between pore relative humidity and radius of curvature is considered as:

$$\ln(RH) = \frac{2 \cdot \gamma \cdot V_m}{R \cdot T \cdot r} \qquad \text{Eq. 2.2}$$

where,

RH = pore humidity

R = the gas constant

T = the temperature (K)

V_m = the molar volume of water

And thus the relation between capillary tension and relative humidity is given by Kelvin equation:

$$P_{cap} = -\frac{RT \ln(RH)}{V_m} \qquad \text{Eq. 2.3}$$

Assuming cylindrical capillary pores, the radius of meniscus curvature decreases with reduction of relative humidity until it equals to the radius of the capillary. Due to the size distribution effect of capillary pores, the evaporation will first take place in the big pores. Further hydration will cause the formation of meniscus in the small pores after the big pore has been emptied. And thus, in hydrating cement paste pores that have radius lower than that of meniscus are filled with water and pores with bigger radius are empty.

Capillary menisci are unstable below about 45% pore humidity [Soroka 1979, Mindess 1981], and thus the capillary tension mechanism for autogenous shrinkage should be only effective in the upper pore humidity range, which is about above 45%. Since the pore humidity in capillary pores is not dropping below 75% due to self-desiccation alone [Jensen 1995], it has justification to state that capillary tension mechanism is appropriate to explain autogenous shrinkage deformation.

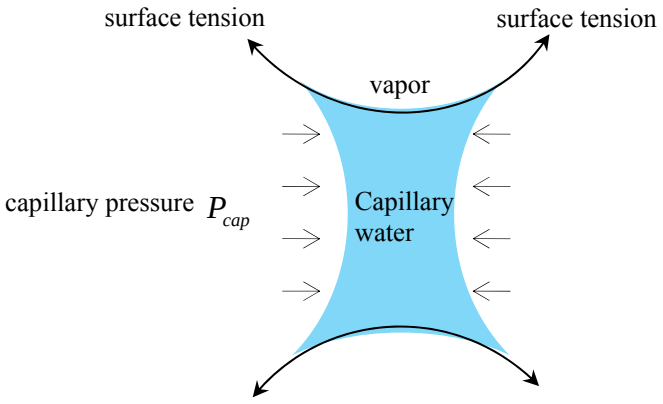

Figure 2.5 Capillary tension as the mechanism of shrinkage

Solid Surface Tension

Solids have surface tension at their interface with other materials. Changes in the surface tension of solid hydration products could result in bulk shrinkage or expansion of the cement paste. The magnitude of solid surface tension is dependent on the thickness of the adsorbed layers of water which lowers the surface tension of the cement gel particles and results in expansion. Conversely, removal of the adsorbed water increases the solid surface tension and creates a net compression of the solid resulting in micro-scale shrinkage [Powers 1968]. Surface tension can induce huge compressive stresses of around 250 MPa in cement gel particles with large specific surface area [Wittmann 1968, Soroka 1979], and thus noticeable bulk shrinkage.

Bangham and Fakhoury [1931] showed an equation that relates length change to the corresponding changes in solid surface tension:

$$\frac{\Delta l}{l} = \lambda \cdot \Delta\gamma \qquad \text{Eq. 2.4}$$

where,

Δl = the length change (m)

l = the length (m)

λ = the proportionality factor (s^2/kg)

$\Delta\gamma$ = the change in surface tension of the solid particles (N/m)

The proportionality factor depends on the internal surface of the porous body, on the density of the solid and on the elastic modulus of the porous material [Hiller 1964]:

$$\lambda = \frac{\sum \cdot \rho}{3E} \qquad \text{Eq. 2.5}$$

where,

$\sum$ = internal pore wall area of the empty pores (m^2/kg)

ρ = the density of the solids (kg/m^3)

E = the elastic modulus of the porous body (MPa)

Koenders [1997] used this relationship between deformation and solid surface tension change to model autogenous shrinkage of a hardening cement paste. However, it has been suggested that surface tension do not become significant until lower pore humidity (less than 50%) where only one or two adsorbed water layers are present [Wittmann 1968, Mindess 1981]. And thus this mechanism does not apply to autogenous deformation since the relative humidity is generally above 75% from self-desiccation alone [Jensen 1995]. Research by Hansen [1987], on the other hand, showed that solid surface tension contributes to shrinkage at higher pore humidity as well.

Disjoining Pressure

The disjoining pressure between the solid particles is the result of van der Waals forces, double layer repulsion, and structural forces [Ferraris and Wittmann 1987]. The layered structures of C-S-H particles have huge surface area which attracts water molecules at interfaces. As water moves into the layers of C-S-H particles, the repulsive forces arise and the attractive van der Waals' force decreases between the solid layers, and thus results volume changes. This swelling pressure from the absorbed water is referred to disjoining pressure. Stresses develop in the solid microstructure to balance the reduction in disjoining pressure, resulting in macro-scale shrinkage [Grasely 2006]. The disjoining pressure varies with the pore humidity. When the pore humidity drops, the disjoining pressure is reduced, causing shrinkage. However, disjoining pressure is quite in debate on at what relative humidity range this mechanism is responsible for volume changes [Mindess and Young 1981].

2.3.3 Experimental Techniques for the Measurement of Autogenous Deformation

Autogenous deformation can be measured in terms of either volume change or length change. For both types of measurements, the samples need to be sealed to avoid moisture exchange between the sample and the environment.

Volumetric measurements are done by taking the weight of a sample sealed in a thin rubber membrane underwater as shown in **Figure 2.6**. The procedure consists of filling the rubber membrane with fresh cement paste or mortar and placing it in a rigid tube. This tube is then immersed in a temperature-controlled water bath and continuously rotated to avoid bleeding. The creation of empty spaces leads to a modification of the buoyancy, making it possible to obtain the variations in volume of the sample by simple weight measurements [Justnes et al. 1996]. However, this technique may subject to measuring less autogenous shrinkage due to the absorption of water from the buoyancy bath through the rubber membrane driven by a lowering of the water activity in the sample due to self-desiccation and to dissolved salts in the pore fluid [Lura and Jensen 2005]. In addition, the volumetric method can not be used for concrete since the aggregates would damage the rubber membrane. The presence of these artifacts makes the volumetric method very difficult to use in practical applications [Lura and Jensen 2005].

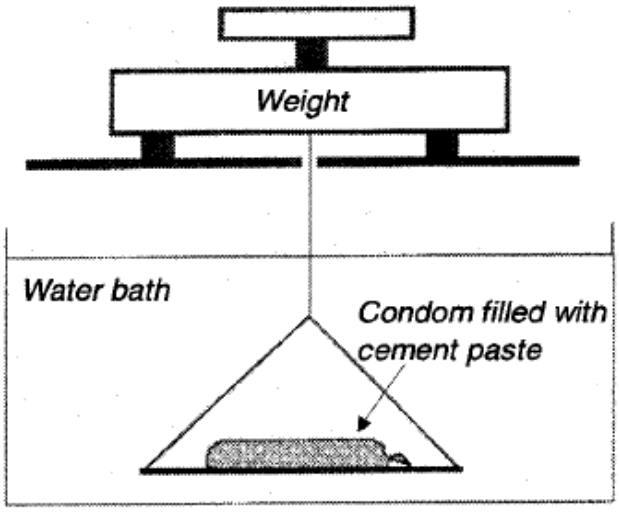

Figure 2.6 Volumetric measurement of autogenous shrinkage [Bjontegaard 1999]

Linear measurements are usually carried out by placing the sample in a rigid mold. The length change of the sample is recorded by a displacement transducer at the end of the specimen (**Figure 2.7**). This linear measurement can measure autogenous deformation not only on cement paste but also on concrete specimens. And it is a more direct way in interpreting autogenous deformation. However, there are a few limitations in the linear measurements. For example, the friction between the sample and the mold may restrain autogenous deformation; the measurement can not be carried out before the sample has set; a sealed curing condition has to be insured. It is essential to overcome the external friction through carefully preparing the mold and the sample. In addition to using a rigid mold, Jensen and Hansen [1995] have developed a method which utilizes a soft corrugated plastic tube to measure the linear autogenous deformation. This technique allows measurements to start 30 minutes after casting. However, this corrugated mould is not applicable for autogenous deformation measurement on concrete mixtures.

In this study, linear measurement is adopted and modified to eliminate artifacts and to achieve the best results.

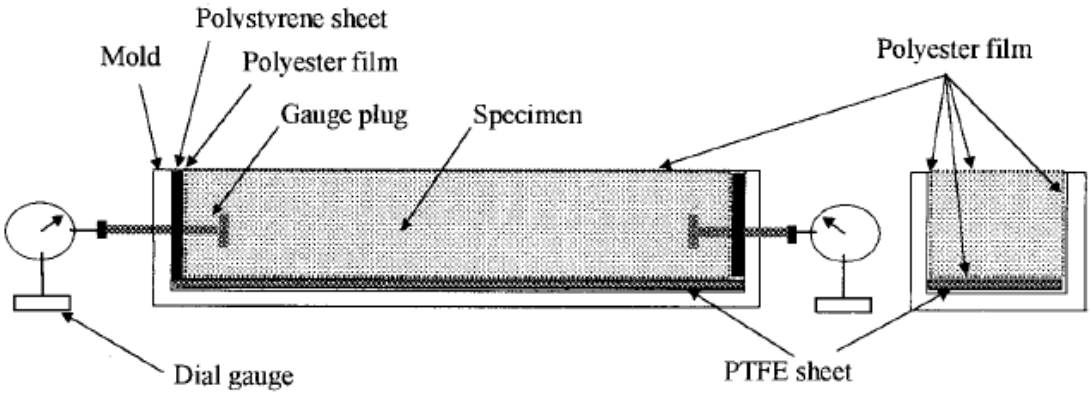

Figure 2.7 Linear measurement of autogenous shrinkage [Japan 1999]

2.4 GROUND GRANULATED BLAST-FURNACE SLAG (GGBFS)

Ground granulated blast-furnace slag (GGBFS) is a waste product in the manufacture of pig iron. The use of GGBFS as a supplementary cementitious material can be less expensive and ecologically friendly alternative. In the cement industry, the thermal transformation of CaO, which is the main component of clinker in the production

of cement, consumes an enormous amount of fuel and energy. In addition, the large scale production of portland cement is a significant source of atmospheric pollution. One ton of clinker generates approximately the same amount of CO_2 [Roy 1999]. However, the addition of 10 tons of pozzolan to the clinker results in a saving of 1 ton of fuel and reduces CO_2 emission [Mehta 1983, Sersale 1983].

GGBFS varies greatly in composition and physical structure depending on the manufacture processes used. The specific density of GGBFS is about 2.9, lower than portland cement of 3.15. Its chemical composition is similar to that of portland cement but not in the same proportions. Compared with portland cement, GGBFS contains higher amount of SiO_2, Al_2O_3 and MgO and lower amount of CaO [Taylor 1997].

GGBFS can be used to make cementitious material in different ways [Neville 1996]: (1) used together with limestone as a raw material for the manufacture of portland cement; (2) used on its own in the presence of an alkali activator or starter if ground to the appropriate fineness; (3) dry blending of portland cement and GGBFS powders before mixing them with water. In this research, the third way is used.

When the blended cement meets with water, the portland cement component begins to react first and with a small amount of immediate reaction of GGBFS that releases calcium and aluminum ions into solution. According to Neville [1996], GGBFS first reacts with alkali hydroxides as they are dissolved immediately when portland cement is mixed with water. Once the concentration of CH from portland cement reaction reaches a certain level, the reaction of GGBFS with CH will become dominant and produce C-S-H.

The hydration products of GGBFS are the same as those of portland cement [Papadakis et al. 1992]. The pozzolanic activity can be reviewed as the following reactions:

$$CaO + H_2O \rightarrow CH \qquad \text{Eq. 2.6}$$

$$2SiO_2 + 3CH \rightarrow C_3S_2H_3 \qquad \text{Eq. 2.7}$$

$$Al_2O_3 + Fe_2O_3 + 8CH + 18H_2O \rightarrow C_8AFH_{26} \qquad \text{Eq. 2.8}$$

$$Al_2O_3 + C\bar{S}H_2 + 3CH + 7H_2O \rightarrow C_4A\bar{S}H_{12} \qquad \text{Eq. 2.9}$$

$$Al_2O_3 + 4CH + 9H_2O \rightarrow C_4AH_{13} \qquad \text{Eq. 2.10}$$

The calcium hydroxide (CH) necessary for the reactions in Eq. 2.7 through Eq. 2.10 comes from the pozzolan itself known as self-pozzolanic activity (Eq. 2.6), while CH provided by the hydration of portland cement for the secondary pozzolanic reactions is known as pozzolanic activity.

Actually, the pozzolanic reaction depends very much on the CH produced by the portland cement hydration, as the amount of lime (CaO) in GGBFS is far from enough for the production of the amount of CH required by the pozzolanic reactions. Eq. 2.11 through Eq. 2.15 lists the portland cement hydration reactions according to Mindess and Young [1981]:

$$2C_3S + 6H_2O \rightarrow C_3S_2H_3 + 3CH \qquad \text{Eq. 2.11}$$

$$2C_2S + 4H_2O \rightarrow C_3S_2H_3 + CH \qquad \text{Eq. 2.12}$$

$$C_4AF + 4CH + 22H_2O \rightarrow C_8AFH_{26} \qquad \text{Eq. 2.13}$$

$$C_3A + C\bar{S}H_2 + 10H_2O \rightarrow C_4A\bar{S}H_{12} \qquad \text{Eq. 2.14}$$

$$C_3A + CH + 12H_2O \rightarrow C_4AH_{13} \qquad \text{Eq. 2.15}$$

Reaction 2.15 takes place only after all the gypsum ($C\bar{S}H_2$) has been consumed by reaction 2.14. It can be seen that the pozzolanic reaction is similar to the hydration reaction in portland cement. The main difference is that the clinker in portland cement reacts in the form of compounds, whereas in pozzolans the amorphous (noncrystalline) form of the oxides reacts with CH.

It has been found fine pore structure of GGBFS cement, which resulting in a lower permeability [Roy and Idorn 1982], and thus the beneficial of resistance to chemical attack. This finer pore structure should be the product of the dissolution of the calcium hydroxide crystals and the precipitation of pozzolanic C-S-H gel.

Recent experimental investigations on autogenous shrinkage indicate that GGBFS blended cements have somewhat greater autogenous shrinkage than neat portland cement paste [Tazawa and Miyazawa 1995, Hanehara et al. 1999, Lura 2003, Lee et al. 2006]. The reasons were generally attributed to the higher chemical shrinkage, the finer pore structure of the blended system, and the pozzolanic reactions that consume calcium hydroxide (CH) crystals and consequently induce shrinkage as a result of removal of shrinkage restraints in the paste.

2.5 STRUCTURAL RESPONSE OF A SLAB TO CEMENT HYDRATION

The structural response of a slab to the hydrating concrete can be moisture or temperature related. Large temperature gradients, typically a negative temperature gradient during the curing period, can develop if the concrete surfaces are exposed to a low environment temperature while the center undergoes thermal inputs which can not be dissipated quickly. And hence, surface cracks due to the non-uniform distributed thermal strain develop in the finished concrete structure.

Moisture related structural response of a slab can be generated from autogenous shrinkage or drying shrinkage. As a uniform volume reduction, autogenous shrinkage causes joint movement. Early age cracking can be one of the major problems for a slab, or overlay if this horizontal movement is restrained from adjunct structures. In concrete overlay which is cast on top of an old concrete pavement, cracks can initiate at the bottom of young overlay which undergoes autogenous shrinkage restrained by the old pavement (**Figure 2.8**). This type of crack can propagate upward and become a big concern for the durability, especially in North America, where de-icing salts are used extensively in winter times.

Concrete shrinkage was found to be a major contributor to cracking of bridge deck on steel girders [Schmitt and Darwin 1999]. Shrinkage cracking allows moisture and chloride to penetrate and hence accelerates the corrosion of reinforcing steel. It has been found that cracks in concrete, especially those wider than 0.15mm, facilitate the penetration of moisture and other detrimental chemical species into concrete [Reinhardt and Jooss 2003, Schieβl and Raupach 1997, Aldea et. al 1999].

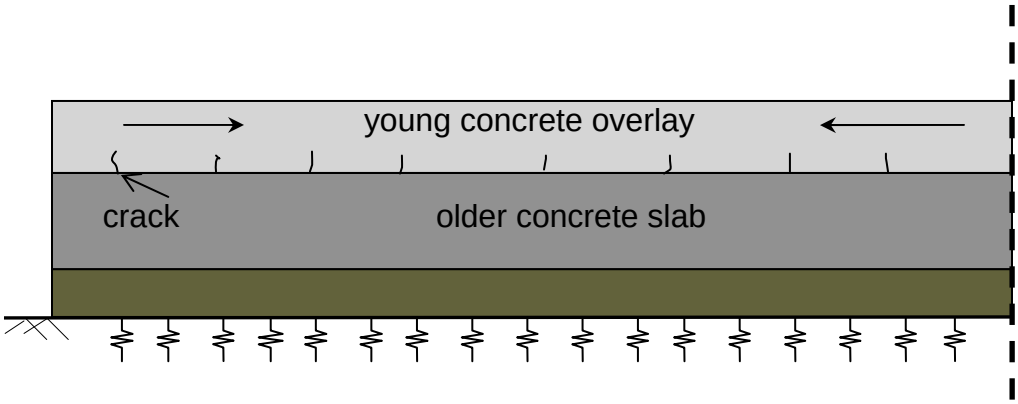

Figure 2.8 Illustration of shrinkage cracking in a concrete overlay

Jointed Plain Concrete Pavements (JPCP) will develop some degree of moisture warping uplift, dependent on the stiffness of grade, at the joints and especially the corners. This is generally attributed to the non-uniform moisture gradient and the associated moisture deformation. Floors exposed to in-door moisture conditions have been found to develop permanent joint corner uplift due to the moisture loss from drying [Ytterberg 1987, Suprenant 2002, Nasvik 2002].

For the case of a concrete slab resting on the ground, drying proceeds from the top surface only. But below about 50 mm (2 in.) from the surface, the moisture level remains at a relatively constant high level which results in a non-linear distributed shrinkage profile along slab depth [Janssen 1987, Suprenant 2002]. Two visible deformations develop as a result of the differential shrinkage, one is the axial movement which is conventionally treated as drying shrinkage and the other one is warping. If restrained, these two deformations can cause axial stress and bending stress, respectively, as shown in **Figure 2.9**. Another stress component is also generated during the drying and described as the residual stress which is due to the internal restraint from the surroundings in order to satisfy translational symmetry in concrete cross-sections. Moisture warping can significantly reduce slab-base contact area and result in early failure of JPCPs [Poblete et al. 1990, Darter et al. 1995, Hansen and Wei 2008].

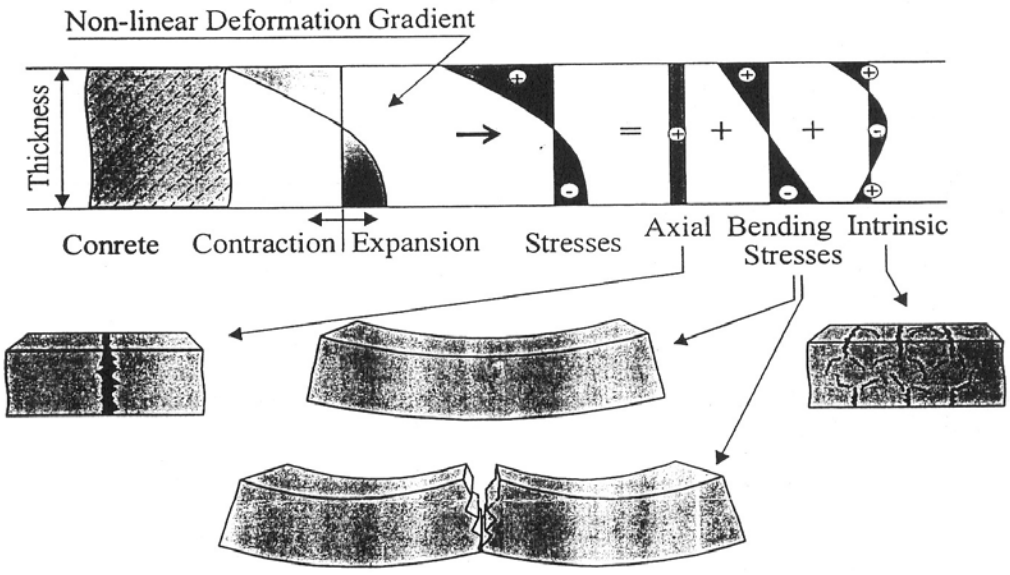

Figure 2.9 Slab deformation and stresses caused by a non-linear shrinkage gradient [Springenschmid 2001]

2.6 CONCLUSIONS

This chapter starts with a literature survey which leads to a state-of-the-art review on the fundamental characteristics of cementitious materials. Substantial research has been conducted on cement hydration, microstructure formation, mechanism of autogenous shrinkage and associated early-age cracking. However, it has not been thoroughly integrated to develop a framework that the engineering profession can use in linking the material-level evidence with the observed problems in the field. This work aims to advance the knowledge on understanding the underlying mechanism of autogenous shrinkage, the associated early-age cracking in concrete, and the extensive warping found in JPCPs through experimental and numerical investigations.

CHAPTER 3

EXPERIMENTAL

3.1 INTRODUCTION

In this chapter, measuring techniques and materials used are discussed. The tests include free autogenous deformation, externally restrained autogenous deformation, chemical and microstructure evolution due to hydration, and strength and modulus are discussed.

The objectives are to obtain experimental data for:

- Evaluating the mechanisms of autogenous shrinkage and the physico-mechanical relationship in cementitious materials.
- Establishing models for predicting autogenous shrinkage in cement paste and concrete.

3.2 MATERIALS

Two types of cement (ordinary portland cement (OPC) and white cement) were used for preparation of cement paste to incorporate the effect of chemical compositions. Ground granulated blast-furnace slag (GGBFS) as a supplementary cementitious material (SCM) was blended with OPC for the purpose of evaluating the effect of pozzolanic reactions. The replacement of GGBFS accounts for 30% and 50% of the total cementitious material by weight. In North America, GGBFS commonly constitutes between 30% and 45% of the cementing material in general purpose concrete. ASTM C 989 classified GGBFS by its increasing level of reactivity as Grade 80, 100, or 120. Grade 120 GGBFS was used in this work. The physical properties and chemical compositions of each cementitious material are listed in **Table 3.1**.

In concrete mixtures, the coarse aggregate was crushed limestone with a bulk specific gravity of 2.64 and water adsorption capacity of 4%. The maximum aggregate size was 12.5 mm (0.5 in.). The fine aggregate was natural sand with Fineness Modulus of 1.56, bulk specific gravity of 2.64, and water adsorption capacity of 1.5%. OPC was used for all concrete mixtures.

The effectiveness of internal curing on mitigating autogenous shrinkage was investigated as well. The internal curing was achieved in concrete through partially replacing the fine aggregate (natural sand) using pre-soaked lightweight fine aggregate (LWFA). The sand-size expanded shale lightweight fine aggregate was used, which have a bulk specific gravity of 1.8 and water content of 15% by weight obtained in a 24-hour pre-soaked condition.

Table 3.1 Physical properties and chemical compositions of cementitious materials

	ordinary portland cement (OPC)	White cement	GGBFS
Blaine fineness, cm^2/g	4290	3910	6020
SiO_2, %	20.4	24.6	37.49
Al_2O_3, %	5.04	2.1	7.77
Fe_2O_3, %	2.51	0.34	0.43
CaO, %	62.39	69	37.99
MgO, %	3.43	0.6	10.69
SO_3, %	2.75	2.03	3.21
Na_2O, %	0.25	0.11	0.28
K_2O, %	0.67	0.03	0.46
Cl, %	0.03	n. a.	n. a.
Total as Oxides	97.47	n. a.	n. a.
C_3S	53.66	74	n. a.
C_2S	18.01	15	n. a.
C_3A	9.11	5.0	n. a.
C_4AF	7.64	1.0	n. a.

n. a. = not available.

3.3 MIX PROPORTIONING

The mix proportioning is provided in **Table 3.2** for cement paste and concrete with different aggregate contents ϕ_A at *w/cm*=0.35 and 0.45 as an example. Mixture with *w/cm*=0.4 was also used but are not shown here. For the same aggregate content, *w/cm*=0.4 mixtures were achieved by varying water and cement contents while maintaining the paste volume the same as other *w/cm* systems. For pastes blended with GGBFS, the mix proportioning is shown in **Table 3.3**.

Cement paste was mixed in a pan mixer. For blended systems, the GGBFS was first dry-mixed with the neat ordinary portland cement (OPC) for several minutes to achieve a uniform distribution of the solid ingredients. Water was then added to the dry ingredients and mixed for another three minutes. The fresh paste was consistent and uniform with no visible agglomerates. For the autogenous shrinkage measurements, to avoid bleeding, the cement paste was remained in the pan mixer after mixing and was allowed to hydrate for about three to four hours dependent on *w/cm* ratios prior to casting, mixing every half an hour to maintain workability.

Concrete shrinks less than cement paste due to the addition of the non-shrinking aggregate particles (sand and coarse aggregates). The addition of aggregates may contribute to the complexity of autogenous shrinkage measurements that the shrinkage can not be fully captured due to the non-shrinking particle proximity effects when using the limited-size specimens. Our previous extensive autogenous shrinkage measurements demonstrated that regular concrete with maximum aggregate size of 25.4 mm (1 in.) and aggregate content ranging from 60% to 80% of the total mixture by volume causes no autogenous shrinkage. Therefore, concretes with different aggregate contents (less than the normal range of aggregate content) and with maximum aggregate size of 12.5 mm (0.5 in.) were examined in this research. The mix proportioning can be found in **Table 3.2** for *w/cm*=0.35 and 0.45 at the aggregate contents of 0%, 40%, and 50% of total mix by volume. Be aware that the concrete with aggregate content of 0% is actually the cement paste. In all the concrete mixtures, the ratio of sand to coarse aggregate by volume was kept the same though the total aggregate content may vary.

For internal curing mixtures, two *w/cm* ratios (0.35 and 0.45) and two LWFA replacement levels (20% and 40% of the total fine aggregate by volume) were used.

Table 3.4 lists the proportioning. In which 20% indicates that 20% sand by volume is substituted by LWFA. For concrete with *w/cm*=0.45, the mix proportioning is not shown here. But it varies only the water and cement contents, the aggregate content was maintained the same as *w/cm*=0.35 systems.

In the concrete mixing process, light adjustment in the amount of high-range water-reducing admixture was performed for low *w/cm* ratio system (*w/cm* =0.35) to achieve consistent rheological properties with adequate workability. Air entraining admixture (AEA) Masterbuilders VR was used as needed to obtain 5-7% air in all concrete mixtures.

Table 3.2 Mix proportioning for paste (ϕ_A=0%) and concrete

Material	*w/cm*=0.35 (ϕ_A=0%)	*w/cm*=0.35 (ϕ_A=40%)	*w/cm*=0.35 (ϕ_A=50%)	*w/cm*=0.45 (ϕ_A=0%)	*w/cm*=0.45 (ϕ_A=40%)	*w/cm*=0.45 (ϕ_A=50%)
Cement (kg/m^3)	1500	763	598	1305	660	520
Water (kg/m^3)	525	267	209	587	297	234
Limestone (kg/m^3)	n. a.	268	341	n. a.	268	341
Sand (kg/m^3)	n. a.	763	974	n. a.	763	974
Water reducer (kg/m^3)	n. a.	3.1	2.4	n. a.	n. a.	n. a.
AEA (kg/m^3)	n. a.	1.5	1.2	n. a.	1.5	1.2

n. a. = not available.

AEA=air-entraining admixture

Table 3.3 Mix proportioning of cement paste blended with GGBFS, *w/cm*=0.35

Material	0% GGBFS	30% GGBFS	50% GGBFS
Cement (kg/m^3)	1500	1050	750
GGBFS (kg/m^3)	n. a.	450	750
Water (kg/m^3)	525	525	525

n. a. = not available.

Table 3.4 Mix proportioning of concrete containing pre-soaked lightweight fine aggregate (LWFA) at different replacement levels, *w/cm*=0.35

Material	0% LWFA (control mix)	20%LWFA	40%LWFA
Cement (kg/m^3)	557	557	557
Water (kg/m^3)	195	195	195
Limestone (kg/m^3)	431	431	431
Sand (kg/m^3)	1224	979	724
pre-soaked LWFA (kg/m^3)	n. a.	526	263
Water reducer (kg)	2.23	2.23	2.23
AEA (kg)	1.11	1.11	1.11

– n. a. = not available.

3.4 AUTOGENOUS DEFORMATION MEASUREMENT

The linear autogenous deformation was measured on sealed specimens with a cross-section of 60 mm (2.4 in.) by 100 mm (3.9 in.) and length of 1000 mm (39.4 in.). For free deformation measurement, the main difficulties to overcome are minimizing friction between the specimen and the rig; preventing moisture exchange with the external; and keeping the curing temperature constant. The following testing procedures were carefully conducted to ensure accurate measurements.

Right after casting into the rig, the external drying was prevented by sealing the specimens using two layers of polystyrene film. External friction was reduced by placing

a soft, flexible, 2 mm-thick foam rubber between the rig and the sealed specimen as shown in **Figure 3.1** [Schleibinger 1999]. The curing temperature was maintained at 23±1 ^{o}C (73±2 ^{o}F) by circulating constant-temperature water through the channels built-into the sides and bottom of the rig. One end of the specimen was fixed to the rig and the other end was free to move horizontally. The free end had an LVDT attached for measuring linear autogenous deformation. This measurement was initiated after final set when a solid skeleton has been formed, as the setting time of the cement paste is usually referenced to the starting point of autogenous shrinkage [Tazawa et al. 1995]. Two replicate specimens were tested and the results of two specimens were plotted for each mix.

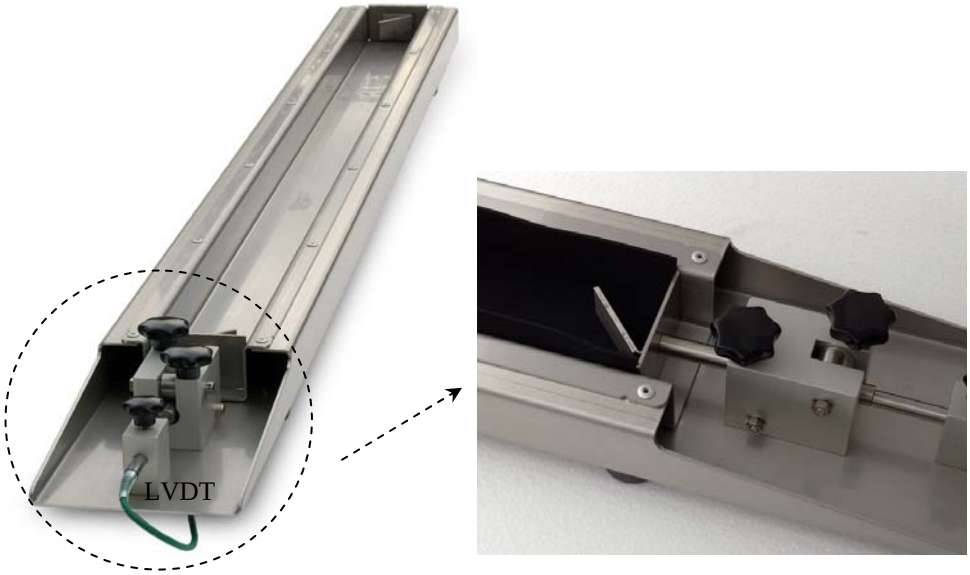

(a)

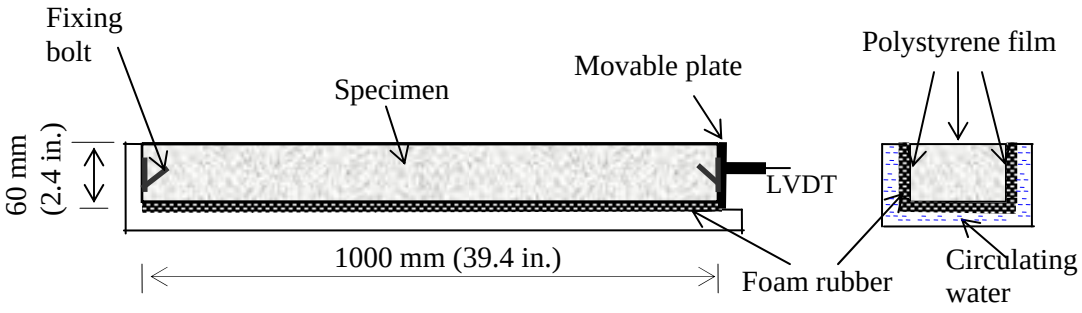

(b)

(c)

Figure 3.1 Linear measurement of autogenous shrinkage (a) photo of an empty rig [after Schleibinger 2007]; (b) schematic illustration of the apparatus; (c) specimens in testing

3.5 SELF-INDUCED STRESS DUE TO RESTRAINED AUTOGENOUS DEFORMATION

Self-induced stress due to restrained autogenous shrinkage in concrete was measured by using a temperature-stress-testing-machine (TSTM). The original development of the TSTM by Springenschmid et al. [1985] has lead to vast improvements in understanding the stress levels that are generated in concrete at early-ages [Weiss 1999]. In this study, TSTM is an improved computer-controlled close loop system which is composed of a load cell and an actuator as illustrated in **Figure 3.2**.

A specimen was directly cast into a rig which is built into TSTM. The total length of the specimen was 810 mm (31.9 in.). Two ends of the specimen were enlarged to ensure a uniform stress distribution in the central part of the specimen. The central part dimension was 254 mm (10 in.) by 100 mm (3.9 in.) by 100 mm (3.9 in.). One enlarged end of the specimen was fixed to the load cell while the other end was connected to the actuator by bolts. To provide a restrained condition, the actuator was computer-controlled to move back and forth at an amplitude of 5 micron strain relative to its original position and a time interval of two seconds. This is done to avoid drift over a long period of time and try to keep the specimen length unchanged. Such restrained mode was designed to

best utilize TSTM's restraining capacity. The load cell recorded the load generated in specimens. During the entire testing, the specimen was sealed cured similar to the one in autogenous shrinkage test. The curing temperature was kept at about 23±1 ^{o}C (73±2 ^{o}F) by circulating constant-temperature water through copper pipes placed around the specimen. Testing was initiated immediately after casting. Two replicate specimens were tested for each mix.

Since TSTM testing is similar to a uniaxial tension test, there are inherent difficulties in this test. For example, the friction between the specimen and the rig was reduced by using the same separator as used in autogenous shrinkage test.

TSTM measures restrained shrinkage stresses with a preset degree of restraint, and the restraining load is transferred to the concrete by four continuously embedded reinforcing bars. Degree of restraint has a large effect on the development of self-induced stress [Kovler 1994, Mizobuchi et al. 2000, Zhang and Qin 2006]. Though the stress ratio (stress under a certain restraint/stress under a complete restraint condition) is not always proportional to the degree of restraint, it is considered acceptable to estimate the stress under 100% restraint using the measured stress by assuming that the stress ratio is proportional to the degree of restraint [Zhang and Qin 2006].

Comparison of the measured autogenous shrinkage and the self-induced stresses enabled the establishment of a restrained stress-strain constitutive relationship for a cementitious system.

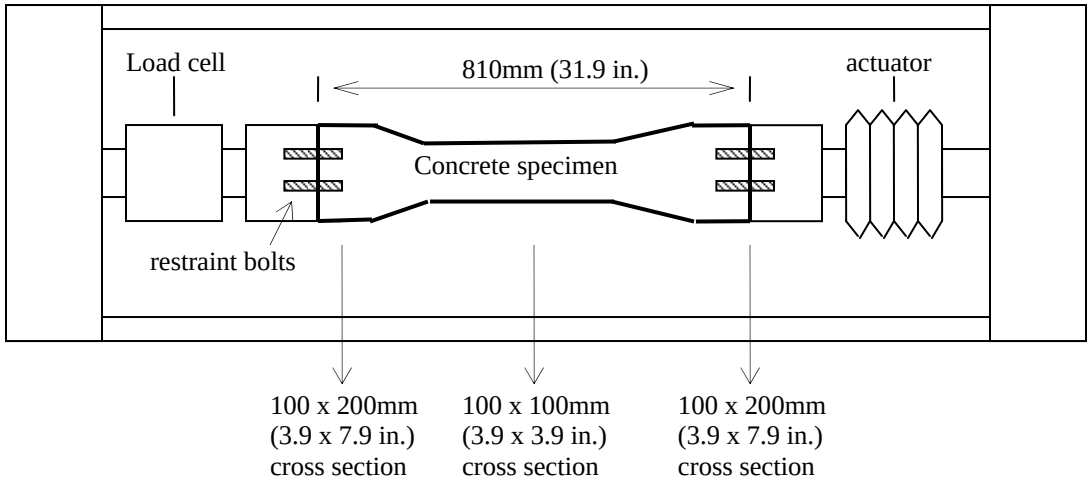

(a)

(b)

Figure3.2 Top view of TSTM (a) schematic illustration of the apparatus; (b) specimens right after casting and prior to testing

3.6 CHARACTERIZATION OF HYDRATION PRODUCTS USING THERMOGRAVIMETRIC ANALYSIS (TGA)

The phase changes in hardening cement paste can be monitored by using thermogravimetric analysis (TGA) through measuring the weight of a sample as it is being heated at a controlled rate in a Mettler TGA (model 851 LF) as shown in **Figure 3.3a**. A weight change of a sample within a specific temperature range identifies the presence of a particular chemical compound. The magnitude of the weight change indicates the amount of the compound in the sample.

In this study, TGA measures the weight loss of a powdered sample which is subjected to heating from 25 ^{o}C to 1000 ^{o}C at a heating rate of 10 ^{o}C/min in a flowing argon (Ar) atmosphere. A typical TGA sample weight versus temperature curve and DTGA (first derivative of the weight loss vs. temperature) curve is shown in **Figure 3.3b** for an OPC paste sample after 180 days of curing.

Thermogravimetric analysis was used to quantify the total chemically bound water or water held in various hydration products. To some extent various hydrate phases decompose (liberate their water) at different temperatures or over different temperature

ranges. Though these ranges overlap considerably, some distinctions can be made between calcium hydroxide (CH) and other hydrates which include the primary product of hydration, calcium silicate hydrate (C-S-H). Consequently, the degree of hydration and the extent of pozzolanic reactions could be determined, from which an explanation or relationship to autogenous shrinkage is expected to be established.

To compare on the same mass basis, these component quantities were normalized by the ignited weight of the sample denoted as per gram ignited cementitious.

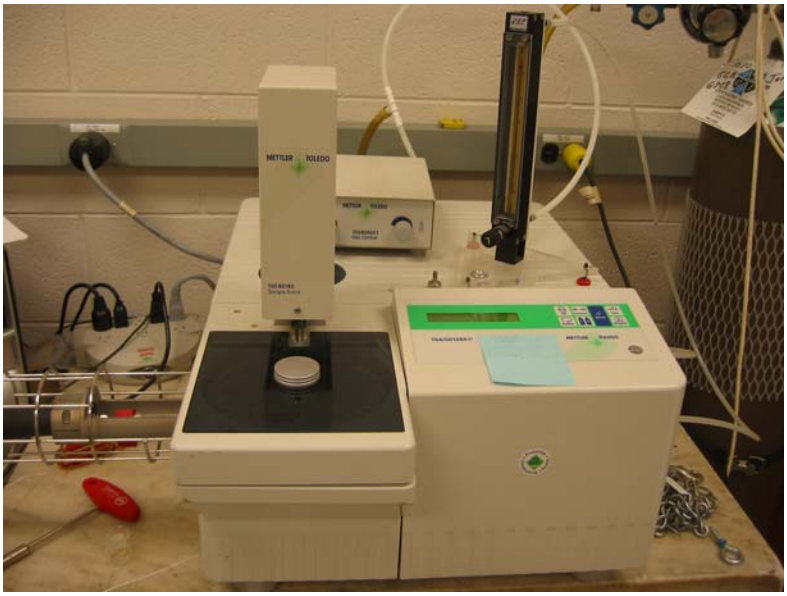

(a)

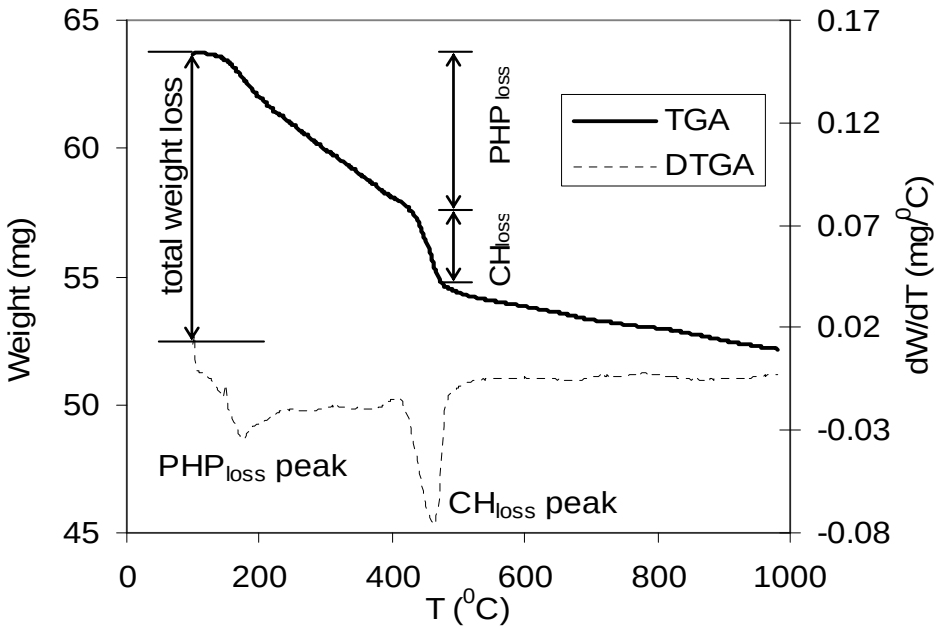

(b)

Figure 3.3 (a) Mettler TGA (model 851 LF); (b) typical TGA and DTGA curves for a cement paste sample after 180 days of hydration

3.6.1 Preparation of Samples

TGA analysis is performed on the cement paste samples at various ages. Two methods (traditional vs. improved) were used in preparing sample.

1. *Traditional method*: after mix, the paste was put in a mold and rotated in a roller until hardening to avoid segregation. The samples are then cured in lime-saturated water until the desired age that a slice of paste sample was cut and then soaked in methanol to stop hydration and prevent carbonation. The methanol soak is continued for at least one week prior to testing. The samples are then ground into a powder, and placed directly into the thermal analyzer for testing. This method was used for OPC paste and OPC paste containing GGBFS.
2. *Improved method*: after mix, the paste sample was cured sealed. Some small pieces were taken carefully at desired ages for testing after being ground into a powder. This method was used for white cement paste measurements.

The improved method is ideal for comparison between TGA analysis and autogenous deformation tests for the degree of hydration and the progress of hydration

products, as they have similar sealed curing conditions. In addition, the improved method reduces the chances of exposure sample to air, and consequently reduces the amount of carbonation. Carbonation is not a hydration reaction. It occurs rapidly when hydrated paste samples are exposed to air.

The ages of testing were 0.25, 0.5, 1, 2, 3, 7, 14, 28, and 180–210 days. The weight of the examined samples ranged from 50 to 100 milligram.

3.6.2 Chemically Bound Water

There are two forms of water in hydrated cement pastes: physically and chemically bound. The physically bound water (or free evaporable water) is not associated with hydration reactions. It is found in the capillary and gel pore spaces, and can be evaporated or boiled off at or below 100^{o}C. The chemically bound water or nonevaporable water, w_n, is the weight loss due to decomposition of the cement paste between about 105 ^{o}C and 1000 ^{o}C less the weight loss contributed by the decomposition of carbonation products (CO_{loss}) which occurs in the temperature range of approximately 600 to 800 ^{o}C [Mackenzie 1970]. Carbonation is not a hydration reaction and should be subtracted from the total weight loss. The carbonation may not be present if care has been taken to prevent carbonation.

The chemically bound water is calculated as:

$$w_n = \left[\frac{w_{105} - w_{1000} + CO_{loss}}{w_{1000} + CO_{loss}} \right] \qquad \text{Eq. 3.1}$$

where,

w_{105} = sample mass at 105^{o}C

w_{1000} = sample mass at 1000^{o}C

CO_{loss} = mass loss due to decomposition of carbonation products

As the chemically bound water is produced by the hydration reactions, it can be used to determine degree of hydration for portland cement. However, in blended system with SCM, w_n is only an indicator of hydration levels as hydration in such systems is rather complex [Pane and Hansen 2005].

For OPC paste, degree of hydration is then calculated as:

$$\alpha = \frac{w_n}{w_{n-ult}} \qquad \text{Eq. 3.2}$$

where,

α = degree of hydration (fraction)

w_{n-ult} = ultimate value of chemically bound water content (fraction)

According to Neville [1996], w_{n-ult}, can vary from as low as 0.18 to as high as 0.25 for different cement types. The degree of hydration or w_{n-ult} is allowed to reach the higher values in a mix with high *w/cm* ratio [Neville 1996]. While for low *w/cm*=0.35, hydration is hindered by the limitation of capillary space where hydration products are generated. Once these spaces have been filled by the hydration products, hydration process will stop. And thus, w_{n-ult} is determined from cement paste with *w/cm*=0.45 in this study. Temperature is another important factor that affects w_{n-ult}. Low curing temperature results in high w_{n-ult} values. To take the temperature effect into account, the relationship between w_{n-ult} and temperature is adopted from the research by Pane and Hansen [2005]. The value of w_{n-ult} taken at 5 ^{0}C was used for determining the degree of hydration.

3.6.3 Calcium Hydroxide (CH)

Thermogravimetric analysis has been widely accepted as an accurate method for the determination of crystalline calcium hydroxide (CH) content [Midgley 1979]. For OPC pastes, the content of CH increases as the hydration proceeds indicating a proportional relation with the degree of hydration or w_n. CH is also known to react with water and pozzolans such as GGBFS. In blended cement paste containing GGBFS, CH content is not only dependent upon how much portland cement has reacted but also upon the extent of pozzolanic reaction of the GGBFS. Therefore, CH content may initially increase then drop as it is consumed more and more by pozzolanic reactions [Shi 1998]. Thus the extent of pozzolanic reactions can be monitored through the variation of CH.

Calcium hydroxide is mostly crystalline and non-porous, and it decomposes between about 400 and 500 ^{o}C. Therefore, the DTGA peak as shown in **Figure 3.3b** is

more narrow and well-defined. Weight loss between 400 and 500 ^{o}C will be referred to as the "calcium hydroxide loss (CH_{loss}).

Though only weight loss from the decomposition of CH is measured, it is shown that this weight loss is very close to the amount of water in CH and therefore proportional to the amount of CH [Midgley 1979]. The weight loss due to chemically bound water in other products during this temperature range should be corrected as well. However, it has been found that the influence of other chemically bound water is insignificant to the measured CH loss [Midgley 1979]. And thus the correction was not conducted.

3.6.4 Calcium Silicate Hydrate (C-S-H)

As demonstrated in **Figure 3.3b**, the presence of mass loss between 105 ^{o}C and 400 ^{o}C includes the loss of water associated with the amorphous and porous hydration products the majority of which is the C-S-H gel [Melo Neto et al. 2008]. Weight loss computed over this temperature range will thus be referred to as the "porous hydration products loss (PHP_{loss})."

Since C-S-H is very difficult to measure directly due to both a lack of crystallinity and an indefinite composition, the weight loss between 100^{0}C and 500^{0}C can be treated due to the decomposition of C-S-H. Though this is not the most accurate method of calculating the C-S-H content for these samples, it was acceptable for our purposes.

By knowing the water held in the various hydrates or hydrate groups, the development of these hydration products, which are of special interest, can be monitored and related to the physico-mechanical properties including autogenous shrinkage.

3.7 STRENGTH AND YOUNG'S MODULUS TESTS

The compressive strength, split tensile strength and Young's modulus were measured according to ASTM C39, ASTM C496, and ASTM C469, respectively, on three 100 × 200 mm (4 x 8 in.) concrete cylinders for each mix. The specimens were demolded after 1 day of sealed curing in the environmental chamber and then water cured until about 1 hour prior to testing. The specimens were capped with a sulfur capping compound to achieve flat surfaces for testing. For elastic Young's modulus test, the axial deformation was measured using two extensometers which were mounted on the specimens and the gage length is 100 mm (3.9 in.). The standard deviation of all tests

meets ASTM C39, ASTM C496, and ASTM C469, respectively, and is less than 7%. The testing was conducted for concrete samples at 1, 3, 7, 28, and 56-90 days. The average results of three cylinders are reported.

3.8 FINITE ELEMENT ANALYSIS TOOL-MLS

The structural response of a concrete element to moisture and temperature changes in the hydrating cementitious materials can be modeled numerically with finite element (FE) programs. These programs make it possible to take into account thermal, hygral and chemical effects occurring at the material level to establish the resulting deformations and crack formation at structural level.

In this work, finite element (FE) analysis using MLS (multi layer system) [MLS 2003] was conducted to evaluate the changes of relative humidity across concrete cross section due to internal and/or external drying and the corresponding slab responses. A new experimental program was presented to first calibrate the predictions from MLS.

MLS (multi layer system) is a module of the 2-D FE package named FEMMASSE, capable of computing the physical (temperature, hydration, and pore humidity) and mechanical behavior (tensile and compressive stresses, displacement, and evolution of the crack width) of hardening concrete and taking varying environmental conditions into account. The preprocessor in MLS gathers the input data for the computation, provides a user-friendly interface to draw objects, such as concrete slabs and cooling pipes, defines how temperature varies at the boundaries of the drawn structures. The possibility to include reinforcement, cooling circuits and interfaces between different materials makes the program particularly suitable to deal with the building practice. **Figure 3.4** shows an example for modeling temperature and stress development in a hardening concrete structure with thermal and autogenous shrinkage being considered in the simulation.

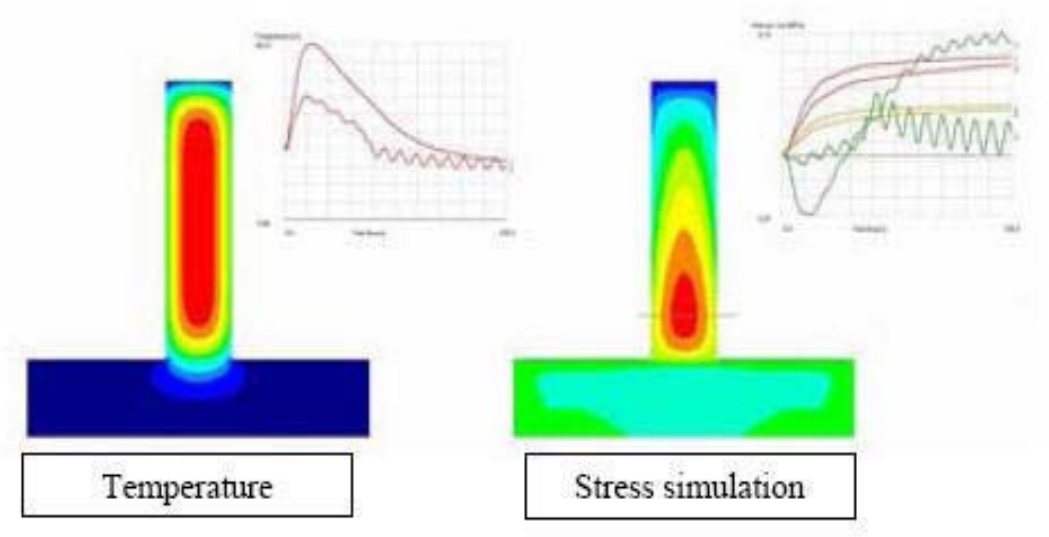

Figure 3.4 Temperature and stress contour in a concrete member simulated by using MLS [2003]

3.9 CONCLUSIONS

In this chapter, the materials, mix proportioning, and the experimental approaches used in this work were discussed in detail. Attention to the measurement of autogenous deformation, restrained stress, and thermogravimetric analysis will eventually lead to a better understanding of the underlying mechanisms and the prediction of behavior. Techniques described for estimating the amount of hydration products in cement paste can be used to evaluate the changes of hydrated compounds and microstructure due to the evolution of hydration.

CHAPTER 4

AUTOGENOUS DEFORMATION AND THERMOGRAVIMETRIC ANALYSIS OF CEMENT PASTE

4.1 INTRODUCTION

Autogenous deformations of hydrating cement paste are influenced by many parameters [Powers 1947, Tazawa 1995, Jensen and Hansen 2001, Holt 2002, Lura 2003]. Most of the recent investigations have been focused on experimental verification the influence of the various parameters such as cement compositions, cement fineness, *w/cm* ratios, supplementary cementitious materials (SCM), and exposure temperature. However, few efforts were done to explain autogenous shrinkage in hydrating cement paste with emphasis on the evolution of microstructures and hydration products.

The influence of *w/cm*, cement type and the addition of supplementary cementitious materials: ground granulated blast-furnace slag (GGBFS) on paste deformation under sealed-cured conditions is experimentally investigated in this chapter. These autogenous shrinkage results along with thermogravimetric analysis lay a solid foundation for better understanding the mechanism of autogenous shrinkage from the hydration product point of view. The major hydrate that controls autogenous shrinkage and the contribution of pozzolanic reactions to autogenous shrinkage in a blended system have been identified and characterized.

4.2 AUTOGENOUS SHRINKAGE AS A RESULT OF SELF-DESICCATION DUE TO CEMENT HYDRATION

4.2.1 Effect of Water-cementitious Ratio

Cement hydration results in the reduction in the relative humidity within the pores of the solid cement paste, known as self-desiccation. Self-desiccation is the driving forces of autogenous shrinkage as the reduction of pore humidity will produce net compressive capillary stresses which cause a measurable physical shrinkage of the material, so-called autogenous shrinkage [Bentz et al. 1998].

Figure 4.1 shows the measured autogenous shrinkage of a neat portland cement pastes at *w/cm* ratios ranging from 0.35 to 0.45. Autogenous shrinkage increases with decreasing *w/cm*. Significantly higher shrinkage is observed for a *w/cm*=0.35 paste suggesting a threshold between 0.40 and 0.35 for neat OPC wherein aggressive self-desiccation is intensified.

This observation agrees with the predicted pore humidity using MLS software that there is more reduction of pore humidity over time for *w/cm*=0.35 paste as shown in **Figure 4.2a**. The predicted pore humidity of *w/cm*=0.45 can drop to 88% after 28 days of sealed curing. The pore humidity of *w/cm*=0.35 paste, however, reaches 77% after 28 days of sealed curing, which is close to the thermodynamic limitation of self-desiccation of 75% wherein cement hydration is hampered. This predicted value is consistent with the measured pore humidity by Baroghel-Bouny and Mounanga [2005].

The lower the pore humidity the less will be the amount of free capillary water held in cement paste. And thus, at low pore humidity the amount of anhydrous cement particles which are exposed to water and the space available for hydration products are reduced [Jensen 1995]. As the hydration products can be produced only in water-filled space, a minimum size of the water-filled space is required. According to the experimental data provided by Jensen [1995], cement hydration is generally hampered at lower pore humidity but remarkably detained at pore humidity lower than 75%. The hampered cement hydration for *w/cm*=0.35 cement paste can be seen from **Figure 4.2b** that the chemically bound water w_b is lowest for *w/cm*=0.35 paste and started to level off after 28 days of sealed curing.

Autogenous shrinkage is pronounced at early ages (for the first 7 days) in paste systems. This suggests that autogenous shrinkage is responsible for a significant amount of the total shrinkage and may be a major cause of early age cracking, especially for low *w/cm* concretes. The lower the *w/cm*, the faster and earlier the autogenous shrinkage develops in cement paste since the available capillary water is used up quickly in these systems.

There is expansion followed by shrinkage observed within the first day for cement paste with *w/cm*=0.4 and higher. The initial expansion is most likely due to the formation of the ettringite needles inside the still very weak solid skeleton of the cement paste [Roy and Idorn 1986, Bjontegaard 1999]. Another reason for the initial expansion may attribute to the reabsorption of the free water in the mixture. This expansion happens during the acceleration period of cement hydration when the demand for water increases due to the initial formation of calcium silicate hydrate (C–S–H). The formation of C-S-H drives free water, bleeding water, to the sites where self-desiccation is more intense. This movement of water generates an increase in the relative humidity of the pores, which reduces the capillary tension that causes shrinkage [Melo Neto et al. 2008]. Factors such as paste stiffness and water movement have a direct influence on the principal mechanisms of shrinkage.

Degree of hydration alone, as the cause of self-desiccation and consequently autogenous shrinkage, is found not directly proportional to autogenous shrinkage and cannot be used to normalize the effect of *w/cm*. This can be seen from **Figure 4.3a** wherein autogenous shrinkage differs even at the same degree of hydration. High *w/cm* paste shows lower autogenous shrinkage due to less intensive self-desiccation as more free capillary water is available for hydration and capillary stress build-up is reduced or minimized by the presence of excess water.

Figure 4.3b, however, shows that there is a unique correlation between the autogenous shrinkage and the pore humidity for sealed-cured portland cement paste regardless of the different *w/cm* rations. This strong correlation demonstrates that the reduction of pore humidity or self-desiccation is the underlying driving force of

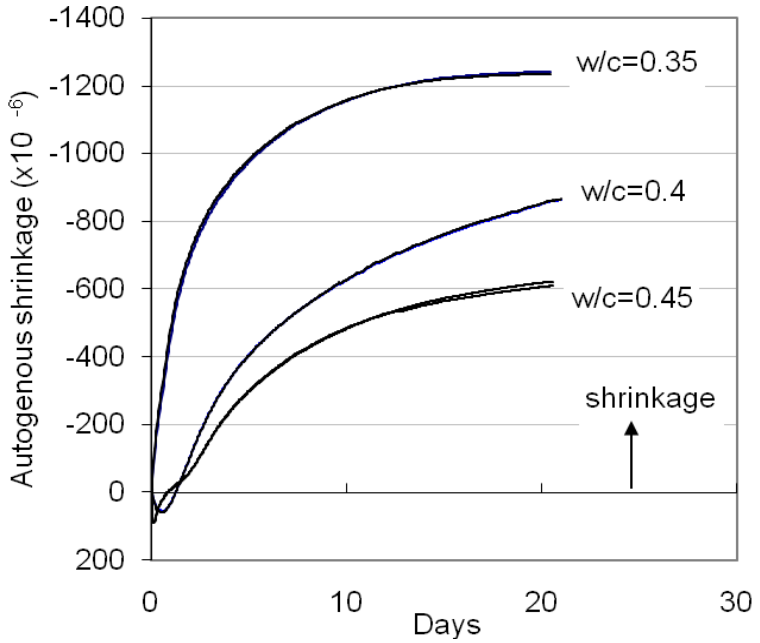

(a)

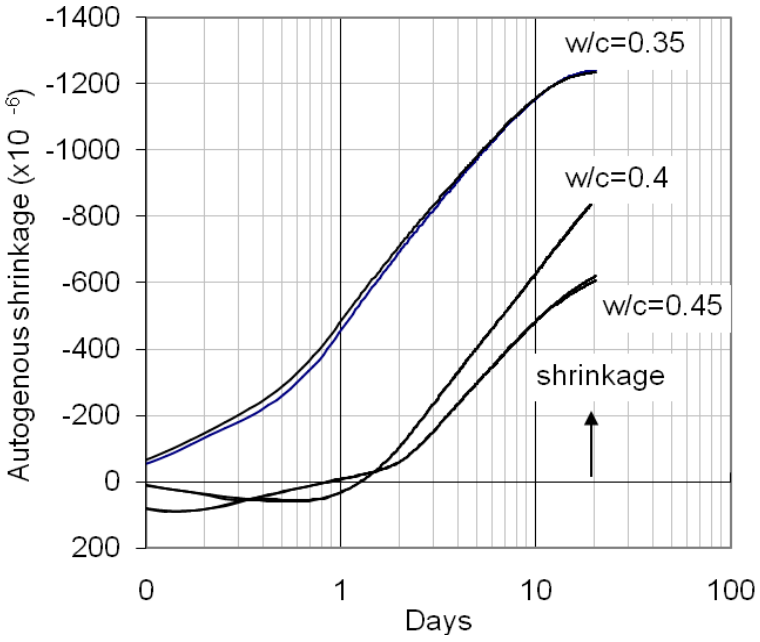

(b)

Figure 4.1 Measured autogenous shrinkage of OPC paste at three *w/cm* ratios (a) linear time scale; (b) logarithmic time scale

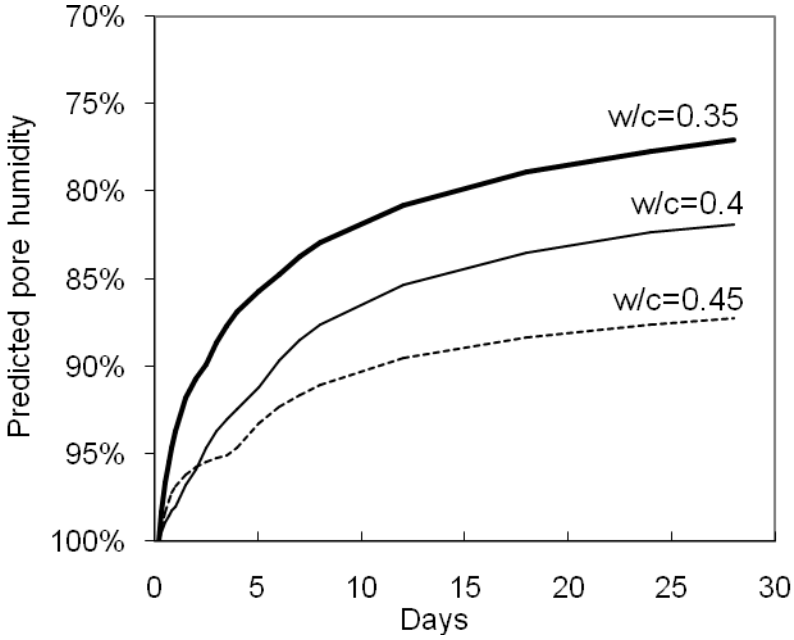

(a)

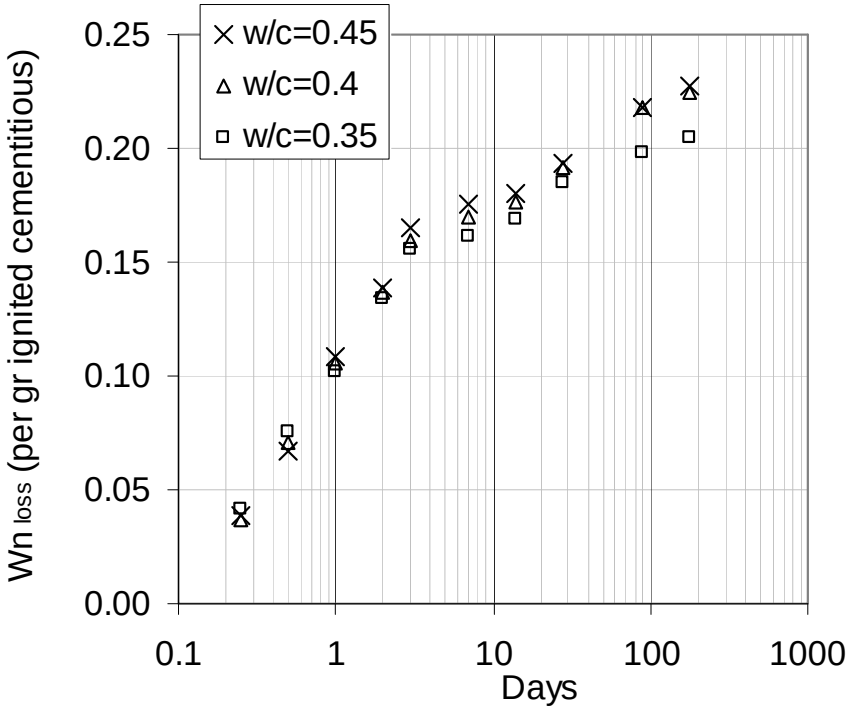

(b)

Figure 4.2 (a) MLS predicted reduction of pore humidity in the sealed-cured OPC paste at three *w/cm* ratios; (b) measured development of chemically bound water in OPC paste at three *w/cm* ratios

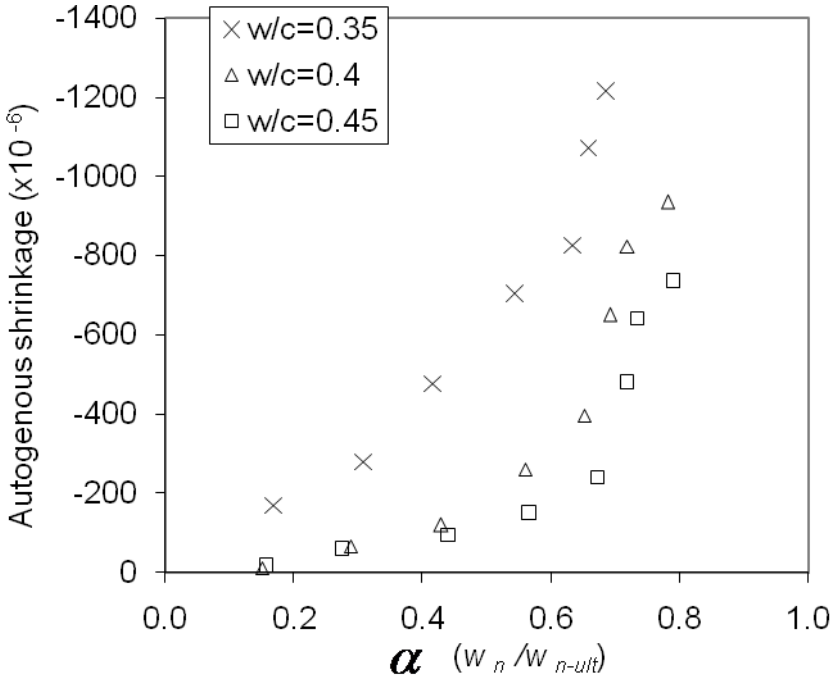

(a)

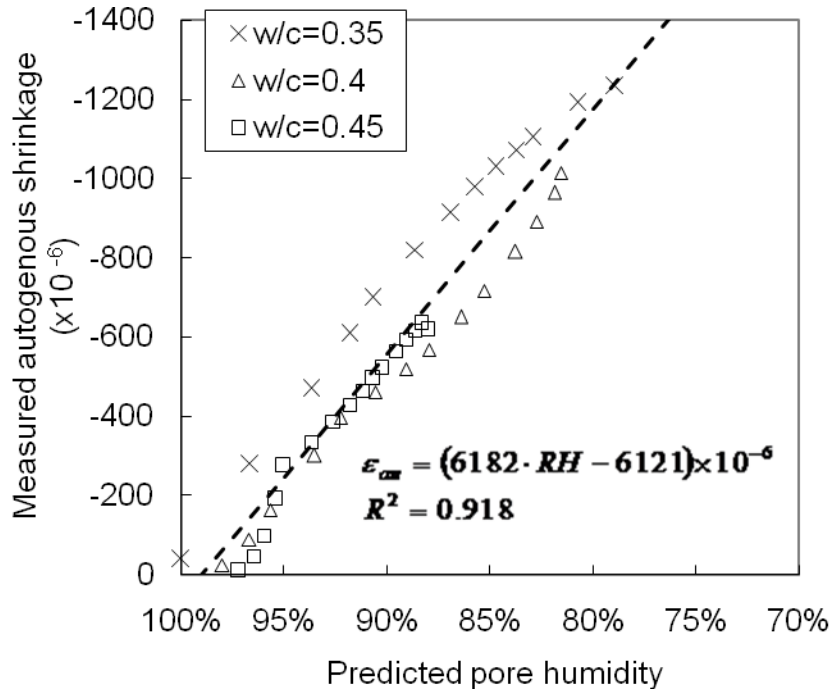

(b)

Figure 4.3 Relationship between measured autogenous shrinkage and (a) degree of hydration; (b) MLS predicted pore humidity of OPC paste

autogenous shrinkage. The effect of chemical shrinkage on autogenous shrinkage is thus prominent only before setting time. After final set, autogenous shrinkage is exclusively the result of the self-desiccation process [Wei et al. 2008]. This is also true at the concrete level. Jonasson et al. [1998] reported the similar linear relationship between measured pore humidity and autogenous shrinkage for concrete mixtures (**Figure 4.4**).

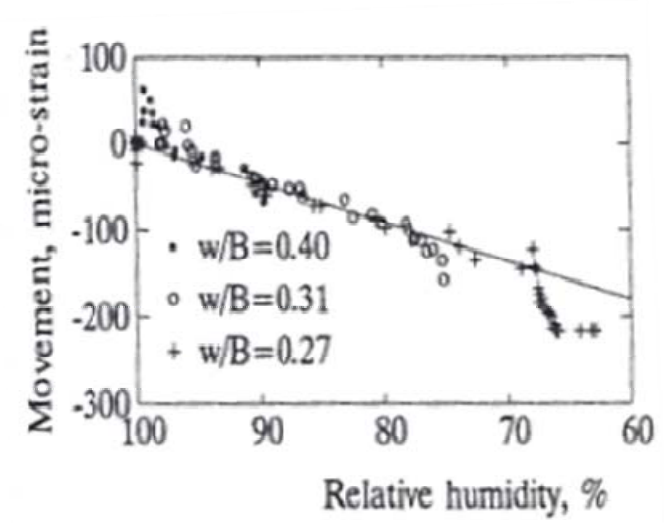

Figure 4.4 Measured internal (pore) humidity and the associated autogenous shrinkage for three concrete mixes [Jonasson et al. 1998]

4.2.2 Effect of Cement Chemical Compositions

Autogenous shrinkage of cement paste is strongly dependent on cement chemical compositions. The comparison of OPC paste and white cement paste is made in this work.

Autogenous shrinkage of white cement paste is shown in **Figure 4.5**. It can be seen from **Figure 4.1** and **Figure 4.5** that OPC paste develops greater autogenous shrinkage than white cement paste at the same *w/cm*. This may be related to the contents of C_3A and C_4AF in cement. As shown in **Table 3.1** in Chapter 3, portland cement contains higher amount of C_3A and C_4AF and less amount of C_3S than white cement. Tazawa and Miyazawa [1995] have pointed out that autogenous shrinkage of paste depends to a large degree on the hydration of C_3A and C_4AF and increases as their contents increase, because the hydration of aluminate and ferroaluminate consumes more water at an early stage and hence self-desiccation increases at this stage. This causes a

faster development of autogenous shrinkage within the first three to five days as illustrated in **Figure 4.1** [Beltzung and Wittmann 2002].

While a dormant period, when autogenous shrinkage is hardly developing, is observed in white cement paste due to a lack of trigger from the hydration of aluminate and ferroaluminate. The higher the *w/cm* ratio, the longer the dormant period will be. This is because there is less intense relative humidity reduction in high *w/cm* paste. As shown in **Figure 4.5** for *w/cm*=0.45, autogenous shrinkage will not develop until after 7 days.

On the other hand, there is more expansion found in portland cement paste than the white cement paste. This may attribute to the greater amount of C_3A and C_4AF contained in portland cement as well. The hydration of C_3A and C_4AF was found to result ettringite formation and consequently expansion in the presence of gypsum [Beaudoin et al. 1991, 1992, Tazawa and Miyazawa 1995].

A formula (Eq. 4.1) proposed by [Tazawa and Miyazawa1995] further demonstrates that the chemical components of C_3A and C_4AF are of significance in terms of autogenous shrinkage of cement paste. Eq. 4.1 was obtained through multiple regressions of the compositions with the autogenous shrinkage measured from different types of cements at different ages, and can be used for calculating autogenous shrinkage of cement paste from its chemical compositions:

$$\varepsilon(t) = 0.012 \cdot \alpha_{C_3S(t)} \cdot (\%C_3S) + 0.070 \cdot \alpha_{C_2S(t)} \cdot (\%C_2S) - 2.256 \cdot \alpha_{C_3A(t)} \cdot (\%C_3A) - 0.859 \cdot \alpha_{C_4AF(t)} \cdot (\%C_4AF) \quad \text{Eq. 4.1}$$

where,

$\varepsilon(t)$ = autogenous shrinkage of cement paste at age t

α = degree of hydration of each component at age t

% = content of each component by mass

As shown in Eq. 4.1 that the coefficient for C_3A and C_4AF is greater than C_3S and C_2S indicating greater contribution from C_3A and C_4AF to the autogenous shrinkage. The minus sign represents expansion. By just looking at Eq. 4.1, it may be concluded that the more the C_3A and C_4AF contents, the less the autogenous shrinkage will be. However, it is not the case as can be seen from the measured autogenous shrinkage that portland cement paste contains more C_3A and C_4AF but develops greater autogenous shrinkage,

because besides chemical compositions there is another driving force known as self-desiccation which affects autogenous shrinkage the most. All these factors work together resulting autogenous shrinkage.

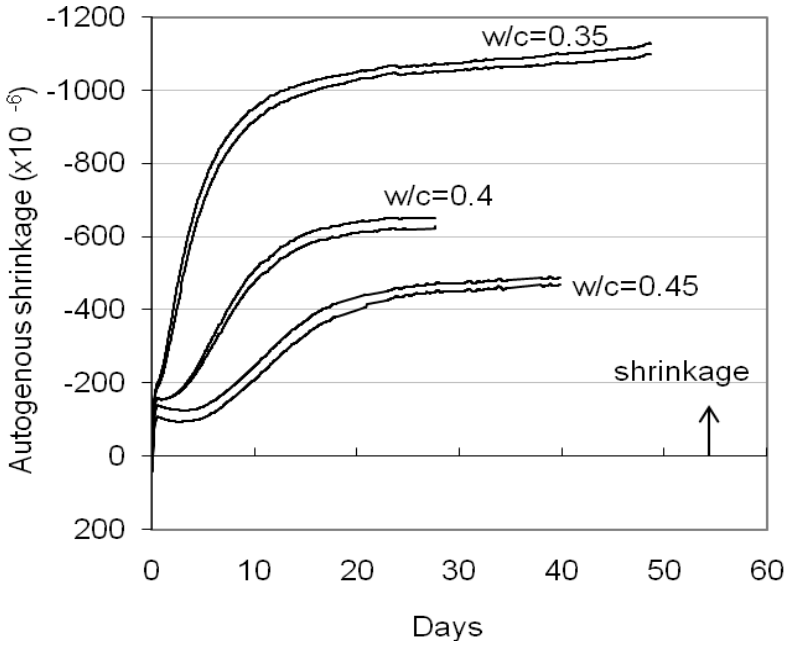

(a)

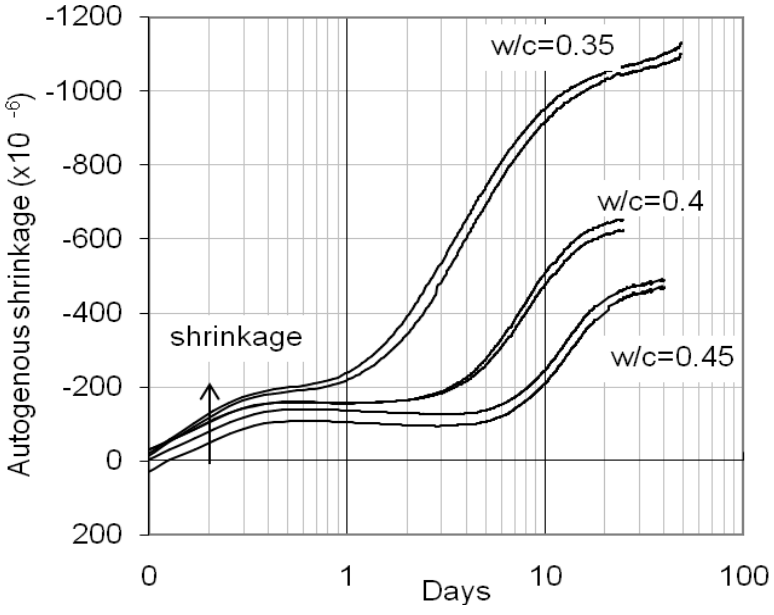

(b)

Figure 4.5 Measured autogenous shrinkage of white cement paste at three *w/cm* ratios (a) linear time scale; (b) logarithmic time scale

4.3 AUTOGENOUS SHRINKAGE OF PASTE BLENDED WITH GGBFS

4.3.1 Experimental Results

For the influence of GGBFS on autogenous shrinkage, much of the literature has indicated that cement paste blended with GGBFS has greater autogenous shrinkage to some degree than the neat portland cement paste [Tazawa and Miyazawa 1995, Hanehara et al. 1999, Lura 2003, Lee et al. 2006]. The reasons were generally attributed to the higher chemical shrinkage, the finer pore structure of the blended system, and the pozzolanic reactions that consume calcium hydroxide (CH) crystals and consequently induce shrinkage as a result of removal of shrinkage restraints in the paste. Unfortunately, there is a lack of agreement on the causes and the extent of the influence of GGBFS on the autogenous shrinkage.

In this study, the autogenous deformations for portland cement pastes containing GGBFS ranging from 0% to 50% of the total cementitious material by weight were measured and plotted in **Figure 4.6** on both linear and logarithmic time scales for mixes having *w/cm*=0.35. These experimental results show that, the addition of GGBFS affects the development of autogenous shrinkage. A direct interpretation from **Figure 4.6** suggests that GGBFS will cause less autogenous shrinkage at earlier ages and there is a continuous growth in autogenous shrinkage found in the blended systems at later ages. This finding agrees with the previous research by Roy and Idorn [1986], Jensen and Hansen [1995] shows that the pozzolanic reaction and the related shrinkage can proceed steadily at later ages, and also at reduced internal relative humidity for years.

Initial expansion is found within the first day for both 30% and 50% GGBFS systems unlike the portland cement paste which exhibits immediate shrinkage. This may be attributed to the dilution effect in a blended system wherein more free water is available for portland cement hydration prior to the onset of significant GGBFS reaction, effectively producing a higher *w/cm* ratio on a pozzolan-free basis.

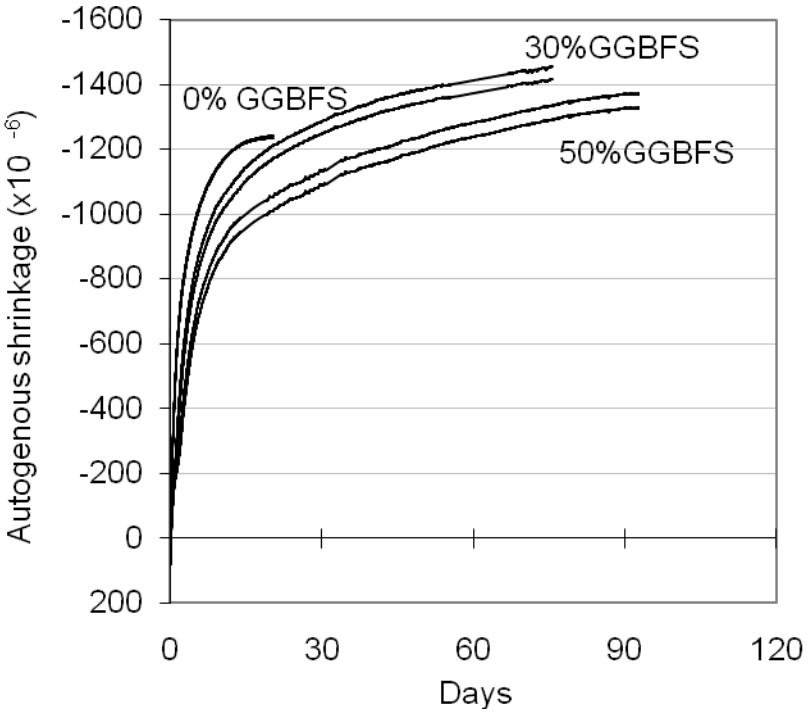

(a)

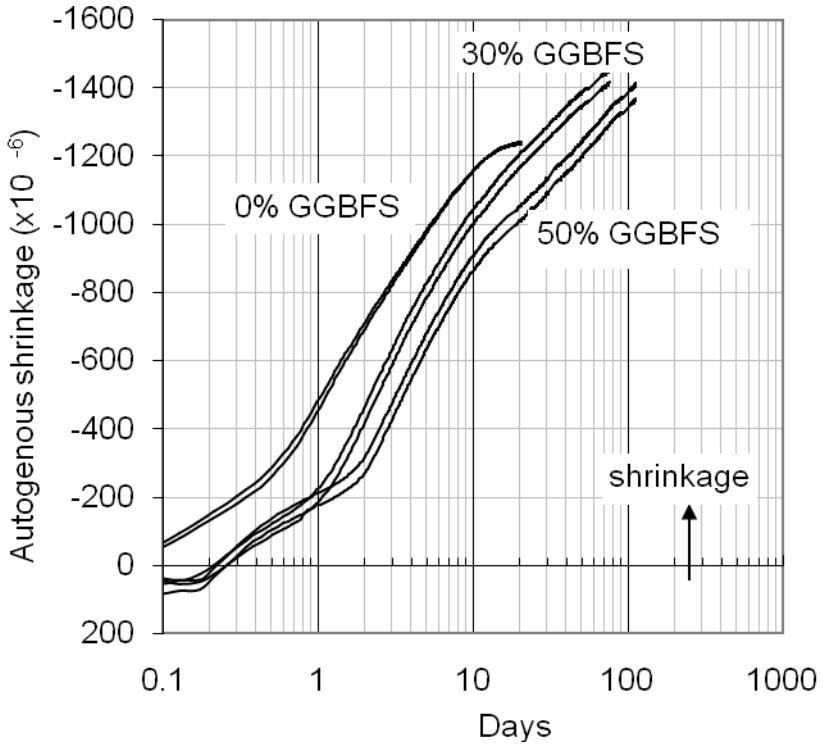

(b)

Figure 4.6 Measured autogenous shrinkage of paste blended with GGBFS, *w/cm*=0.35 (a) linear time scale; (b) logarithmic time scale

4.3.2 Thermogravimetric Analysis

Since there is a lack of agreement on the causes and the extent of influence of the GGBFS on the autogenous shrinkage, an effort has been made to combine the experimental autogenous shrinkage results with the thermogravimetric analysis for the same systems to provide information for better understanding the underlying mechanism of autogenous shrinkage.

Hydration products of cement pastes are investigated using thermogravimetric analysis and differential thermogravimetric analysis (TGA/DTGA) to identify the water held in different hydration products such as porous hydration products (PHP) the majority of which is the C-S-H gel, calcium hydroxide (CH), and the total chemically bound water w_n. By knowing the water held in the various hydrates or hydrate groups, the development of these hydration products, which are of special interest, can be monitored and related to the physico-mechanical properties such as autogenous shrinkage and compressive strength.

Figure 4.7 illustrates the DTGA curves measured at 1 day and 90 days for paste blended with GGBFS at *w/cm*=0.35. It can be seen that both the PHP_{loss} and CH_{loss} are increasing over time due to the progress of cement hydration. The PHP_{loss} of the blended systems with 30% and 50%GGBFS is initially less than and then exceeds the neat cement paste at the age of 90 days. This is due to the contribution from pozzolanic reaction that more C-S-H, which is the majority of PHP has been produced. Water loss from CH, on the other hand, is found less in the blended systems due to the less production of CH from OPC hydration and the consumption of crystalline CH from pozzolanic reaction.

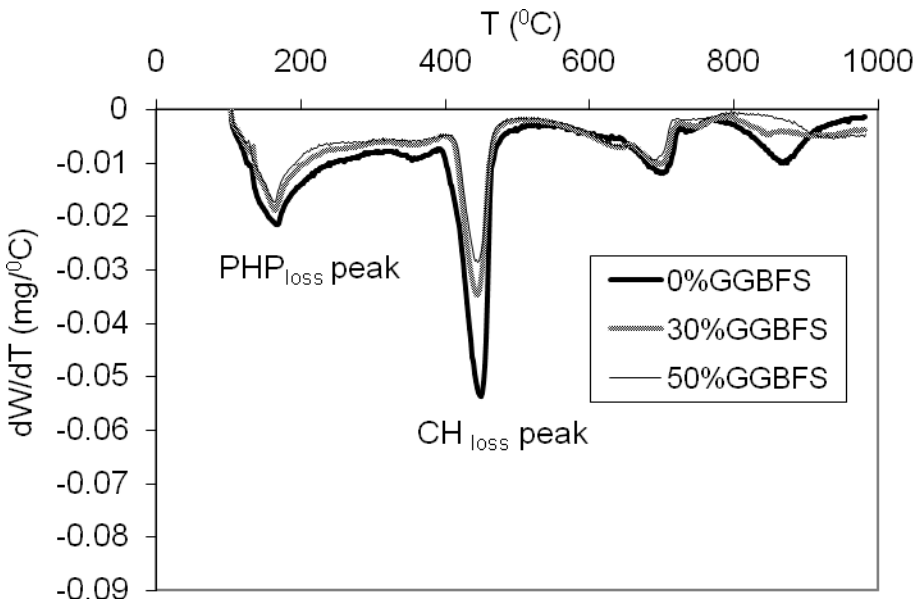

(a)

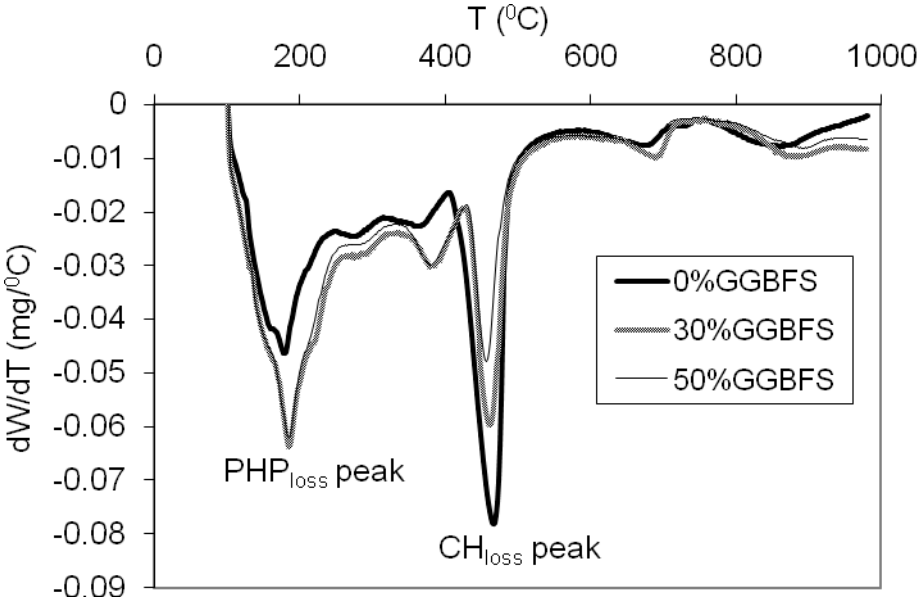

(b)

Figure 4.7 DTGA curves of blended paste with *w/cm*=0.35 at the age of (a) 1 day; (b) 90 days

The calculated PHP $_{loss}$, CH $_{loss}$, and $w_{n_{loss}}$ over time due to the evolution of hydration are plotted in **Figure 4.8** for different systems with *w/cm*=0.35. They are determined based on per gram of the ignited total cementitious materials.

The cement hydration is enhanced in the presence of the GGBFS. It can be seen from **Figure 4.8a** that PHP content (indicated by PHP $_{loss}$) in a blended cement paste exceeds the neat cement paste after about 1 to 2 days of hydration, indicating the beginning of pozzolanic reaction through which more PHP is produced. This is consistent with the research by Roy and Idorn [1982] on other supplementary cementitious materials such as fly ash that more combined water generates from the pozzolanic reaction than the hydrates normally produced through the reaction of pure cement. As one of the major hydration products, C-S-H or PHP is responsible for the development of many mechanical and physical properties such as strength, permeability and shrinkage [Neville 1996]. This provides justification for relating the hydration products to cement paste properties.

The amount of calcium hydroxide (CH) seems to be decreasing with the increasing replacement of GGBFS as demonstrated in **Figure 4.8b**. This is understandable as pozzolanic reaction consumes CH. In addition, the reduced content of portland cement which produces majority of CH in a blended system will cause less production of CH. The growth rate of CH becomes significantly slow after 1 to 2 days of hydration in a blended system, which tells the beginning of the pozzolanic reaction as well.

PHP $_{loss}$ and CH $_{loss}$ are the two major components of chemically bound water w_n. As shown in **Figure 4.8c**, w_n of systems blended with GGBFS is less than the neat portland cement paste at early age and it catches up at later age as a result of competing between the production of PHP and depletion of CH. The chemically bound water can be used to determine degree of hydration for neat cement paste. However, for the blended systems, w_n is only an indicator of hydration level.

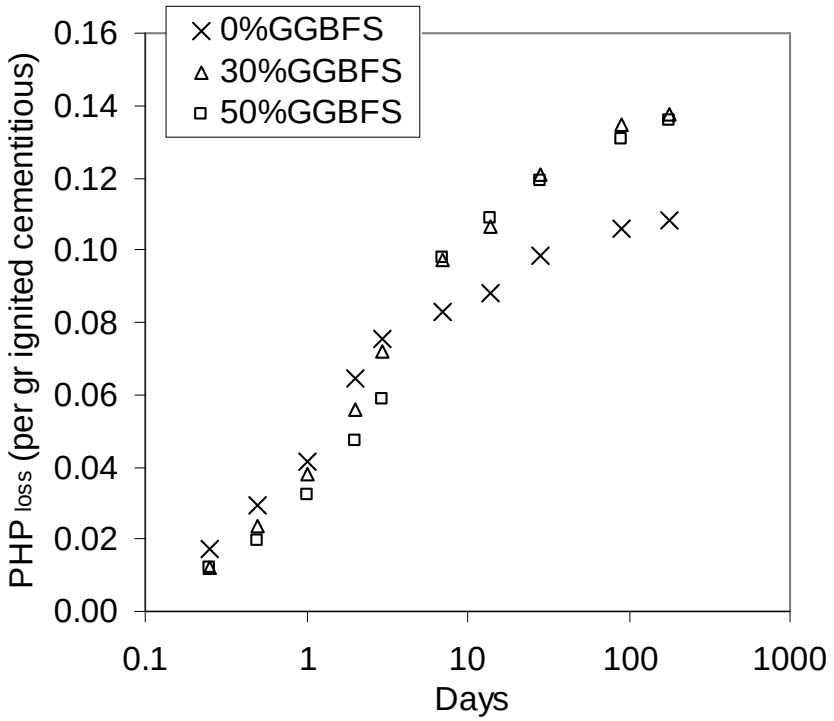
0%GGBFS
30%GGBFS
50%GGBFS
PHP loss (per gr ignited cementitious)
0.16
0.14
0.12
0.10
0.08
0.06
0.04
0.02
0.00
0.1
1
10
100
1000
Days

(a)

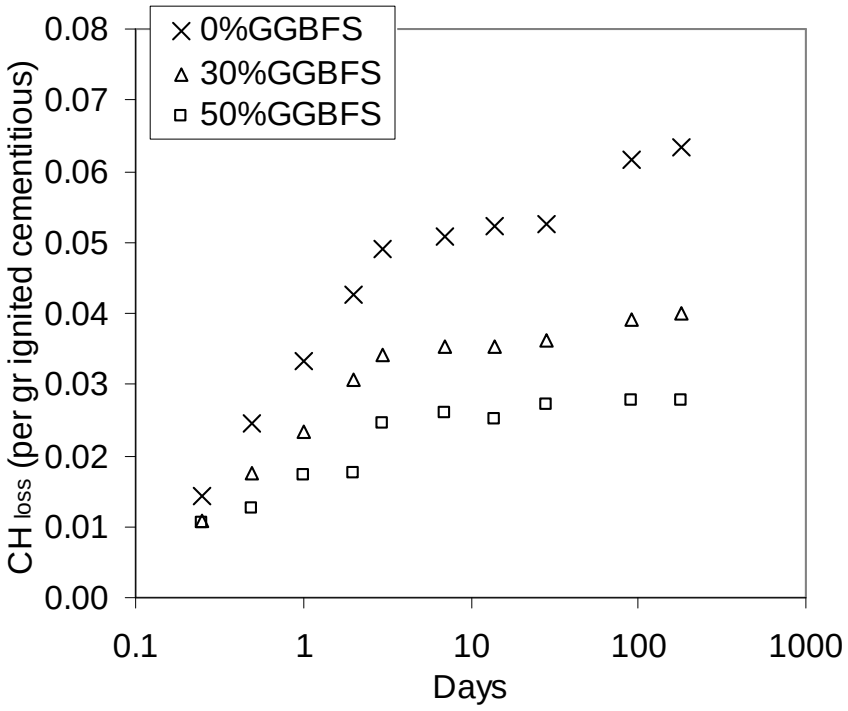
0%GGBFS
30%GGBFS
50%GGBFS
CH loss (per gr ignited cementitious)
0.08
0.07
0.06
0.05
0.04
0.03
0.02
0.01
0.00
0.1
1
10
100
1000
Days

(b)

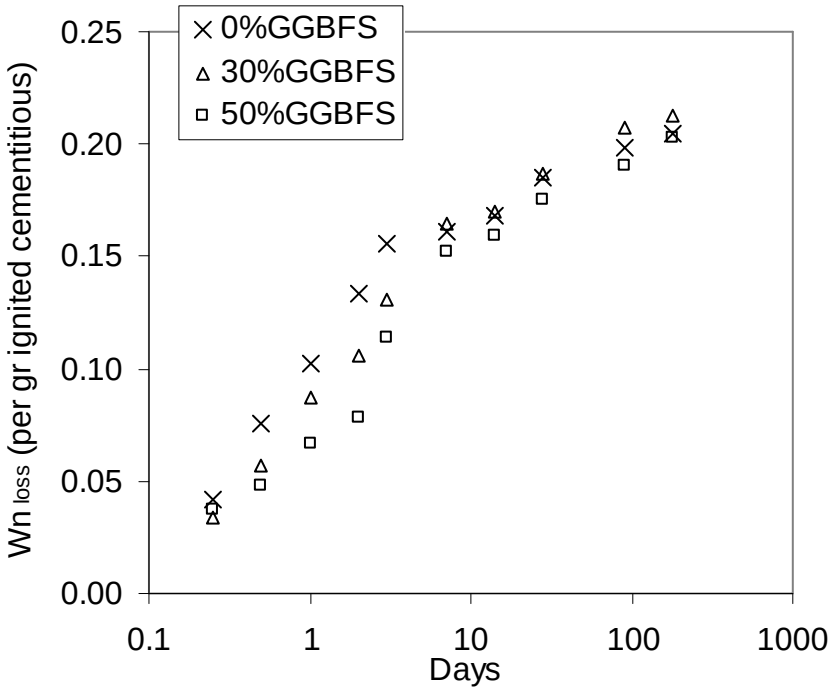

(c)

Figure 4.8 TGA results over time for paste blended with GGBFS at *w/cm*=0.35 (a) PHP_{loss}; (b) CH_{loss}; (c) Wn_{loss}

4.3.3 Quantifying Pozzolanic Contribution to Autogenous Shrinkage

The influence of GGBFS on the autogenous shrinkage can be evaluated using a new equation (Eq. 4.2) proposed in this work [Wei et al. 2008]. This equation quantifies the difference between the observed shrinkage and the expected shrinkage corrected for dilution (assuming no pozzolanic interaction):

$$\varepsilon_{au,P} = \varepsilon_{au,blended} - (100 - C_{SCM}\,\%)\cdot \varepsilon_{au,C} \qquad \text{Eq. 4.2}$$

where,

$\varepsilon_{au,P}$ = contribution from pozzolanic reaction,

$\varepsilon_{au,blended}$ = measured autogenous shrinkage of a blended system,

C_{SCM} = the SCM content by mass in a blended system (%), in this case the SCM is GGBFS,

$\varepsilon_{au,C}$ = measured autogenous shrinkage of a control mix, here it is OPC.

Equation 4.2 quantifies the incremental autogenous shrinkage for a system containing C% GGBFS when compared to the same system in which the C% of GGBFS is assumed not reactive. This concept more clearly illustrates the contribution from pozzolanic reaction than looking only at the total amount of autogenous shrinkage that has been developed in a blended system.

The contribution of pozzolanic reaction to the autogenous shrinkage can be seen from the hatched area shown in **Figure 4.9** for paste containing 30% and 50% GGBFS. This analysis demonstrates that the pozzolanic reaction accelerates autogenous shrinkage starting at around the age of two days when shrinkage curves of blended paste deviate from the scaled OPC curves. The contribution to autogenous shrinkage increases with time. This can also be seen from **Figure 4.10a** in which the contribution of GGBFS to the autogenous shrinkage is plotted versus time for both 30% and 50% GGBFS systems. The curves take off at around two days indicating the beginning of the pozzolanic contribution. High GGBFS content results in slightly greater contribution to autogenous shrinkage. At later ages, the contributed autogenous shrinkage from 50% GGBFS can account for 50% of the total shrinkage. Since pozzolanic reaction is the secondary reaction which follows the primary reaction of ordinary portland cement (OPC), the pozzolanic contributions were plotted vs. degree of hydration of OPC. As shown in **Figure 4.10b**, the start time of pozzolanic contribution was found to be at 50% to 60% degree of hydration of OPC.

This is consistent with the TGA results that the PHP_{loss} in a blended paste increases rapidly after 50% to 60% degree of hydration of OPC has been reached after two days of sealed curing as shown in **Figure 4.11a**. Pastes blended with GGBFS have the largest amount of PHP_{loss} at later ages. This explains the pronounced later-age autogenous shrinkage found in paste blended with GGBFS. The porous hydration products (PHP) such as C-S-H have substantial surface area, greater than 200 m^2/g, which is at least an order of magnitude greater than any other components in hardened portland cement paste [Roy and Idorn 1982]. This magnifies the effect of the capillary tension which is the driving force for the development of autogenous shrinkage. Though an increase in PHP results in a decrease in porosity, it appears that the increase in net surface area out weights the reduction in coarse capillary pore volume. The CH_{loss} in a

blended paste starts to level off after 50% to 60% of hydration of OPC due to the depletion from pozzolanic reaction (**Figure 4.11b**).

Hence, extent of hydration is found to normalize the effect of pozzolanic reaction, illustrating that for same *w/cm* ratios, all GGBFS content pastes behave the same with respect to extent of reaction (hydration). Thus, autogenous shrinkage and TGA results can be used to determine both time of initiation of pozzolanic reaction and its contribution to autogenous shrinkage.

In summary, pozzolanic reactions increase amount of porous hydration products at later stages of hydration and thus pronounced autogenous shrinkage. Though GGBFS may increase the later age autogenous shrinkage, it has been found to improve the later age compressive strength as well. As demonstrated in **Figure 4.12**, the development of compressive strength follows the same trend as autogenous shrinkage does.

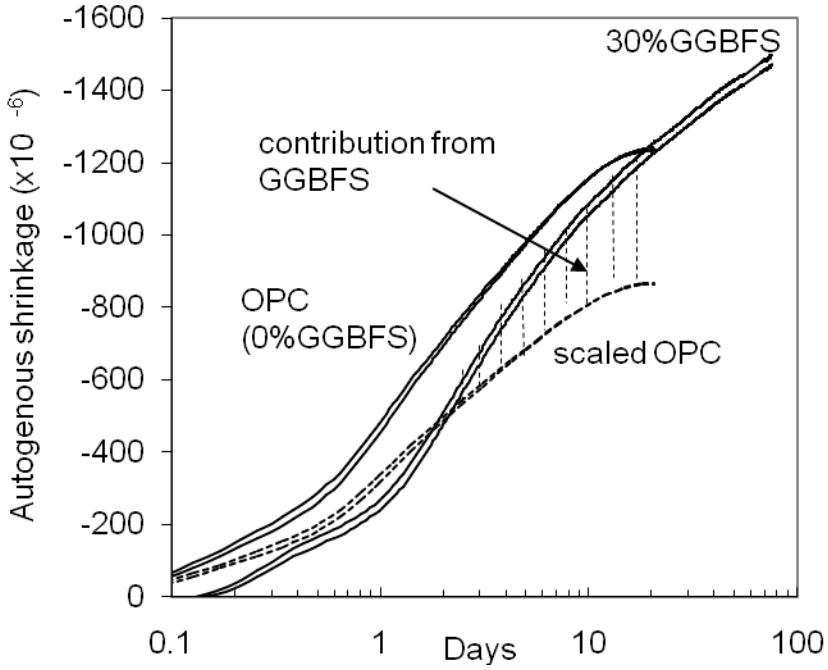

(a)

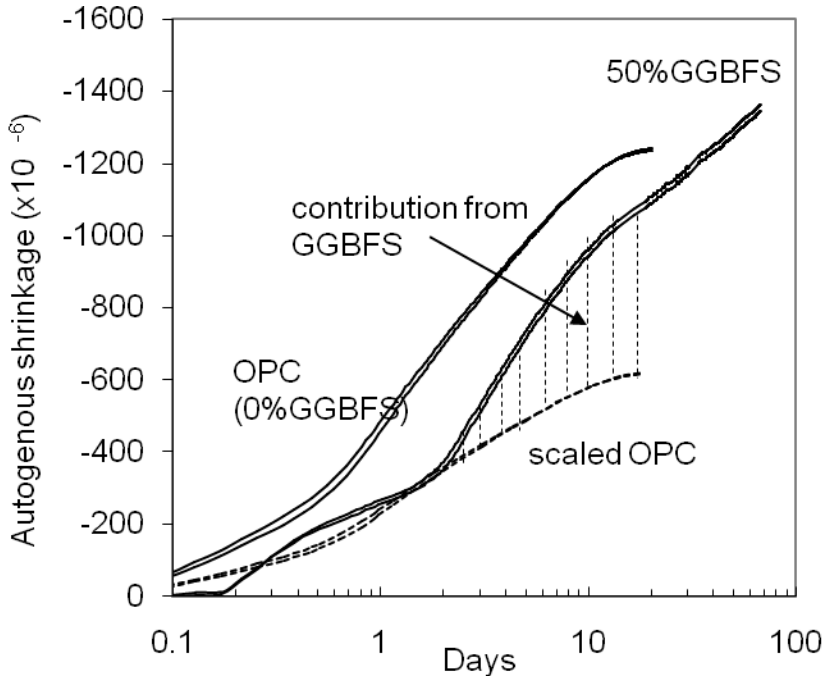

(b)

Figure 4.9 Normalization of pozzolanic contribution to autogenous shrinkage of blended cement paste, *w/cm*=0.35 (a) 30%GGBFS; (b) 50%GGBFS

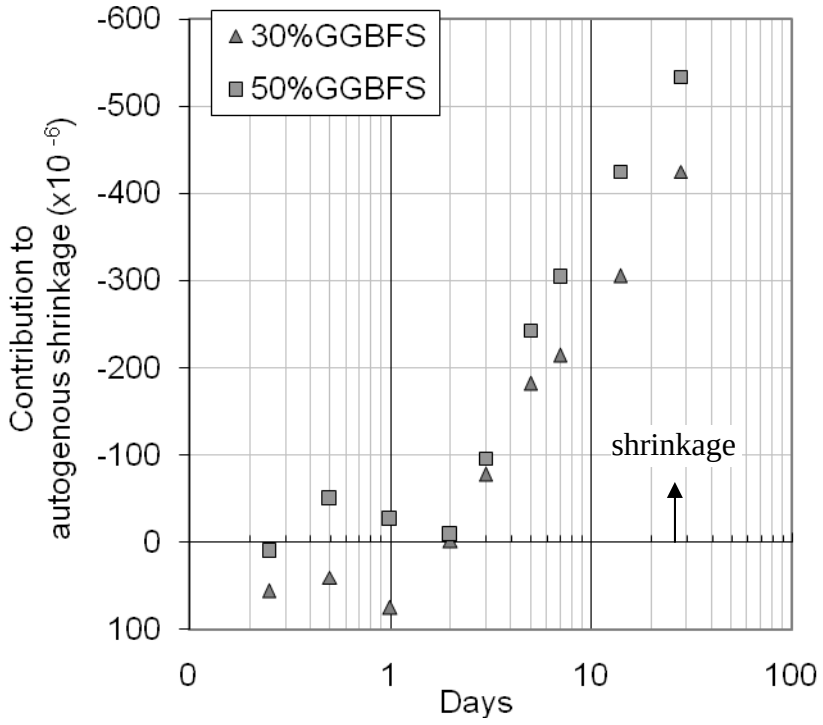

(a)

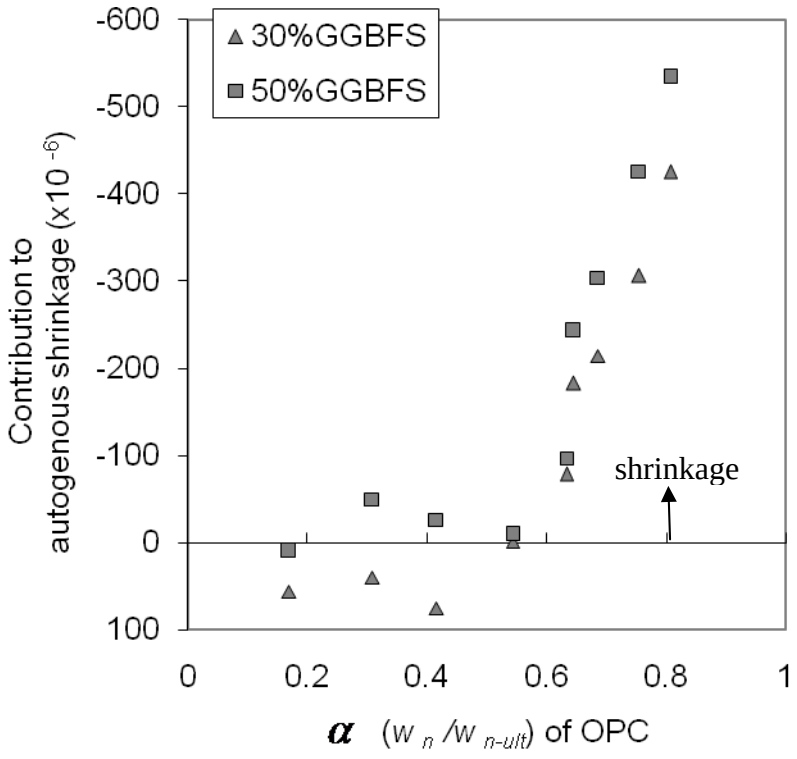

(b)

Figure 4.10 Contribution of pozzolanic reactions to autogenous shrinkage as a function of (a) time; (b) degree of hydration of OPC, *w/cm*=0.35

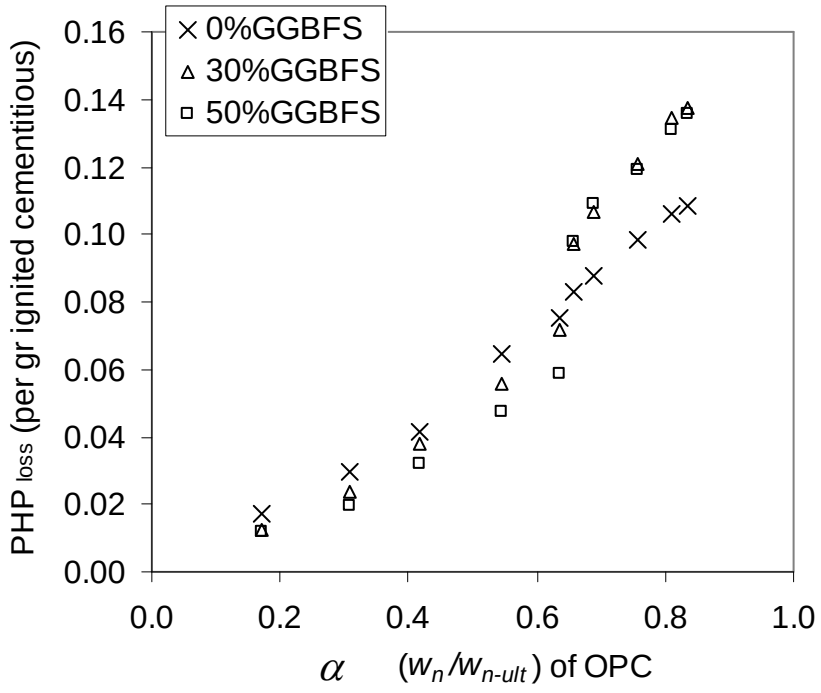

(a)

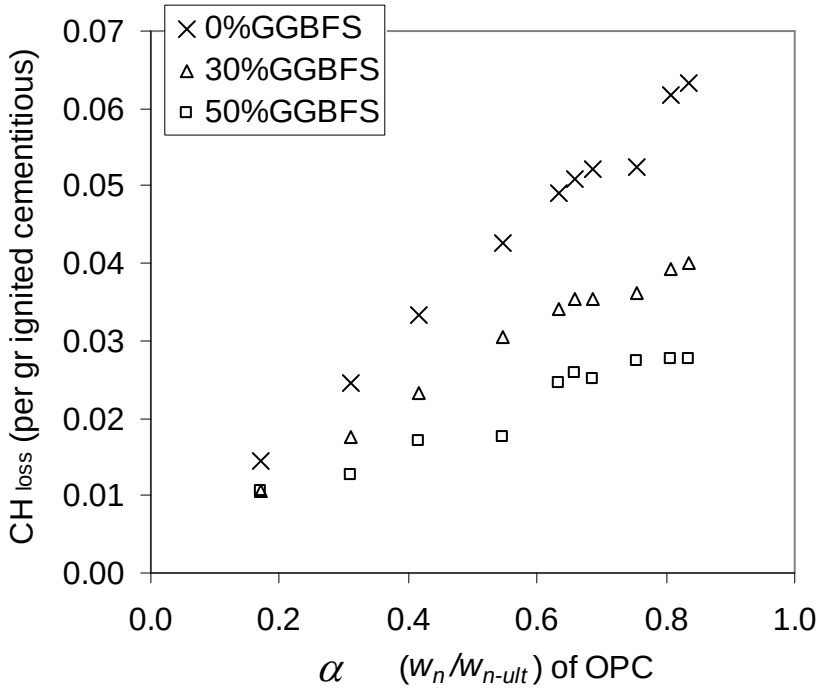

(b)

Figure 4.11 (a) PHP $_{loss}$ as a function of degree of hydration of OPC; (b) CH $_{loss}$ as a function of degree of hydration of OPC in a blended paste, *w/cm*= 0.35

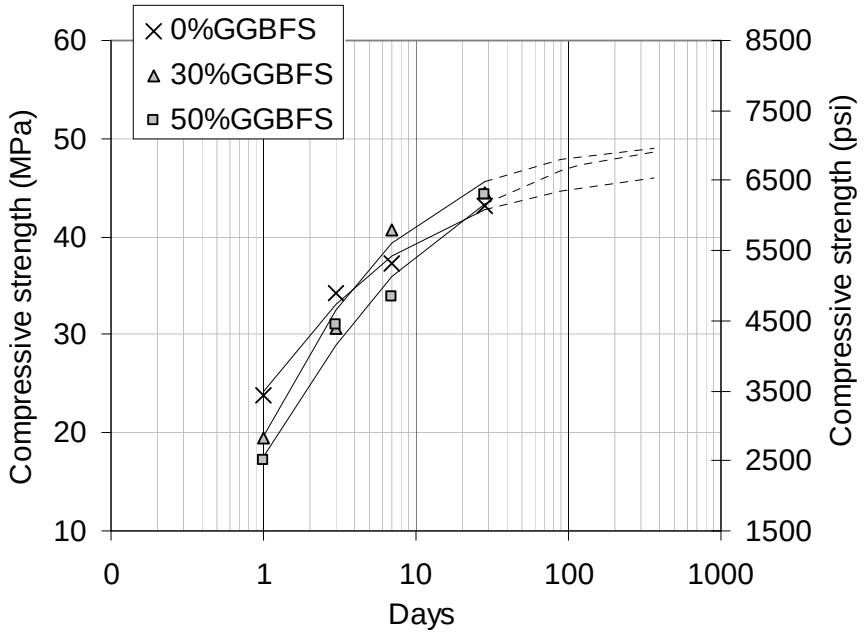

Figure 4.12 Compressive strength development of concrete blended with GGBFS, *w/cm*= 0.35

4.3.4 Primary Hydration Products Controlling Autogenous Shrinkage in a Blended System

It is found in this study that the amount of autogenous shrinkage of a system blended with GGBFS depends on the age and the GGBFS content. Much of the literature has indicated that cement paste blended with GGBFS has greater autogenous shrinkage to some degree than neat cement paste [Tazawa and Miyazawa 1995, Hanehara et al. 1999, Lura 2003, Lee et al. 2006]. One of the explanations cited suggests that the pozzolanic reaction, which consumes calcium hydroxide (CH) crystals, induces shrinkage as a result of removal of shrinkage restraints in the paste, e.g. the crystalline CH. The present study tests this hypothesis by relating the production and consumption of major hydration products to the amount of autogenous shrinkage.

The autogenous shrinkage and TGA results, clearly support a hypothesis that the porous hydration products (PHP) are the principle hydrates that are responsible for the greater autogenous shrinkage found in the blended system. This is confirmed by plotting autogenous shrinkage vs. PHP_{loss} as shown in **Figure 4.13**. A strong correlation is found

between the autogenous shrinkage and the PHP $_{loss}$ for both neat and blended cement pastes at the same *w/cm* of 0.35. This correlation applies to the pozzolanic contribution as well, indicating that from the hydration product point of view it is porous hydration products and the associated pore drying in these products that control autogenous shrinkage. Note that the pozzolanic contribution to autogenous shrinkage is calculated from Eq. 4.2. The pozzolanic contribution to PHP $_{loss}$ is calculated similarly, which quantifies the difference between the measured PHP $_{loss}$ and the expected PHP $_{loss}$ corrected for dilution (assuming no pozzolanic interaction):

$$PHP_{loss,P} = PHP_{loss,blended} - (100 - C_{SCM}\,\%) \cdot PHP_{loss,C} \qquad \text{Eq. 4.3}$$

where,

$PHP_{loss,p}$ = contribution from pozzolanic reaction,

$PHP_{loss,blended}$ = measured PHP $_{loss}$ of a blended system,

C_{SCM} = the SCM content by mass in a blended system (%), in this case the SCM is GGBFS,

$PHP_{loss,C}$ = measured PHP $_{loss}$ of a control mix, here it is OPC.

Finally, the hypothesis that CH_{loss} is somehow linked to autogenous shrinkage was tested. As indicated in **Figure 4.14**, no systematic correlation was found between autogenous shrinkage and CH $_{loss}$. The same autogenous shrinkage may occur at different CH $_{loss}$ values. In addition, the autogenous shrinkage contributed from pozzolans keeps developing though there is no CH depletion. These results clearly dispute the hypothesis that suggests that one of the reasons for the greater autogenous shrinkage found in the blended system is the consumption of calcium hydroxide crystals which results in the removal of shrinkage restraints in the paste.

Rather, the present results find that high PHP content, e.g. high C-S-H content, along with the pore drying in these porous hydration products is responsible for the development of autogenous shrinkage. Therefore, it is proposed that future efforts in this field be directed towards a greater understanding of the (nano) structures of cement hydration products, particularly the calcium silicate hydrate gel, and their influence on performance properties.

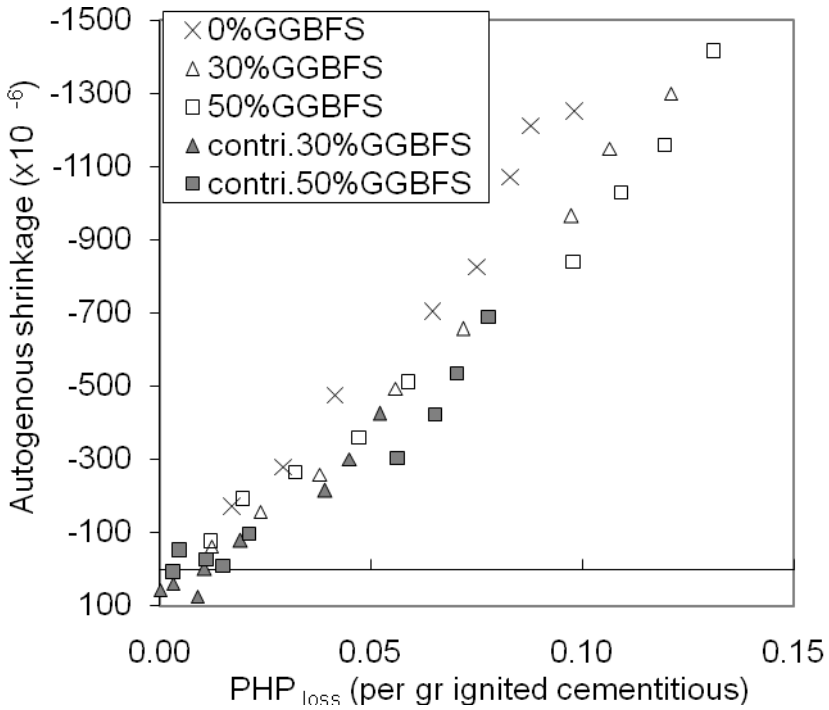

Figure 4.13 Relationship between autogenous shrinkage and PHP $_{loss}$ for blended systems, *w/cm*= 0.35

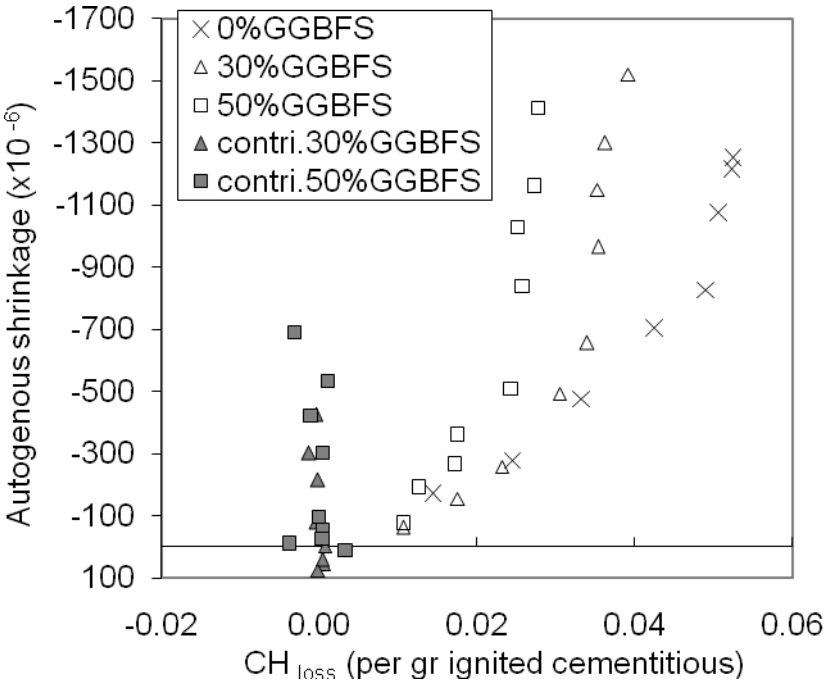

Figure 4.14 Relationship between autogenous shrinkage and CH $_{loss}$ for blended systems, *w/cm*= 0.35

4.3.5 Relating Chemically Bound Water to the Physico-Mechanical Properties of Blended Systems

Though autogenous shrinkage has been realized as one of the major factors causing cracking and durability problems in concrete elements, a standard measuring procedure has not yet been developed due to debate over measuring techniques, such as how to overcome external friction, control temperature, and achieve sealed curing conditions. Alternatively, it would be beneficial if autogenous shrinkage could be related to properties that would not require such stringent test conditions and elaborate apparatus.

A quantitatively good correlation is found between autogenous shrinkage and the chemically bound water w_n for systems of the same *w/cm*. This finding has its justification as the majority of the chemically bound water is coming from PHP as demonstrated in **Figure 4.15**. Though calcium hydroxide is not directly related to the development of autogenous shrinkage as suggested in **Figure 4.14**, the consumption of free water in the capillary pores to produce CH will cause the reduction of the pore humidity as well and consequently the development of autogenous shrinkage.

Figure 4.16 illustrates the relationship between autogenous shrinkage and chemically bound water for systems at the same *w/cm* of 0.35, which suggests an approach to predict autogenous shrinkage. A regression equation of the following form was shown as the dashed line in **Figure 4.16** and considered as [Wei et al. 2008]:

$$\varepsilon_{au} = A \cdot w_n^{\,B} \qquad \text{Eq. 4.4}$$

where, A and B are regression parameters.

Figure 4.16 suggests as well that unlike PHP the chemically bound water w_n is not the controlling factor of autogenous shrinkage from the hydration product point of view, because the contribution of pozzolanic reaction to w_n and to autogenous shrinkage does not follow the same curve. This can be seen from **Figure 4.13** and **4.16**.

Though measuring the chemically bound water can be an alternative technique to determine autogenous shrinkage of a cement paste, further investigation is needed to verify this approach on systems with different *w/cm* ratios. As indicated in **Figure 4.17,** due to decreased self-desiccation for high *w/cm* pastes, lower autogenous shrinkage is

seen in the neat portland cement paste. It is expected that the blended systems with GGBFS fall on the same curve as the neat paste systems at these higher *w/cm* ratios.

The chemically bound water seems to be an important indicator of strength development as well for the blended systems as illustrated in **Figure 4.18**. Compressive strength of concrete is found to be in good correlation with chemically bound water. However, unlike autogenous shrinkage, this relationship is true for different *w/cm* systems as indicated in **Figure 4.18**. The compressive strength is determined on 100 mm by 200 mm concrete cylinders.

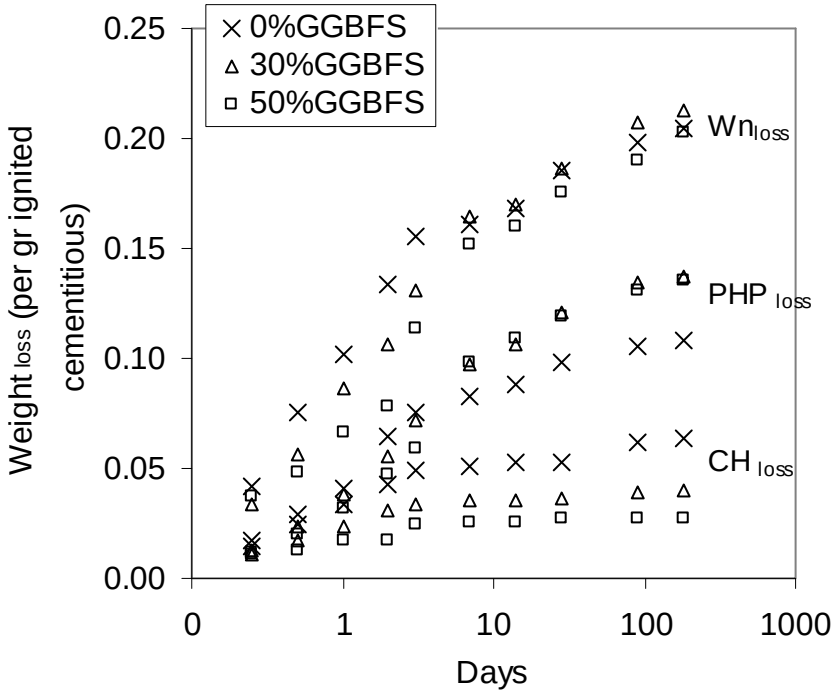

Figure 4.15 TGA results of various phases in blended systems, *w/cm*= 0.35

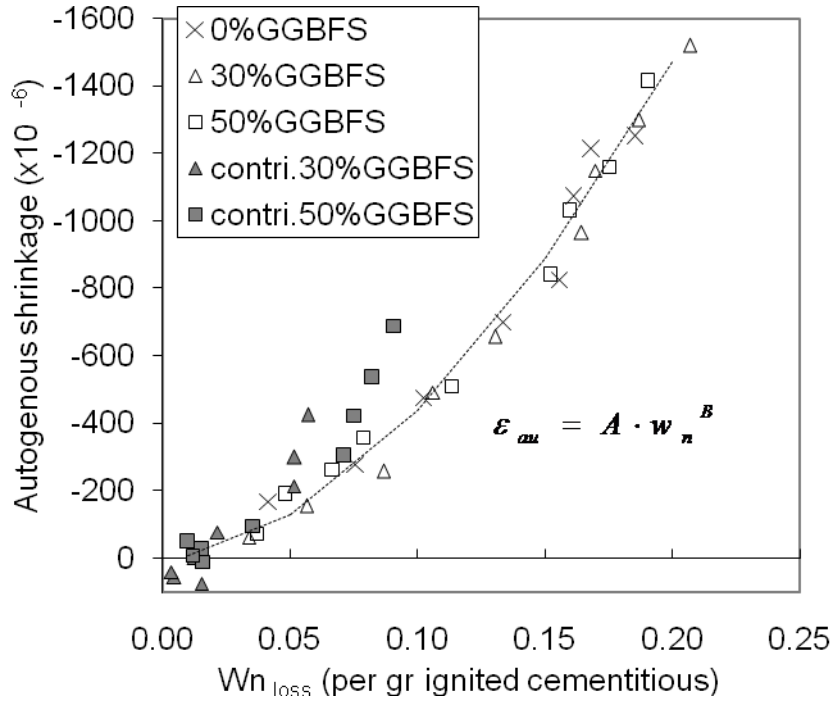

Figure 4.16 Relationship between autogenous shrinkage and Wn $_{loss}$ for blended systems, *w/cm*= 0.35

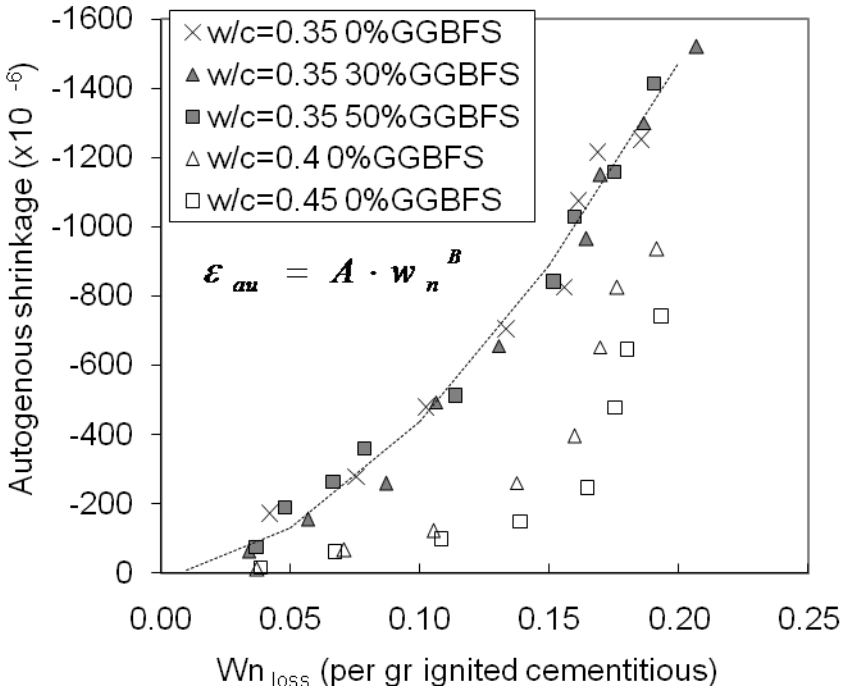

Figure 4.17 Relationship between autogenous shrinkage and Wn $_{loss}$ for systems with different *w/cm*

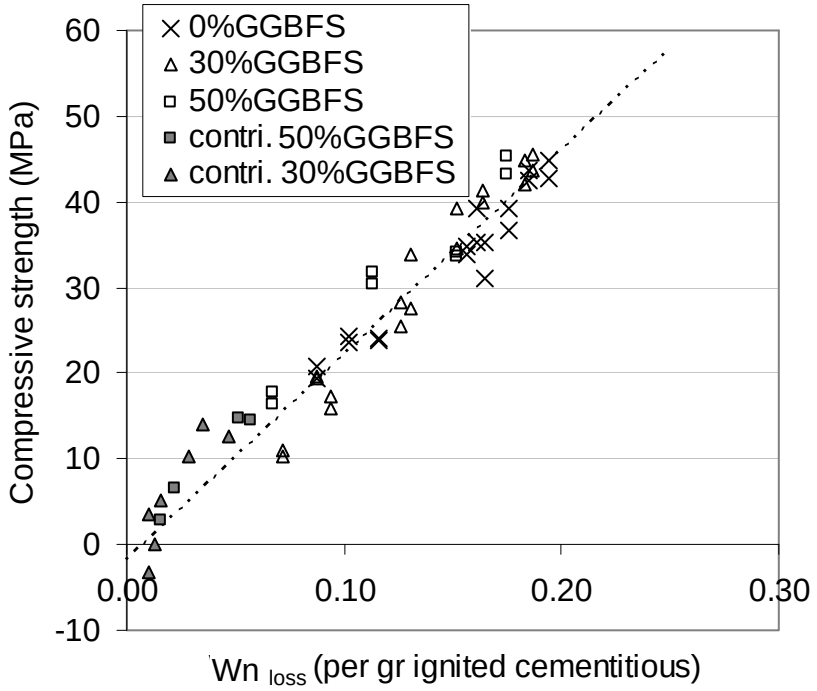

Figure 4.18 Relationship between compressive strength and Wn $_{loss}$ for concrete blended with GGBFS, *w/cm*=0.35 and 0.45

4.3.6 Relating Autogenous Shrinkage to Chemical Shrinkage

Chemical shrinkage is the absolute volume reduction associated with the hydration reactions. It creates the underlying driving force to the occurrence of autogenous shrinkage. Autogenous shrinkage has shown to be equal to chemical shrinkage as long as the paste is liquid. Around the time of setting, however, a solid skeleton is formed allowing empty pore to form, and the resulting autogenous shrinkage becomes much smaller than the underlying chemical shrinkage. The part of the autogenous shrinkage that occurs after setting is self-desiccation shrinkage normally termed as autogenous shrinkage.

Sellevold et al. [1994] showed a relationship between the chemical and autogenous shrinkage for a cement paste with *w/cm* of 0.4 (**Figure 4.19**). The chemical shrinkage was measured for a continuously rotated specimen and thus there was no load bearing microstructure being formed. The autogenous shrinkage was measured for specimen without being rotated. The difference between these two types of shrinkage can

be attributed to the formation of the load bearing microstructure where self-desiccation occurs. If the space created by chemical shrinkage is not fully filled with water the surface tension generated at the water-solid surface creates under pressure that induces autogenous shrinkage.

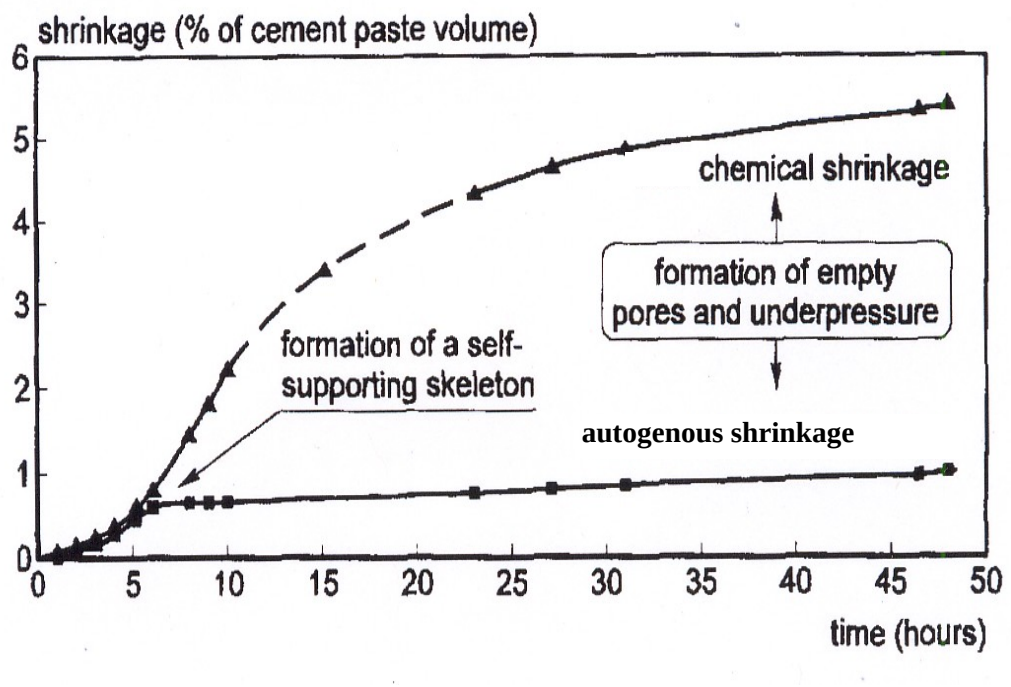

Figure 4.19 Chemical and autogenous shrinkage of cement paste with *w/cm*=0.4 [Sellevold et al. 1994]

Relating autogenous shrinkage to chemical shrinkage helps better understanding the shrinkage mechanism. The chemical shrinkage of portland cement has been shown to be a sensitive indicator of the progress of the cement hydration. Powers' model [1947] is adopted to predict chemical shrinkage as a function of degree of hydration and *w/cm* of cement paste:

$$\frac{\Delta V}{V} = \frac{0.0584 \cdot \alpha}{0.321 + {}^{w}\!/_{cm}} \qquad \text{Eq. 4.5}$$

where, $\frac{\Delta V}{V}$ is the volumetric chemical shrinkage; α is the degree of hydration; ${}^{w}\!/_{cm}$ is water/cementitious ratio of cement paste.

The chemical shrinkage can be calculated from Eq. 4.5 after obtaining the degree of hydration from TGA results. The relationship between the measured autogenous shrinkage and the predicted chemical shrinkage are then shown in **Figure 4.20** and **4.21** for different systems.

It is observed that autogenous shrinkage increases nonlinearly with the chemical shrinkage. The growth of autogenous shrinkage becomes very sensitive to the increase of chemical shrinkage after the chemical shrinkage of 0.04 has been reached for all systems indicating another factor may become dominant in producing autogenous shrinkage. This factor should be self-desiccation.

Figure 4.22 shows the relationship between the predicted pore humidity and chemical shrinkage of OPC paste. It can be seen that chemical shrinkage of 0.04 corresponds to pore humidity greater than 90%, indicating the effect of self-desiccation on autogenous shrinkage becomes pronounced even at high pore humidity. This finding confirms previous studies that it is primarily capillary tension that causes autogenous shrinkage rather than surface tension or disjoining pressure, as capillary tension works in the upper pore humidity range, which is above 45% [Soroka 1979, Mindess 1981]. **Figure 4.22** further illustrates that the pronounced effect of pore humidity begins at low pore humidity for low *w/cm* system because the free water in the capillary pores is used up quickly in such system. At the same amount of chemical shrinkage, self desiccation causes low pore humidity in low *w/cm* system. This is consistent with finding in **Figure 4.20** that for the same chemical shrinkage, greater autogenous shrinkage results in low *w/cm* cement paste. According to Lura [2003], at the same *w/cm*, blended systems with GGBFS are found to have lower pore humidity than pure portland paste. This supports the finding shown in **Figure 4.21** that even at the same chemical shrinkage level, blended systems show greater autogenous shrinkage due to its intensive pore drying.

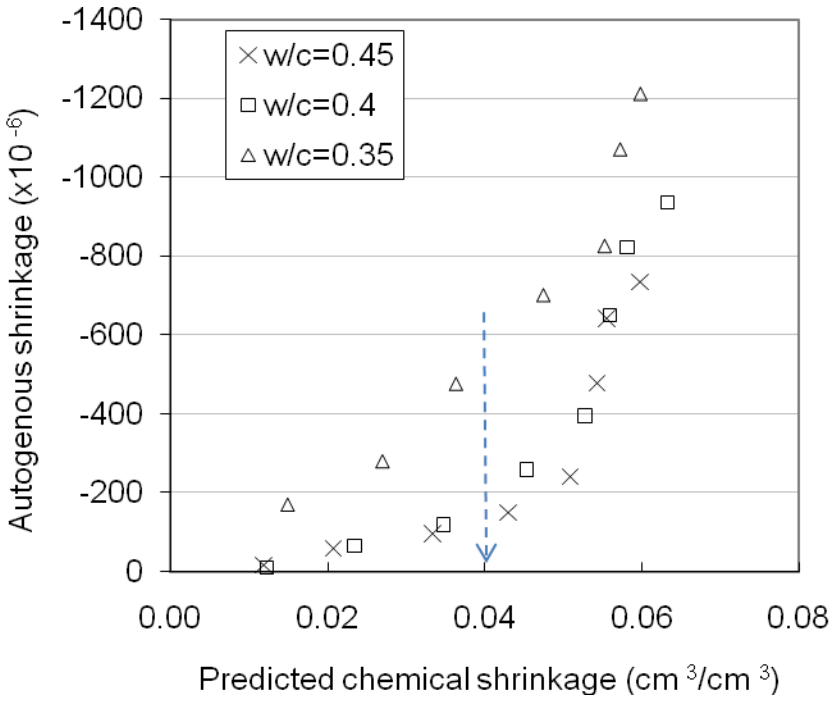

Figure 4.20 Relationship between measured autogenous shrinkage and predicted chemical shrinkage for OPC paste

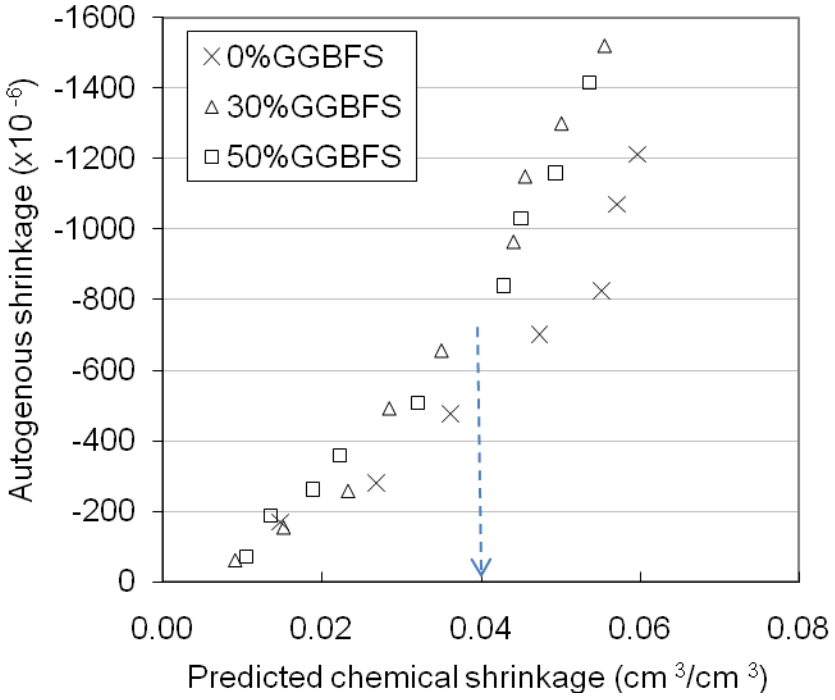

Figure 4.21 Relationship between measured autogenous shrinkage and predicted chemical shrinkage for blended systems, *w/cm*=0.35

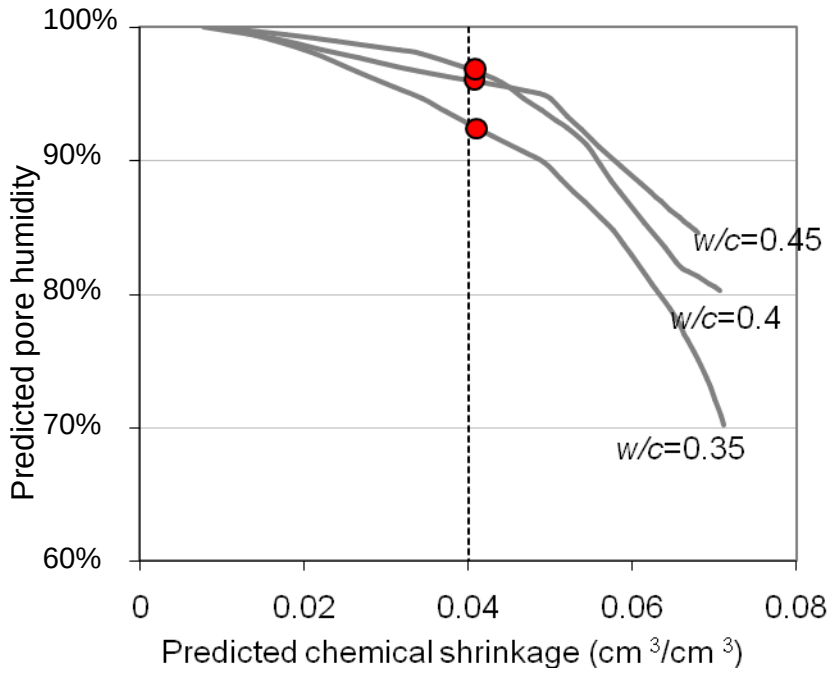

Figure 4.22 The reduction of pore humidity with chemical shrinkage for OPC paste

4.4 CONCLUSIONS

The results of the experimental investigation provide a basis for better understanding the autogenous shrinkage of cement pastes. In particular, the following findings either support prior inferences or new interpretations:

- Autogenous shrinkage was found to be a result of hydration of the cement and associated reduction in pore-humidity with increasing hydration level and decreasing *w/cm* ratio. Lower pore humidity develops faster with decreasing *w/cm* ratio and thus explains why autogenous shrinkage is more pronounced in lower *w/cm* ratio pastes.
- Pozzolanic reactions increase the amount of porous hydration products and therefore autogenous shrinkage. Pozzolanic reactions are secondary reactions as they require cement hydration for initiation. In this study GGBFS-OPC initiation of pozzolanic reactions was found to start after about two days, corresponding to 50% to 60% hydration level. Thus, GGBFS decreases initial autogenous shrinkage of the cementitious blends as it dilutes the amount of porous hydration

products and associated capillary pore-volume, while increasing long-term (greater 28 days) shrinkage.

- A basic microstructure-property relationship has been established between the autogenous shrinkage and the chemically bound water that suggests that chemically bound water may be used as a robustness indicator of autogenous shrinkage.

CHAPTER 5

MODELING OF AUTOGENOUS SHRINKAGE AND AGGREGATE RESTRAINING EFFECT IN CONCRETE

5.1 INTRODUCTION

Quantifying autogenous shrinkage of concrete systems becomes increasingly important in order to assess and control the risk of early-age cracking, especially in systems with low water-cementitious ratios where extensive pore-drying and thus autogenous shrinkage develops with the extent of hydration (or time). And consequently the risk of early-age cracking due to restrained autogenous shrinkage increases in these systems. However, there is very little data available on autogenous deformation due to the challenges in measurement which requires sealed curing conditions and low frictions between the specimen and the surrounding.

This chapter reports the experimental results on the autogenous deformation of concrete containing various aggregate contents and with three *w/cm* ratios from time of final set, and subsequent development of procedures for predicting autogenous shrinkage. New models are developed for the prediction of both cement paste and concrete autogenous shrinkage by incorporating a shrinkage-stress equilibrium model developed by Pickett with a time-domain model developed by Freiesleben-Hansen and Pedersen. The new methodology has been verified to be able to provide improved prediction of concrete autogenous shrinkage.

5.2 PREDICTION OF PASTE AUTOGENOUS SHRINKAGE

5.2.1 Background

The experimental results presented in Chapter 4 show that autogenous shrinkage of hydrating cement paste is influenced by many factors, for example, water/cementitious ratio, cement chemical compositions, and supplementary cementitious material content. The predictions of autogenous shrinkage of cement paste have involved treating autogenous shrinkage as a material property [Bjontegaard 1999] or the mechanical response to the internally applied stresses known as capillary stress [Lura 2003, Grasley 2006]. Unfortunately, there is a lack of agreement on the prediction approaches. For example, treating autogenous shrinkage as a material property had lead to using maturity concept for shrinkage predictions. However, conflicting results were obtained regarding the applicability of the maturity concept [Bjontegaard 1999]; the capillary tension approach is considered advantageous when compared to other modeling strategies, since it has a sound mechanical and thermodynamic basis [Lura 2003, Grasley 2006]. However, this approach requires stringent inputs which are difficult to obtain, including pore relative humidity, saturation factor of the porous body, bulk modulus of the porous body and the solid phase, creep properties of the hydrating paste. In addition, calculation of autogenous shrinkage based on the capillary tension approach could explain only part of the measured autogenous shrinkage of cement paste, as some other driving forces causing autogenous shrinkage may involve [Lura 2003].

For the purpose of practical use, in this chapter, a new predicting procedure based on experimental measurements is presented for paste systems with varying *w/cm* ratios, cement compositions, and GGBFS contents.

5.2.2 Prediction Based on F-H Model

According to Powers [1947] and Tazawa et al. [1995], the autogenous shrinkage of cement paste is a linear function of the shrinkage of each individual constituent which is dependent on the degree of hydration of each component. A close look at the development of autogenous shrinkage plotted on a logarithmic time scale for different paste systems as shown in **Figure 5.1**, **5.2** and **5.3**, it is suspected that the autogenous

shrinkage of cement paste can be modeled using the S-shaped F-H model proposed by Freisleben-Hansen and Pedersen [1977] originally to fit hydration curves. This model fits well with the hydration-related properties, such as the development of degree of hydration, heat of hydration, compressive strength, and Young's modulus.

For autogenous shrinkage, the F-H model can be written as:

$$\varepsilon_{au} = \varepsilon_{au-ult} \exp[-(\frac{\tau}{t})^{a}] \qquad \text{Eq. 5.1}$$

where, ε_{au} = autogenous shrinkage at time t

ε_{au-ult} = the "ultimate" value for autogenous shrinkage at a given *w/cm* ratio, in this study it is referred to as the three-year autogenous shrinkage $\varepsilon_{au,3-yrs}$

τ = the time characteristic, days

a = the curvature parameter

As can be seen from **Figure 5.1** through **Figure 5.3**, the F-H model fits the measured autogenous shrinkage data fairly well for pastes with different cement types and GGBFS contents. The predicted long-term shrinkage data from F-H model are shown as the dashed lines. For the white cement paste, the F-H model does not capture the early-age (during the first few days) autogenous shrinkage very well due to the complexity of it early-age deformations. Be aware that the autogenous shrinkage curves shown are relative to the point where shrinkage begins to develop while maintaining time axis unchanged.

According to the predictions, lower *w/cm* paste develops greater autogenous shrinkage at all times. The magnitude of ultimate or long-term autogenous shrinkage depends on the type of cement used. For the same *w/cm*, OPC paste shows greater long-term autogenous shrinkage than the white cement paste. Paste blended with GGBFS shows slightly greater autogenous shrinkage at later ages than the neat paste.

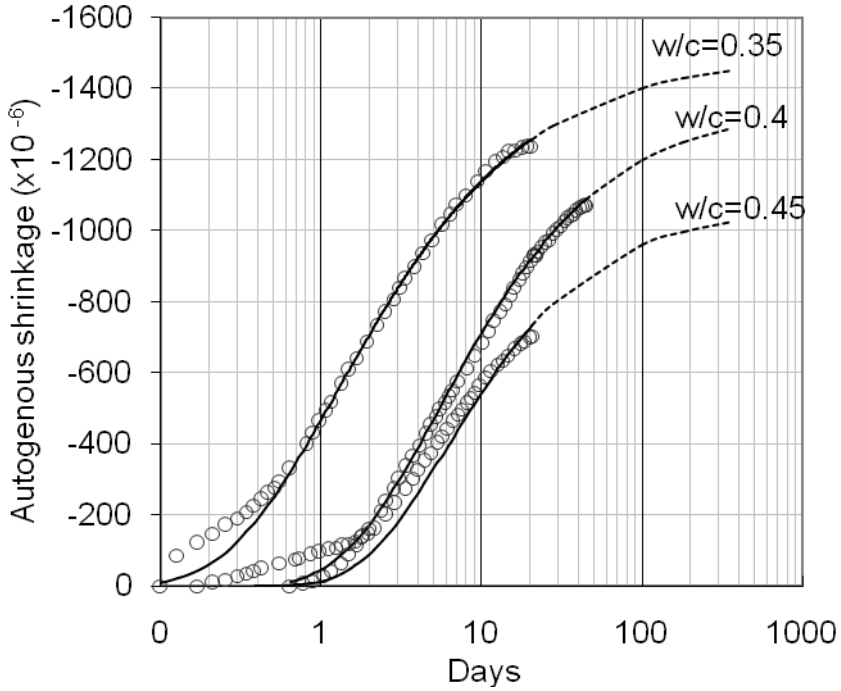

Figure 5.1 Measured autogenous shrinkage and the curve fit using F-H model for OPC paste

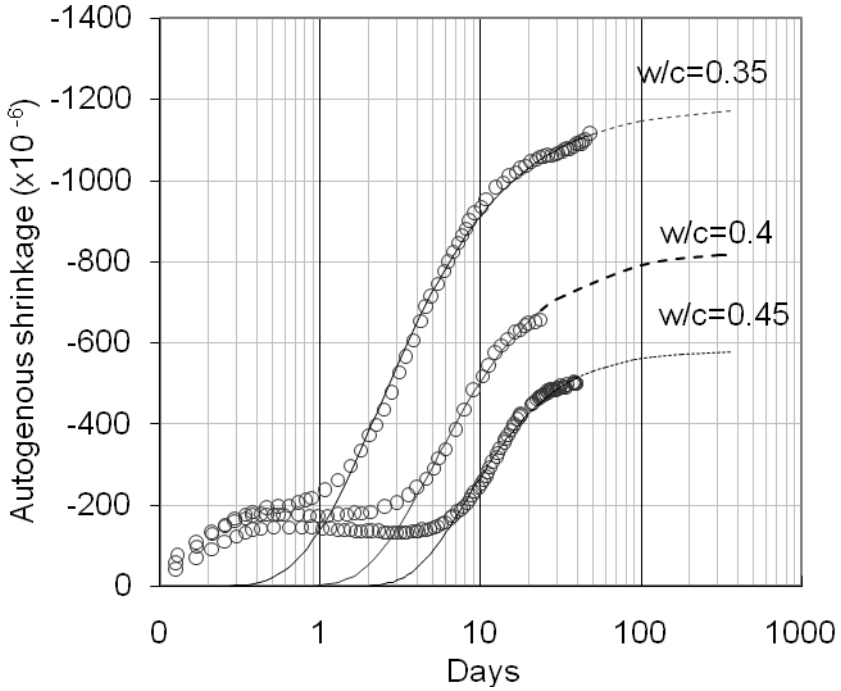

Figure 5.2 Measured autogenous shrinkage and the curve fit using F-H model for white cement paste

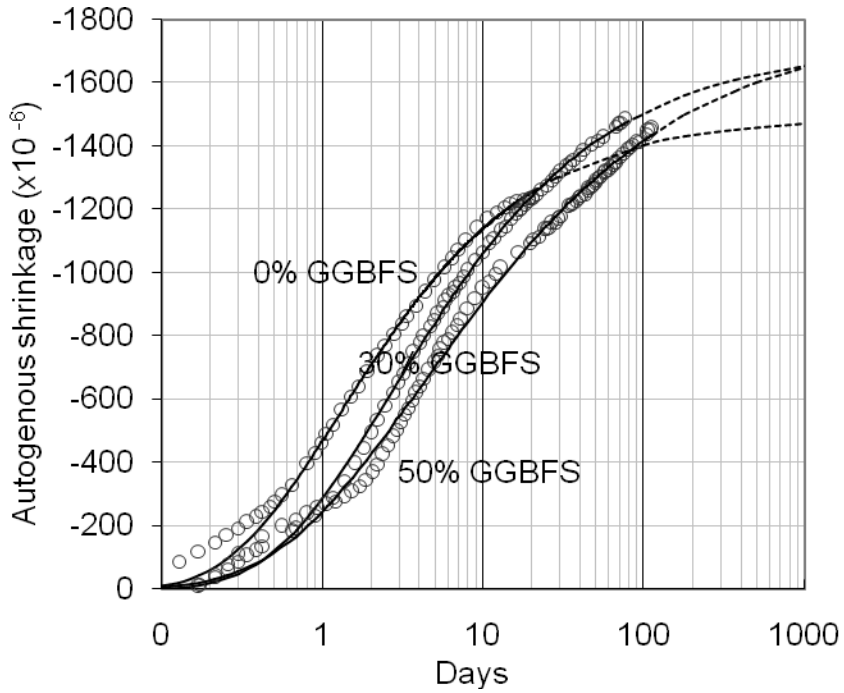

Figure 5.3 Measured autogenous shrinkage and the curve fit using F-H model for blended cement paste

F-H model is also known as the "three-parameter model" as the three parameters in Eq. 5.1 are essential in determining the shape and curvature of the fitting curves. The three parameters are: the ultimate value ε_{au-ult} or $\varepsilon_{au,3-yrs}$; the time characteristic τ; and the curvature parameter a. They can be determined from curve fitting and are shown in **Figure 5.4** through **Figure 5.6** for each system. These three parameters are found to be linear functions of *w/cm* for neat cement paste (see **Figure 5.4** for OPC paste and **Figure 5.5** for white cement paste) and of GGBFS contents for blended paste (see **Figure 5.6**).

The three-year autogenous shrinkage decreases linearly with the increasing *w/cm*. As suggested in **Figure 5.4a** and **Figure 5.5a**, there is no autogenous shrinkage expected when *w/cm* is above 0.7 for OPC paste and 0.55 for white cement paste. Baroghel-Bouny and Mounanga [2005] reported the same value of 0.7 for cement paste studied. These *w/cm* limits are higher than the previous findings by [Powers and Brownyard 1948, Taylor 1997]. Research by Powers and Brownyard [1948] demonstrated that autogenous shrinkage occurs only when the *w/cm* ratio is less than 0.42, as further hydration will draw free water from the capillary pores, and thus reduces the pore humidity and causes

self-desiccation. For *w/cm* greater than 0.42, a complete hydration can be reached without consuming water from capillary pore and thus no autogenous shrinkage is expected [Powers and Brownyard 1948]. According to Taylor [1997], this *w/cm* limit can vary from 0.36 to 0.48 dependent on the cement type.

From the results shown in this work, the later-age autogenous shrinkage can be pronounced even in a cement paste with *w/cm* greater than 0.5. For *w/cm* ranging from 0.4 to 0.5, which is normally seen in highway concrete mixture, the autogenous shrinkage of cement paste is substantial of about 300 $x10^{-6}$ to 1200 $x10^{-6}$. Though the autogenous shrinkage of concrete is much less than paste shrinkage and may not cause significant structural-level shrinkage due to the fact that concrete shrinkage decreases with the increase of the aggregate content [Pickett 1956], micro-cracking may result in the paste phase of a highway concrete when the pronounced paste shrinkage is restrained by aggregates.

The three-year autogenous shrinkage of a blended system is linearly proportional to the GGBFS content (**Figure 5.6a**). Increase of GGBFS content will result in slightly greater later-age autogenous shrinkage. However, the GGBFS effect on the autogenous shrinkage depends on the age as well. For example, the 50%GGBFS system shows even less autogenous shrinkage than the 0%GGBFS system at the age of 28 days.

The second parameter τ, as a time characteristic, represents the time shift of autogenous shrinkage curve. The lower the *w/cm*, the earlier the shrinkage will start. And thus, low *w/cm* mixture has small τ. For paste blended with GGBFS, the autogenous shrinkage starts late due to the dilution effect, and thus has large τ values as indicated in **Figure 5.6b**. The third parameter a is the curvature parameter. It is found linearly proportional to the *w/cm* and GGBFS content as well.

These parameters are of significance for predicting autogenous shrinkage of cement paste with wide range of *w/cm* ratios and GGBFS contents. The regression equations for each parameter are listed for each paste systems as follows:

For neat OPC paste:

$$\varepsilon_{au,3-year} = 4281 \cdot \left(w/cm\right) - 3016 \qquad \text{Eq. 5.2}$$

$$\tau = 48.589 \cdot \left(w/cm\right) - 15.175 \qquad \text{Eq. 5.3}$$

$$\alpha = 1.764 \cdot \left(w/cm\right) + 0.0162 \quad \text{Eq. 5.4}$$

For neat white cement paste:

$$\varepsilon_{au,3-year} = 5992 \cdot \left(w/cm\right) - 3260 \quad \text{Eq. 5.5}$$

$$\tau = 59.286 \cdot \left(w/cm\right) - 18.491 \quad \text{Eq. 5.6}$$

$$\alpha = 3.865 \cdot \left(w/cm\right) - 0.45 \quad \text{Eq. 5.7}$$

For portland cement paste blended with GGBFS at *w/cm*=0.35:

$$\varepsilon_{au,3-year} = -5.915 \cdot C_{GGBFS} - 1504 \quad \text{Eq. 5.8}$$

$$\tau = 0.06 \cdot C_{GGBFS} + 1.17 \quad \text{Eq. 5.9}$$

$$\alpha = -0.0032 \cdot C_{GGBFS} + 0.644 \quad \text{Eq. 5.10}$$

where, C_{GGBFS} is the GGBFS content, %.

Be aware that there is limitation of using this approach for predicting paste autogenous shrinkage, as the temperature effect is not considered. This can be part of further research to develop a comprehensive model capable of incorporating the effects of *w/c*m, GGBFS content and curing temperature together for the purpose of practical use.

Obtaining paste autogenous shrinkage is the first step toward concrete autogenous shrinkage predictions by using composite models, which will be discussed in section 5.3 in this Chapter.

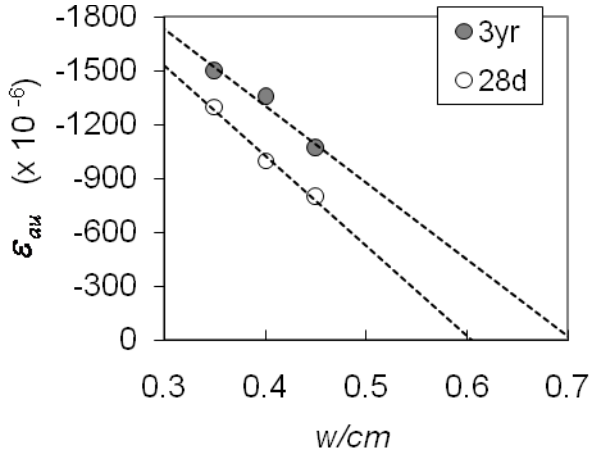

(a)

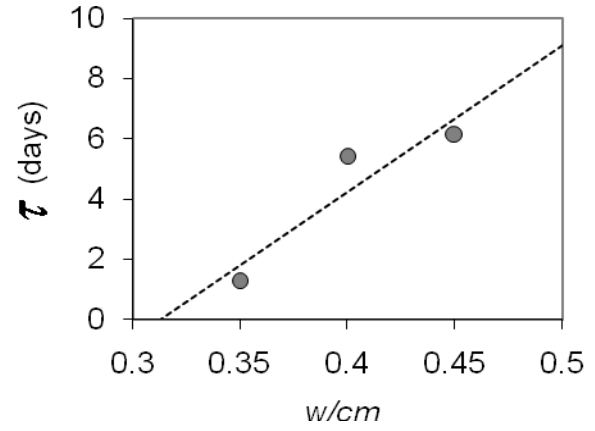

(b)

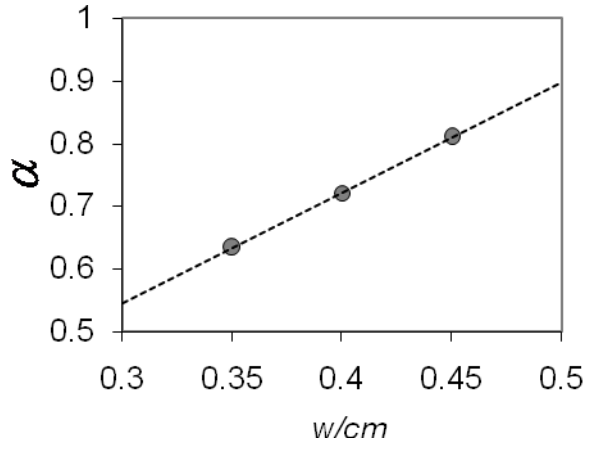

(c)

Figure 5.4 Parameters in F-H model vs. *w/cm* for predicting autogenous shrinkage of OPC paste

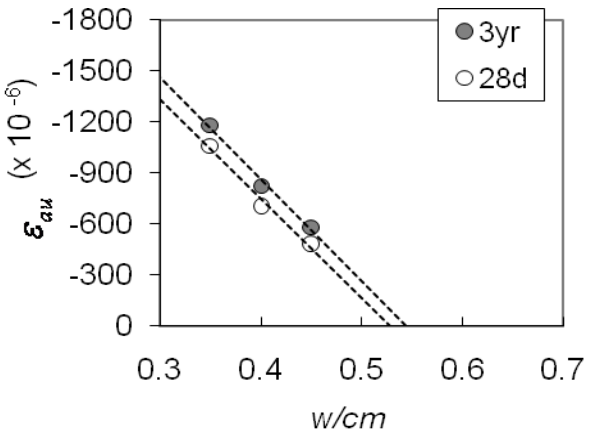

(a)

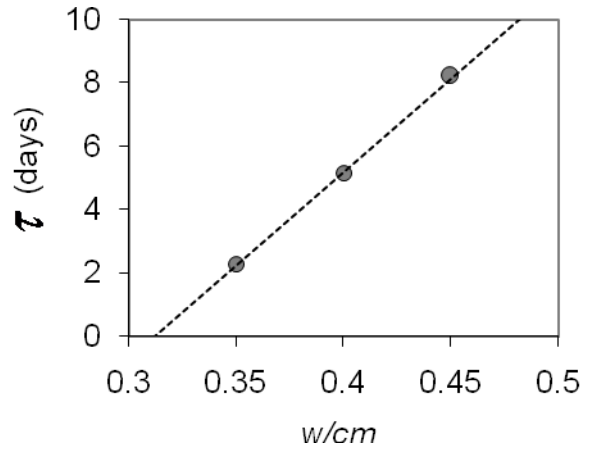

(b)

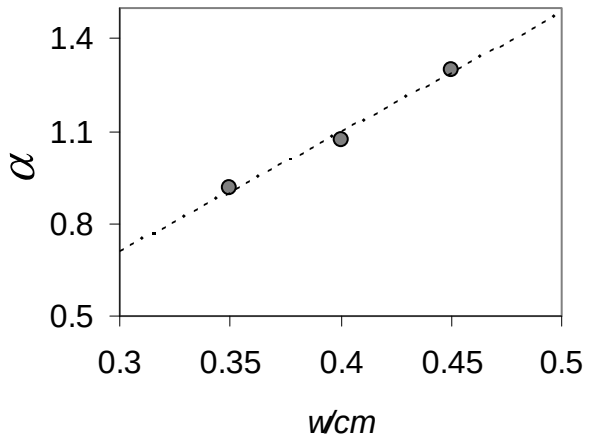

(c)

Figure 5.5 Parameters in F-H model vs. *w/cm* for predicting autogenous shrinkage of white cement paste

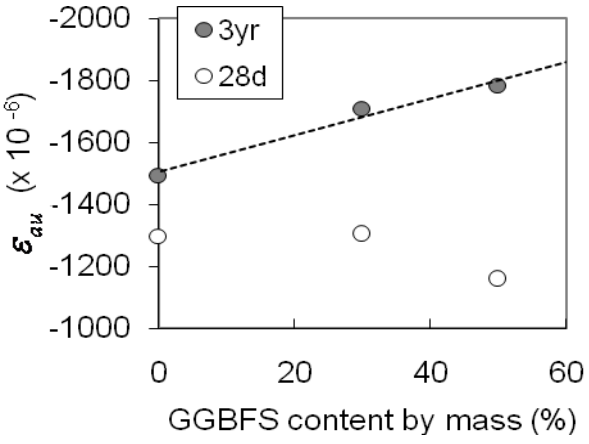

(a)

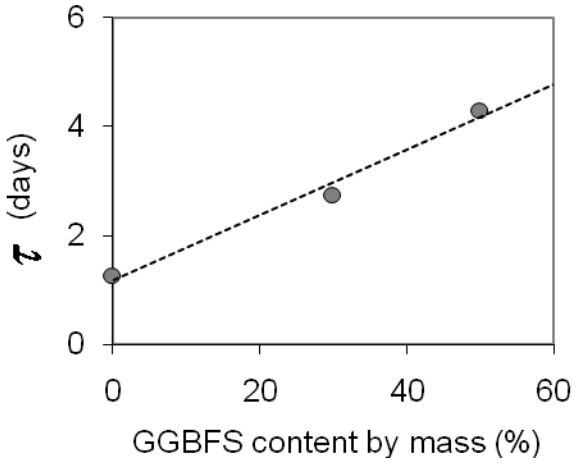

(b)

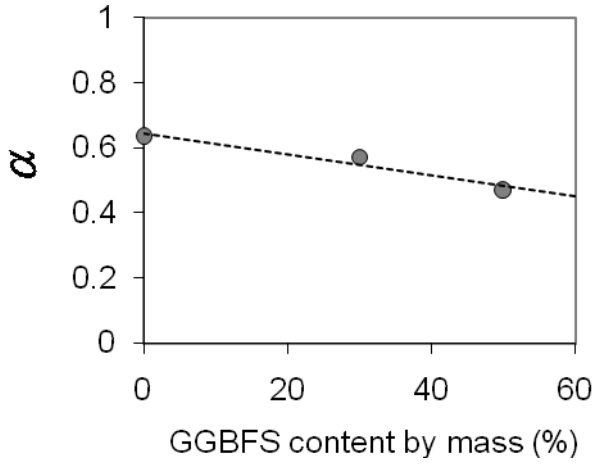

(c)

Figure 5.6 Parameters in F-H model vs. GGBFS content for predicting autogenous shrinkage of blended paste, *w/cm*=0.35

5.2.3 Prediction as a Function of Chemically Bound Water

As discussed in Chapter 4, the autogenous shrinkage of paste has a good correlation with the chemically bound water w_n for systems at the same *w/cm*. This suggests a way to predict autogenous shrinkage using parameter (chemically bound water) that can be easily measured. As illustrated in **Figure 5.7**, the autogenous shrinkage ε_{au} can be expressed as a function of chemically bound water for the blended systems with *w/cm* of 0.35:

$$\varepsilon_{au} = A \cdot w_n^{\,B} \qquad \text{Eq. 5.11}$$

where, A and B are regression parameters; they are, in this case, A=-24630 and B=1.7506.

The chemically bound water is a function of time (see **Figure 5.8**), similar to degree of hydration, which can be modeled using the F-H model:

$$w_n = w_{n,3-yrs} \cdot \exp\left(-\left(\frac{\tau}{t}\right)^{\alpha}\right) \qquad \text{Eq. 5.12}$$

where, w_n = chemically bound water at time t

$w_{n,3-yrs}$ = the "ultimate" value for chemically bound water, referred as the three-year value

τ and a are defined the same as in Eq. 5.1.

The three parameters: $w_{n,3-yrs}$, τ, and a are linear functions of GGBFS contents as plotted in **Figure 5.9**. $w_{n,3-yrs}$ increases with the increasing GGBFS content due to the secondary pozzolanic reaction following the primary portland cement hydration and thus more free water is consumed. The regression equations for each parameter in Eq. 5.12 are listed:

$$w_{n,3-year} = 0.0005 \cdot C_{GGBFS} + 0.208 \qquad \text{Eq. 5.13}$$

$$\tau = 0.019 \cdot C_{GGBFS} + 0.486 \qquad \text{Eq. 5.14}$$

$$\alpha = -0.0033 \cdot C_{GGBFS} + 0.587 \qquad \text{Eq. 5.15}$$

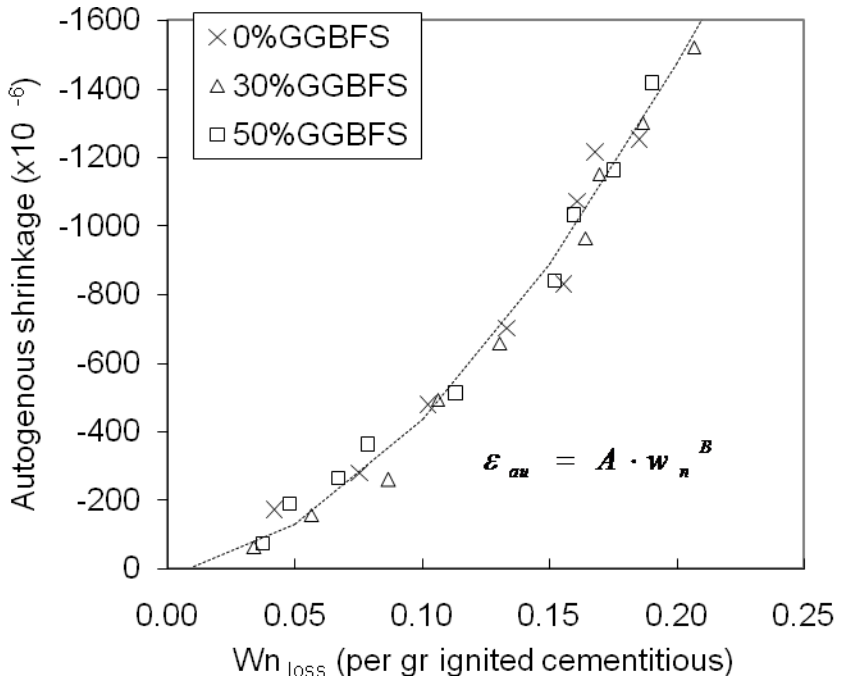

Figure 5.7 Autogenous shrinkage as a function of chemically bound water for blended cement paste, *w/cm*=0.35

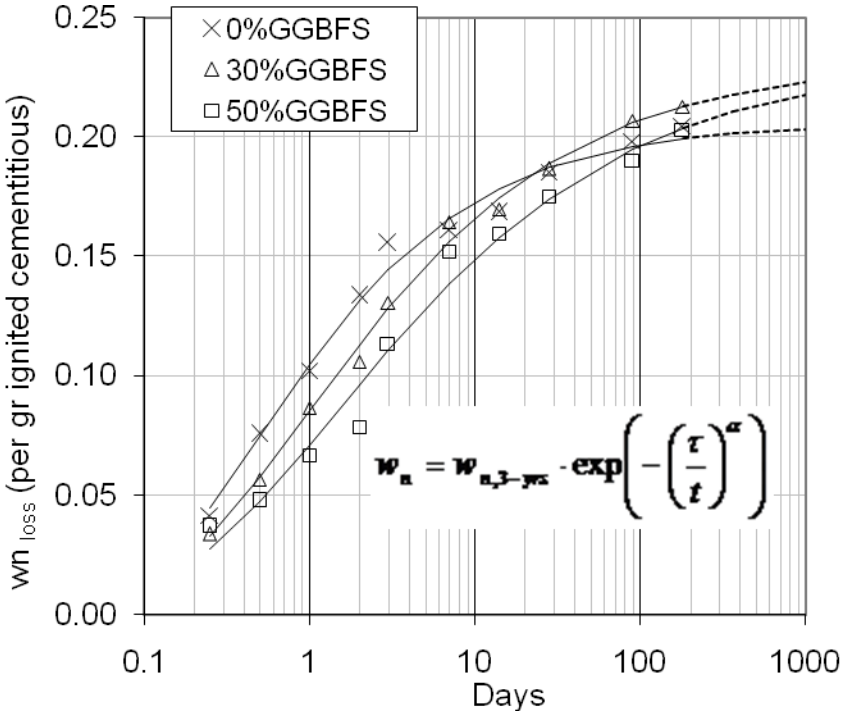

Figure 5.8 Chemically bound water as a function of time for blended cement paste, *w/cm*=0.35

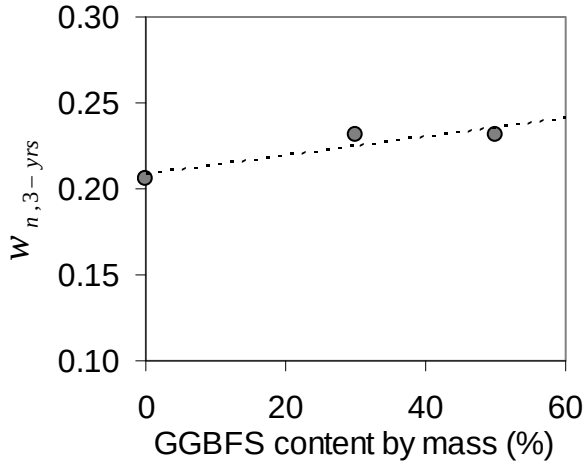

(a)

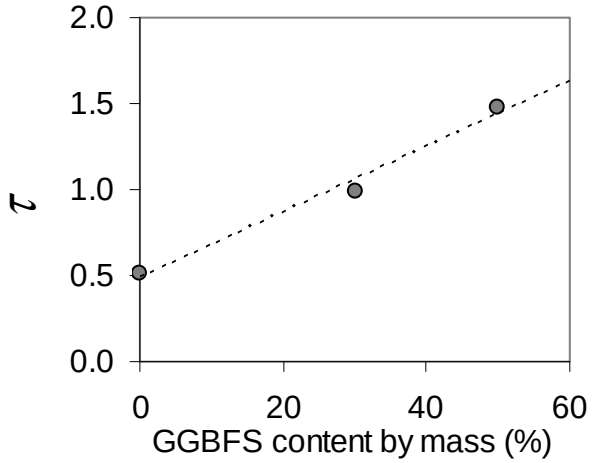

(b)

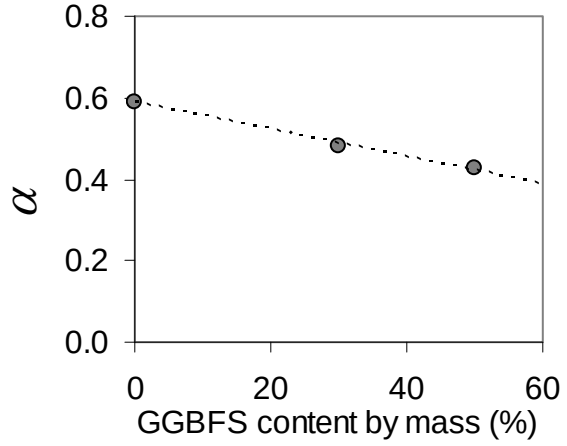

(c)

Figure 5.9 Parameters in F-H model vs. GGBFS content for predicting chemically bound water of blended paste, *w/cm*=0.35

It will be convenient to correlate autogenous shrinkage to time by relating Eq. 5.11 with Eq. 5.12, which results in:

$$\varepsilon_{au} = A \cdot \left(w_{n,3-yrs}\right)^{B} \cdot \exp\left(-\left(\frac{B^{\frac{1}{\alpha}} \cdot \tau}{t}\right)^{\alpha}\right) \quad \text{Eq. 5.16}$$

Eq. 5.16 is actually a three-parameter function, which can be considered as:

$$\varepsilon_{au} = n_1 \cdot \exp\left(-\left(\frac{n_2}{t}\right)^{n_3}\right) \quad \text{Eq. 5.17}$$

where, $n_1 = A \cdot \left(w_{n,3-yrs}\right)^{B}$, $n_2 = B^{\frac{1}{\alpha}} \cdot \tau$, $n_3 = \alpha$.

The measured and predicted autogenous shrinkage using Eq. 5.17 agree very well as demonstrated in **Figure 5.10**. The predicted long-term autogenous shrinkage is shown as the dashed lines. It can be seen from **Figure 5.10** that the predicted autogenous shrinkage using chemically bound water is similar to the F-H model prediction (**Figure 5.3**). The autogenous shrinkage is more pronounced in the blended paste at later age, especially for 30% GGBFS system. This is consistent with the development of chemically bound water as indicated in **Figure 5.8** for *w/cm*=0.35 systems that 30%GGBFS system exhibits more chemically bound water after the age of 28 days. This may suggest that a more complete cement hydration can be reached in system blended with 30%GGBFS, leading to more chemically bound water and possibly self-desiccation shrinkage.

The three parameters in Eq. 5.17: n_1, n_2, and n_3 are plotted as a function of GGBFS shown in **Figure 5.11**. Similar trend is found when compared to the F-H model prediction (**Figure 5.6**). Below is the regression equation for each parameter shown in Eq. 5.17:

$$n_1 = -7.439 \cdot C_{GGBFS} - 1581 \quad \text{Eq. 5.18}$$

$$n_2 = 0.081 \cdot C_{GGBFS} + 1.156 \quad \text{Eq. 5.19}$$

$$n_3 = -0.0033 \cdot C_{GGBFS} + 0.587 \quad \text{Eq. 5.20}$$

In summary, measuring the chemically bound water can be an alternative technique to determine autogenous shrinkage of a cement paste. However, further research may be needed to verify this approach on systems with different *w/cm* ratios.

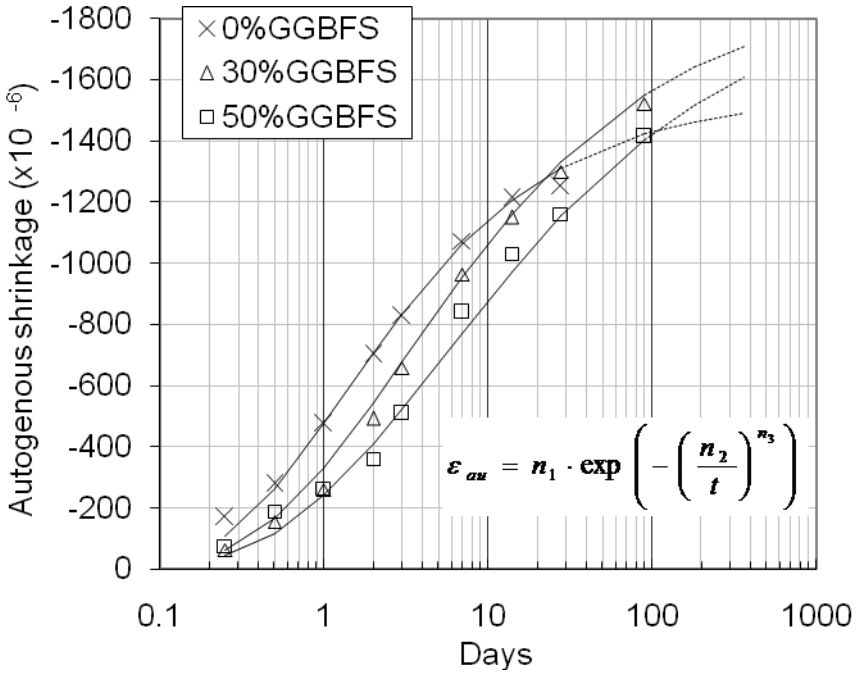

Figure 5.10 Measured and predicted autogenous shrinkage using chemically bound water for blended cement paste, *w/cm*=0.35

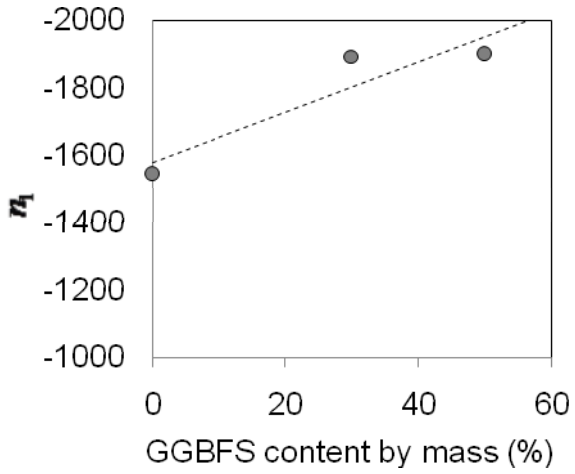

(a)

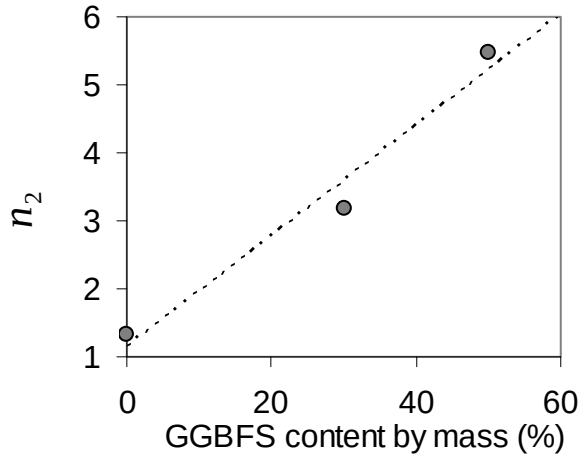

(b)

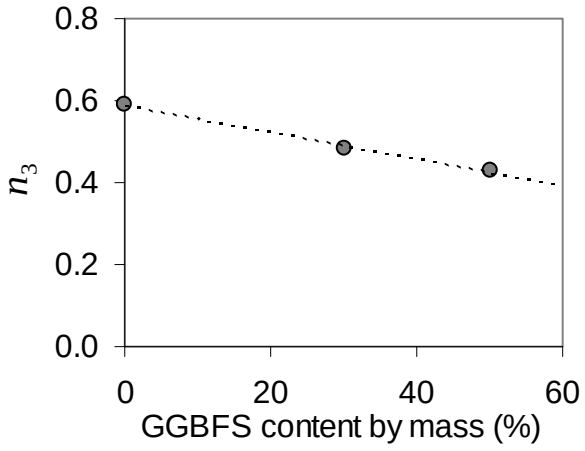

(c)

Figure 5.11 Parameters (obtained through chemically bound water) in F-H model vs. GGBFS content for predicting autogenous shrinkage of blended paste, *w/cm*=0.35

5.3 MODELING OF CONCRETE AUTOGENOUS SHRINKAGE AND AGGREGATE RESTRAINING EFFECT

5.3.1 Experimental Results

Knowing that the autogenous shrinkage takes place only in the paste phase, an increase of the aggregate fraction in a concrete mixture should cause a reduction of the autogenous shrinkage due to the restraints from the aggregate [Pickett 1956, Tazawa 1995, Holt 2002].

The measured autogenous deformations of cement pastes and concretes with different aggregate contents and *w/cm* ratios are plotted vs. ages in days starting from the final set time (see **Figure 5.12**). The aggregate fraction includes both fine and coarse aggregate. Two measured values are reported for each mixes.

Substantial autogenous shrinkage is observed in cement paste and it decreases dramatically with the increase of aggregate content. **Figure 5.13** illustrates the neat autogenous shrinkage in both cement paste and concrete mixtures, which is obtained by normalizing the measured autogenous shrinkage relative to the point where shrinking starts while maintaining the time axis unchanged. It can be seen from **Figure 5.13** that the autogenous shrinkage of concrete is not linearly proportional to the volume fraction of cement paste. Instead, a much less autogenous shrinkage is observed in concrete. For example, concrete containing 40% aggregate by volume shows much less autogenous shrinkage than cement paste times 0.6 (the paste volume fraction). This is possibly due to the residual stress generated from the aggregate restraint which results in nonlinearities associated with creep and micro cracking. Moon et al. [2005] discovered that higher internal stresses and thus microcracking develop with higher volume fraction of aggregate. The nonlinearities can also delay the start time of the shrinking phase in concrete. As shown in **Figure 5.13**, there is a time lag between the shrinking start time of the cement paste and the concrete.

Concrete shows longer expansion phase than cement paste. The higher the aggregate content, the longer the expansion period will be. This is probably related to the changes of water distribution in concrete due to the addition of aggregates that water is originally absorbed to the small pores in aggregates during the mixing and then released to the surrounding cement paste after mixing. The extra water released from aggregate pores will slightly increase the pore humidity in the cement paste and consequently delay the shrinkage. This is somewhat similar to the process of internal curing, however, being much less intensive as the pore volume available in the regular aggregates is much less than that of the lightweight aggregate. And thus, after a short period of expansion, the deformation will eventually turn into shrinkage.

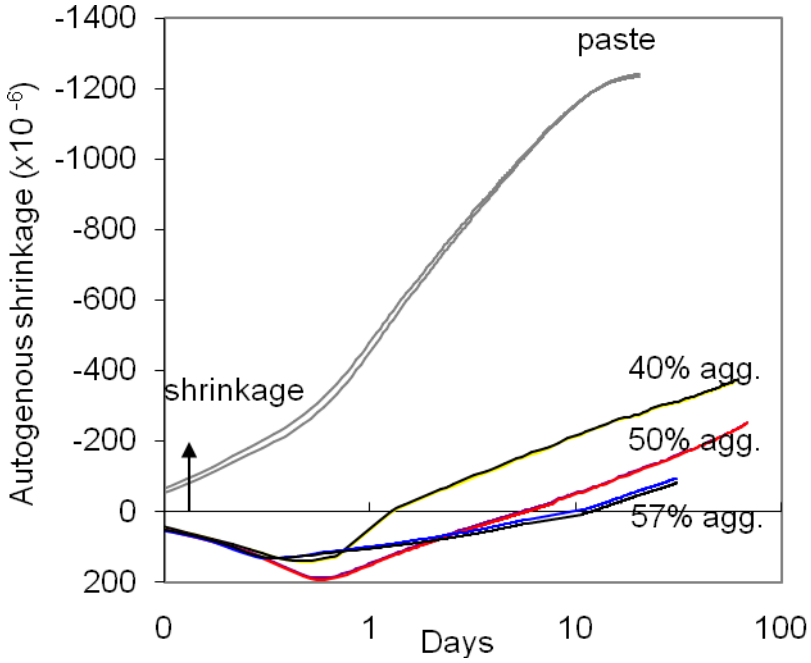
-1400
-1200
-1000
-800
-600
-400
-200
0
200
Autogenous shrinkage (x10 -6)
paste
shrinkage
40% agg.
50% agg.
57% agg.
0
1
Days
10
100

(a)

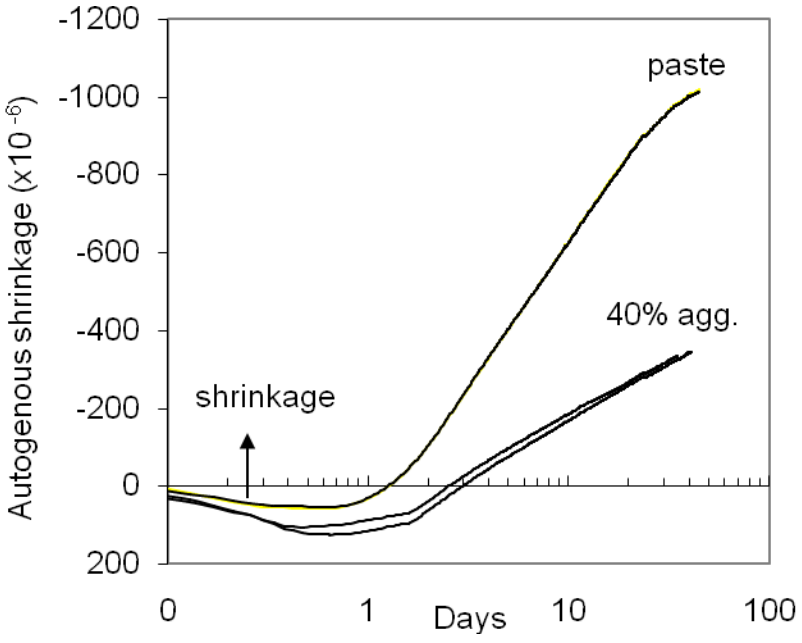
-1200
-1000
-800
-600
-400
-200
0
200
Autogenous shrinkage (x10 -6)
paste
40% agg.
shrinkage
0
1
Days
10
100

(b)

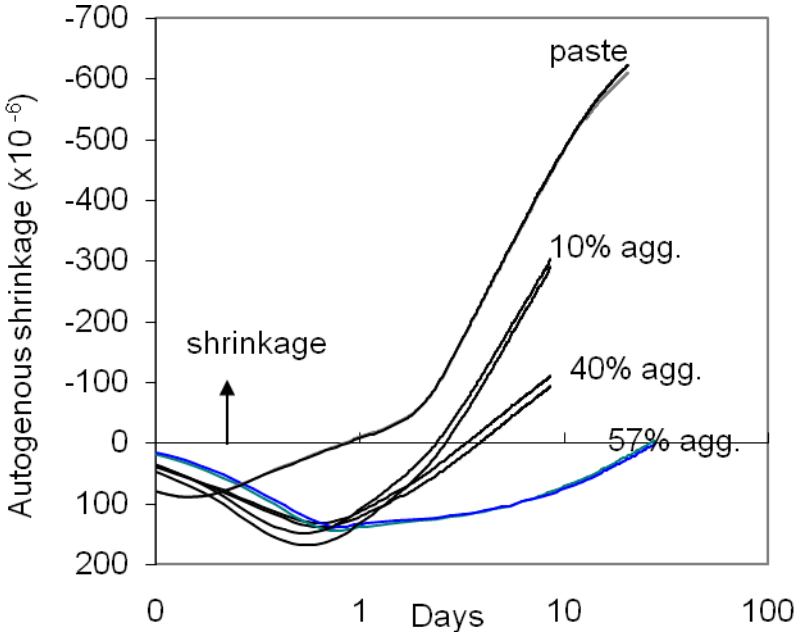

(c)

Figure 5.12 Measured autogenous shrinkage of cement paste and concrete with different aggregate contents (a) *w/cm*=0.35; (b) *w/cm*=0.4; (c) *w/cm*=0.45

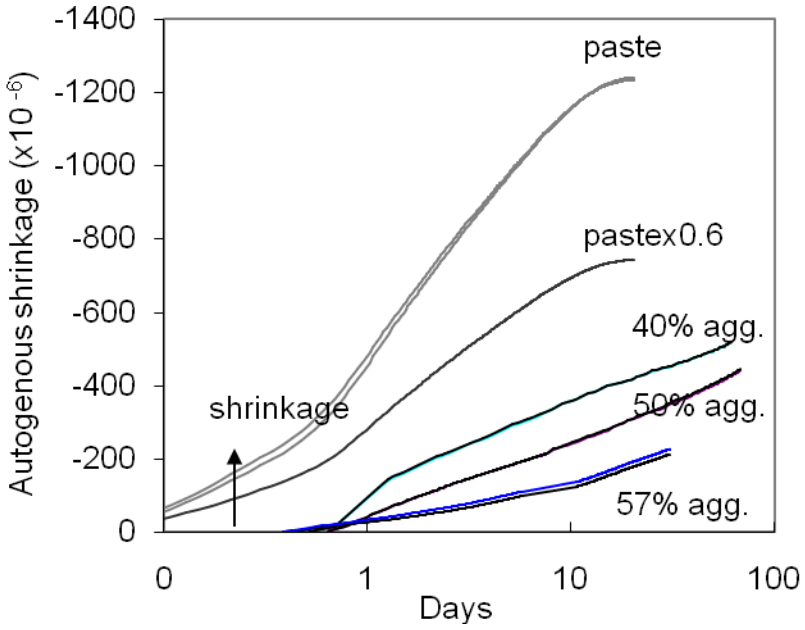

(a)

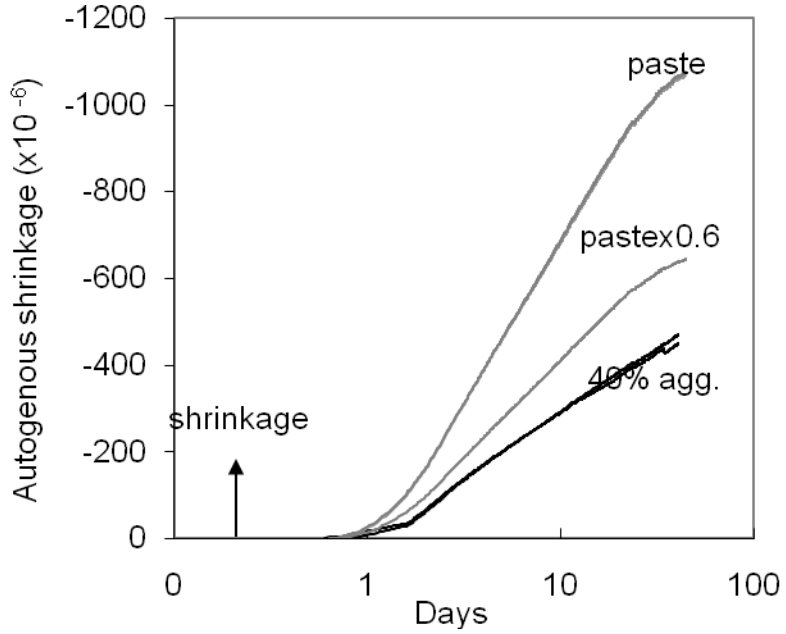

(b)

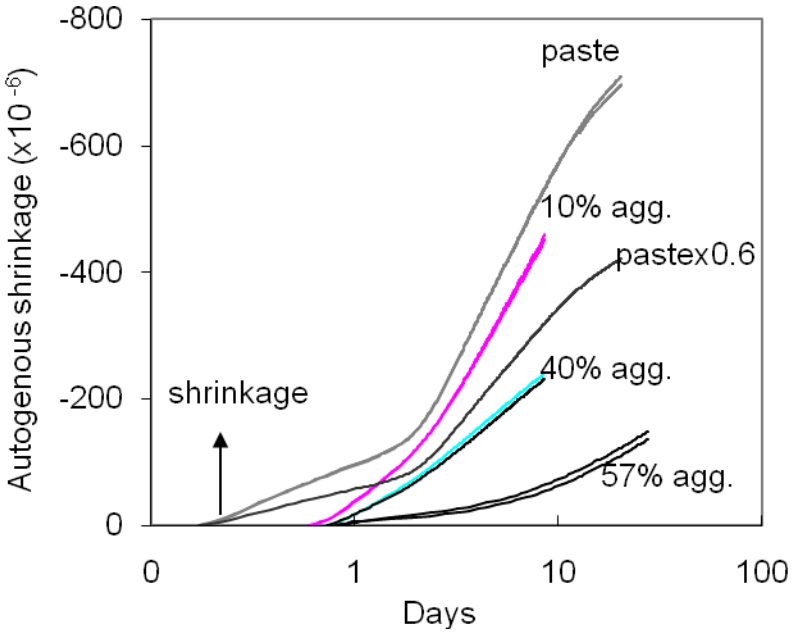

(c)

Figure 5.13 Normalized autogenous shrinkage of cement paste and concrete with different aggregate contents (a) *w/cm*=0.35; (b) *w/cm*=0.4; (c) *w/cm*=0.45

5.3.2 Composite Models

The autogenous shrinkage of concrete mixtures is difficult to capture due to many techniques involved during the measurements, i.e. the specimen size, the external friction reduction, sealing conditions. And thus, fewer data can be found in literature for concrete mixtures. However, some composite models [Pickett 1956, Hansen and Nielsen 1965, Hobbs 1969] originally developed for predicting concrete drying shrinkage might be useful in predicting autogenous shrinkage of concrete.

In these models, concrete is assumed to consist of two phases, namely aggregate particles dispersed in a cement paste matrix. Concrete shrinkage is a function of the paste shrinkage, the stiffness of the paste and of the aggregate, and the aggregate volume concentration.

For Pickett's model which is extensively studied and improved in this work, the formula is derived by considering the restraining effect of one small spherical aggregate particle embedded in a large body of a shrinking concrete [Pickett 1956]. The concrete surrounding the aggregate particle is considered as a homogeneous material and both the aggregate particles and the concrete are assumed to be elastic. If the particle is small compared to the shortest distance from it to the concrete surface, no great error will be introduced by treating the concrete as spherical with a radius equal to that distance as demonstrated in **Figure 5.14**. According to Timoshenko and Goodier [1951], the restraint of the small sphere as the large sphere tends to shrink will cause the following stresses in the large sphere:

$$\sigma_r = -\frac{qa^3}{r^3}\frac{b^3 - r^3}{b^3 - a^3} \qquad \text{Eq. 5.21}$$

$$\sigma_t = \frac{qa^3}{2r^3}\frac{b^3 + 2r^3}{b^3 - a^3} \qquad \text{Eq. 5.22}$$

where, σ_r = normal stress in the radial direction

σ_t = normal stresses perpendicular to the radius

r = radial coordinate

a = radius of inner sphere

b = radius of outer sphere

q = unit pressure between inner and outer spheres

The radial displacement δ_r in the outer sphere caused by the restraint of the inner sphere, referred to the unrestrained position is:

$$\delta_r = \frac{r}{E_C}\left[(1-\nu_C)\sigma_t - \nu_C\sigma_r\right] \qquad \text{Eq. 5.23}$$

where E_C and ν_C are Young's modulus and Poisson's ratio, respectively, for the outer sphere (concrete).

And thus, the restraint of the inner sphere has reduced the volume shrinkage of the total body by the amount:

$$4\pi b^2 \delta_r\big|_{r=b} = \frac{3q\Delta V}{E_C}\left(\frac{1-\nu_C}{2}\right)\frac{3b^3}{b^3-a^3} \qquad \text{Eq. 5.24}$$

where $\Delta V = \frac{4}{3}\pi a^3$ is the volume of the small sphere.

If the inner restraint was not present, the outer sphere would have reduced in volume by $3SV$, where S is the unit linear shrinkage and V is the total volume. Therefore, the reduction of shrinkage volume expressed as in Eq. 5.24 may be rewritten as:

$$-3\Delta SV = \frac{3q\Delta V}{E_C}\left(\frac{1-\nu_C}{2}\right)\frac{3b^3}{b^3-a^3} \qquad \text{Eq. 5.25}$$

In order to obtain the final form of the Pickett's model, it needs another expression to eliminate the unit pressure q. This is done by considering the reduction in the volume of the inner sphere caused by q, which is equal to the reduced space available to it within the large sphere:

$$\frac{3q\Delta V}{E_A}(1-2\nu_A) = 3S\Delta V - 4\pi a^2 \delta_r\big|_{r=a} \qquad \text{Eq. 5.26}$$

where E_A and ν_A are Young's modulus and Poisson's ratio, respectively, for the inner sphere (aggregate).

Equating Eq. 5.25 and Eq. 5.26 through q and setting $b/a = \infty$ gives:

$$-\Delta SV = \alpha_p S\Delta V \qquad \text{Eq. 5.27}$$

where,

$$\alpha_P = \frac{3 \cdot (1 - \nu_C)}{1 + \nu_C + 2 \cdot (1 - 2\nu_A) \cdot E_C / E_A} \qquad \text{Eq. 5.28}$$

As more particles are added, the increase in particle volume per unit volume of mix will be:

$$\Delta\phi_A = \frac{\phi_A V + \Delta V}{V + \Delta V} - \phi_A = (1 - \phi_A)\frac{\Delta V}{V + \Delta V} \qquad \text{Eq. 5.29}$$

where ϕ_A is the volume fraction of the particles.

Combining Eq. 5.27 and Eq. 5.29 results in Eq. 5.30 and its differential form Eq. 5.31:

$$\frac{\Delta S}{S} = -\frac{\alpha_p \Delta\phi_A}{1 - \phi_A}\frac{V + \Delta V}{V} \qquad \text{Eq. 5.30}$$

$$\frac{dS}{S} = -\frac{\alpha_p d\phi_A}{1 - \phi_A} \qquad \text{Eq. 5.31}$$

By assuming α_p is independent of ϕ_A, Eq. 5.31 integrates to:

$$S = S_0 (1 - \phi_A)^{\alpha_p} \qquad \text{Eq. 5.32}$$

where S_0 is the shrinkage that would occur if no particle were present.

For a concrete mixture, Eq. 5.32 is rewritten as the final form of Pickett's model:

$$\varepsilon_C = \varepsilon_P \cdot (1 - \phi_A)^{\alpha_p} \qquad \text{Eq. 5.33}$$

where, ε_C is the shrinkage of concrete, ε_P is the shrinkage of the paste, and α_P is the aggregate restraining factor.

According to Eq. 5.28 and 5.33, concrete shrinkage equals to paste shrinkage only when the ratio $E_C / E_A \to \infty$, that is $E_A \to 0$.

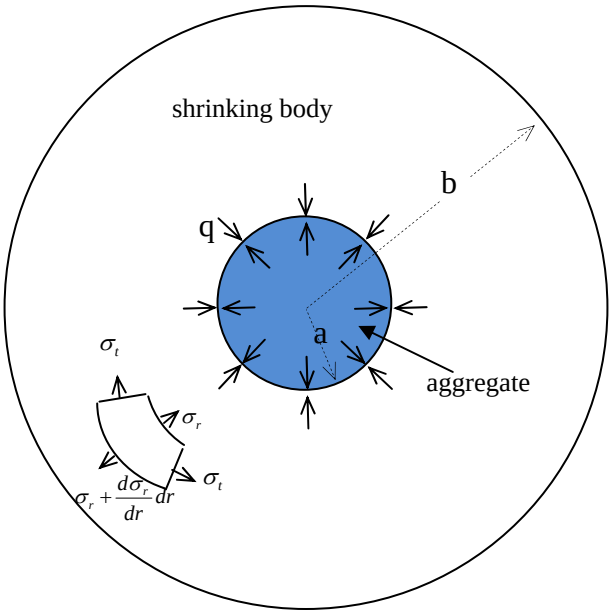

Figure 5.14 Schematic illustration of the small spherical aggregate particle within a concrete sphere [after Hansen and Nielsen 1965]

5.3.3 Application of Pickett's Model to Concrete Autogenous Shrinkage Predictions

Pickett's model was originally developed for predicting concrete drying shrinkage as a function of paste shrinkage and aggregate concentration [Pickett 1956]. However, it is considered more appropriate here in predicting autogenous shrinkage. This is because unlike drying shrinkage, autogenous shrinkage is a result of uniform relative humidity reduction from self-desiccation and no shrinkage gradient exists across the concrete section.

The reduction in concrete autogenous shrinkage has been modelled using Pickett's model by a few researchers [Tazawa et al. 2000, Hammer et al. 2002, Lura 2003, Grasley 2006]. These predictions, however, have arrived rather different conclusions. Tazawa et al. [2000] found good agreement between the measured and the predicted autogenous shrinkage of concrete at 28 days. According to Hammer et al. [2002], on the other hand, it was not successful to use Pickett's model for predicting concrete autogenous shrinkage.

A recent objection to using Pickett's model for predicting concrete autogenous shrinkage may relate to the viscoelastic behavior of cement paste. Lura [2003] has pointed out that the creep of cement paste might need to be considered in the model for

better prediction. According to Grasley et al. [2005], the newly developed theoretical model based on Pickett's model accounting for creep of cement paste gave adequate fit for the materials studied.

However, inappropriate conclusion can be made on Pickett's modeling if the autogenous shrinkage is not measured accurately on cement paste and concrete, as this will certainly cause discrepancy between the predicted and measured autogenous shrinkage.

In this study, the Pickett's model is further justified through fitting measured autogenous shrinkage of concrete with varying paste contents and *w/cm* ratios. According to Eq. 5.28 and 5.33, the inputs to Pickett's model are: ε_P, the measured autogenous shrinkage of cement paste; E_C, measured elastic Young's modulus of concrete (see **Figure 5.15**); E_A =70GPa, the elastic Young's modulus of limestone aggregate and sand, was taken from [Alexander 1996]; the Poisson's ratio for concrete and aggregate were assumed to be v_C =0.2 and v_A =0.2, respectively.

The predicted and measured autogenous shrinkage of concrete is shown in **Figure 5.16** through **Figure 5.18** for *w/cm* ranging from 0.35 to 0.45. All the shrinkage curves presented here are relative to the point where the shrinking starts to develop while maintaining time axis unchanged.

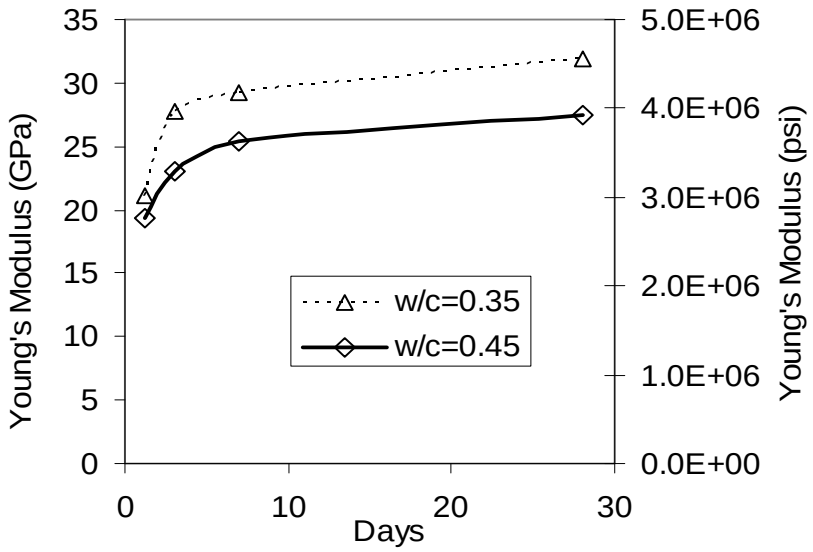

Figure 5.15 Measured Young's modulus for portland cement concrete, aggregate content =57%

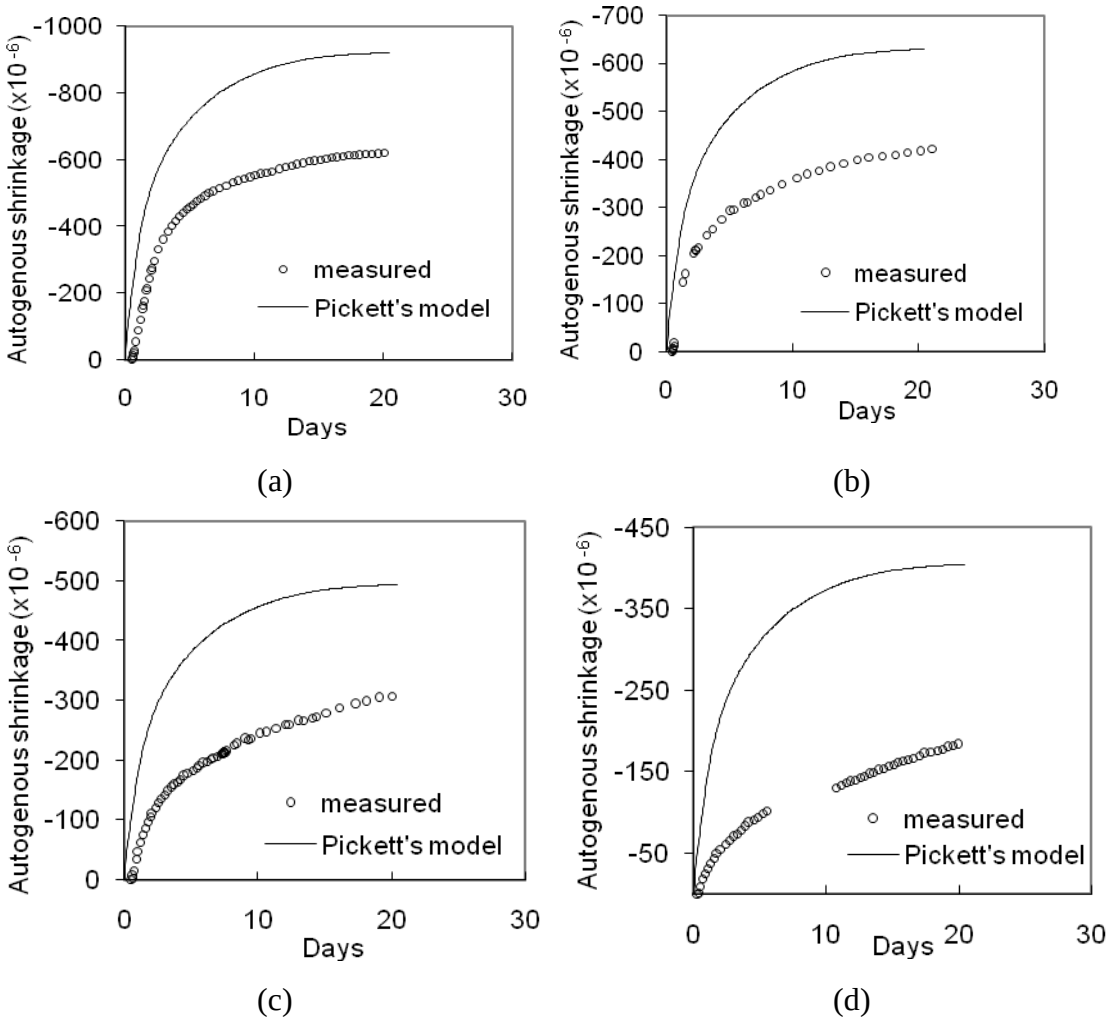

Figure 5.16 Measured and predicted autogenous shrinkage using Pickett's model for concrete with *w/cm*=0.35 and (a) ϕ_A =20%; (b) ϕ_A =40%; (c) ϕ_A =50%; (d) ϕ_A =57%

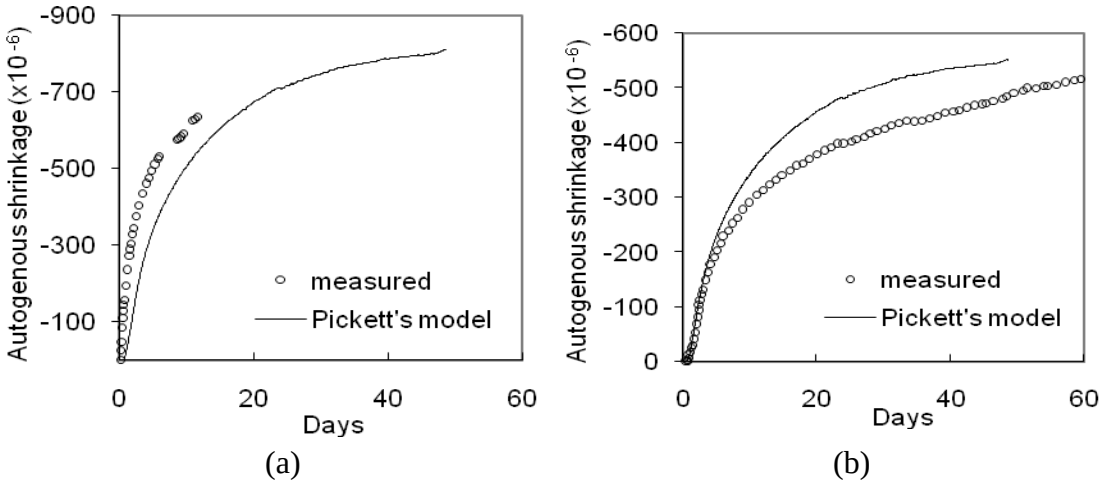

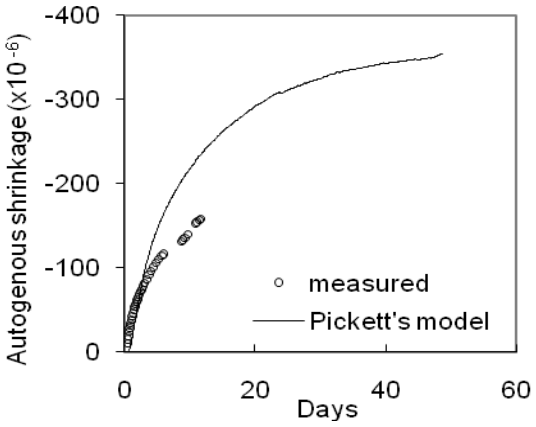

(c)

Figure 5.17 Measured and predicted autogenous shrinkage using Pickett's model for concrete with *w/cm*=0.4 (a) ϕ_A=20%; (b) ϕ_A=40%; (c) ϕ_A=57%

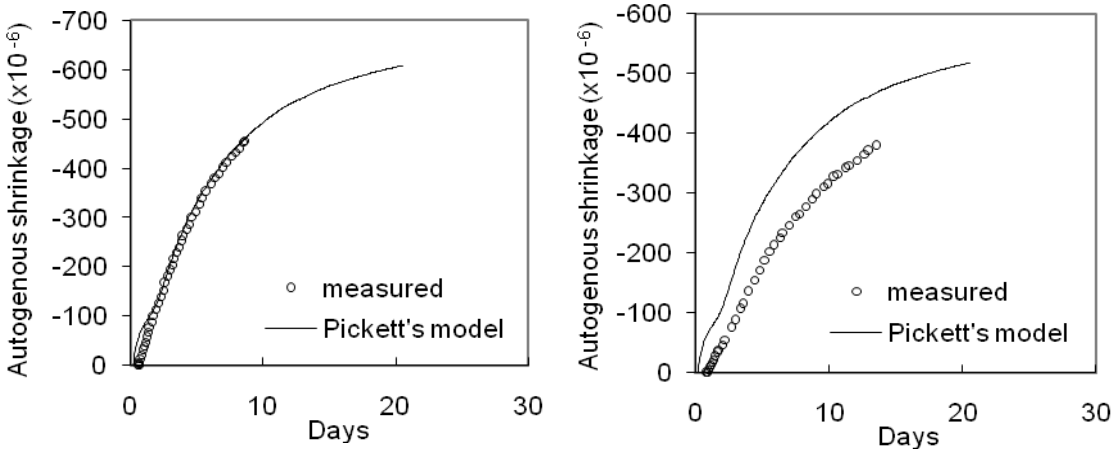

(a)

(b)

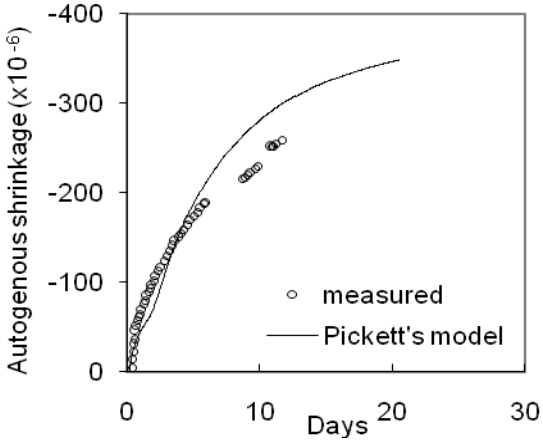

(c)

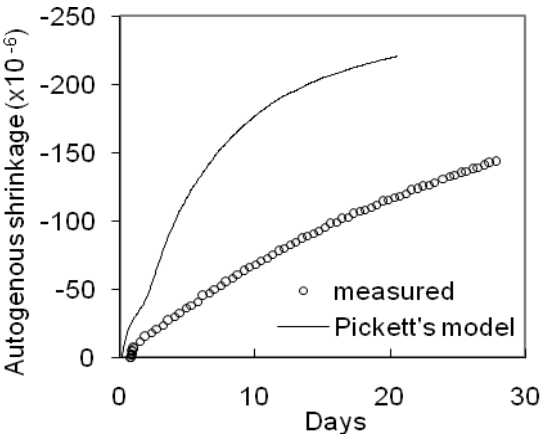

(d)

Figure 5.18 Measured and predicted autogenous shrinkage using Pickett's mode for concrete with *w/cm*=0.45 and (a) ϕ_A=10%; (b) ϕ_A=20%; (c) ϕ_A=40%; (d) ϕ_A=57%

It can be seen that Pickett's model overestimates autogenous shrinkage, especially for concrete with greater aggregate contents and lower *w/cm*. This is possibly attributed to: (1) microcracking which develops on the interface of the shrinking paste and the nonshrinking aggregates. Upon shrinking, cement paste surrounding an aggregate will subject to hoop tensile stress due to the restraining effect from the non-shrinking aggregate as demonstrated in **Figure 5.19**. Cracks perpendicular to the interface may occur in the paste phase. This will result in debonding between paste and aggregate and thus the reduction of the global shrinkage of the concrete. Moon et al. [2005] discovered that higher internal stresses develop in concrete with higher volume fraction of aggregate and thus reduces the overall free shrinkage in a composite material. This explains why the elastic-theory-based Pickett's model overestimates autogenous shrinkage in a composite with high aggregate content. As more shrinkage occurs in low *w/cm* system, larger hoop tensile stresses and more microcracking form in these systems. And thus, less autogenous shrinkage is measured when compared to the Pickett's model predictions; (2) the autogenous shrinkage may not be fully captured for concrete with high aggregate volume because of the aggregate's proximity effects, the external friction and the size limitation of the measuring rig.

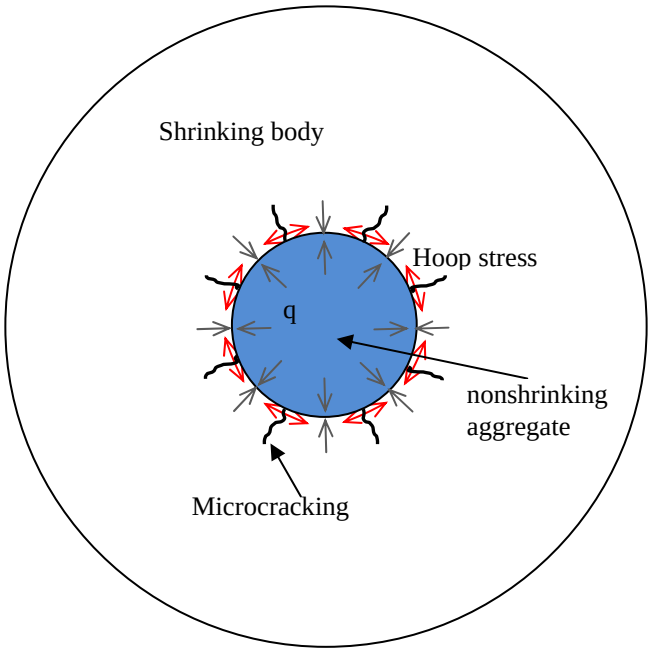

Figure 5.19 Schematic illustration of the microcracking generated on the interface of the nonshrinking spherical aggregate and the shrinking body

Another factor that is worthy to discuss is the creep effect in cement paste. Creep will cause a lower concrete shrinkage as the capillary stresses causing shrinkage are relaxed over time. Concrete containing high paste volume is expected to have more creep [Neville and Dilger 1970], and thus less autogenous shrinkage will be measured when compared to the predictions using Pickett's model. However, this is not the case for the *w/cm*=0.35 and 0.45 systems that the predicted values fit better to the measured autogenous shrinkage for systems with high paste volume. Therefore, the creep effect in cement paste should probably not be considered as a major obstacle in using Pickett's model for predicting concrete autogenous shrinkage. Instead, more efforts may be needed in characterizing the aggregate restraining effect on concrete autogenous shrinkage.

5.3.4 Modified Pickett's Model

Since it is more practically difficult to measure concrete autogenous shrinkage than cement paste, prediction from the paste measurements will be beneficial. As can be seen from **Figure 5.16** to **5.18**, Pickett's model is basically sound in predicting autogenous shrinkage of concrete but there is room for improvement. The autogenous shrinkage is overestimated for concrete with greater aggregate content and lower *w/cm* ratios. It is considered in this study that this discrepancy is due to either the accuracy of the experimental measurement or the microcracking on the paste-aggregate interface rather than the model itself. Following is the procedure of developing modified Pickett's model.

By plotting the aggregate content vs. the measured autogenous shrinkage as shown in **Figure 5.20**, a relationship is observed, that can be fit using Pickett's equation. A unique n value is determined for each age and for different systems as listed in **Figure 5.20**. Thus, Eq. 5.33 can be alternatively expressed as:

$$\varepsilon_c = \varepsilon_p \cdot \left(1 - \phi_A\right)^n \qquad \text{Eq. 5.34}$$

where, n is a time-dependent parameter for a certain system. The autogenous shrinkage of concrete at different aggregate content can be possibly predicted if n is known.

Note that n is determined based on the autogenous shrinkage data of concrete containing aggregate less than 50% by volume. This is because Pickett's model captures concrete autogenous shrinkage very well within this aggregate content range as

demonstrated in **Figure 5.18**. For concretes with aggregate content greater than 50%, the autogenous shrinkage data will be used for verifying the modified Pickett's model.

As a time-dependent factor, n is determined and plotted vs. time for the *w/cm*=0.35, 0.4 and 0.45 systems. As can be seen from **Figure 5.21**, n decreases with ages and ranges between 1 to 3. For drying shrinkage, however, Pickett [1956] found n is 1.7. L'Hermite [1960] gave a range of n which is between 1.2 and 1.7 for mortars and concretes made using different aggregates. According to Neville [1964], n can range from 1 to 2.

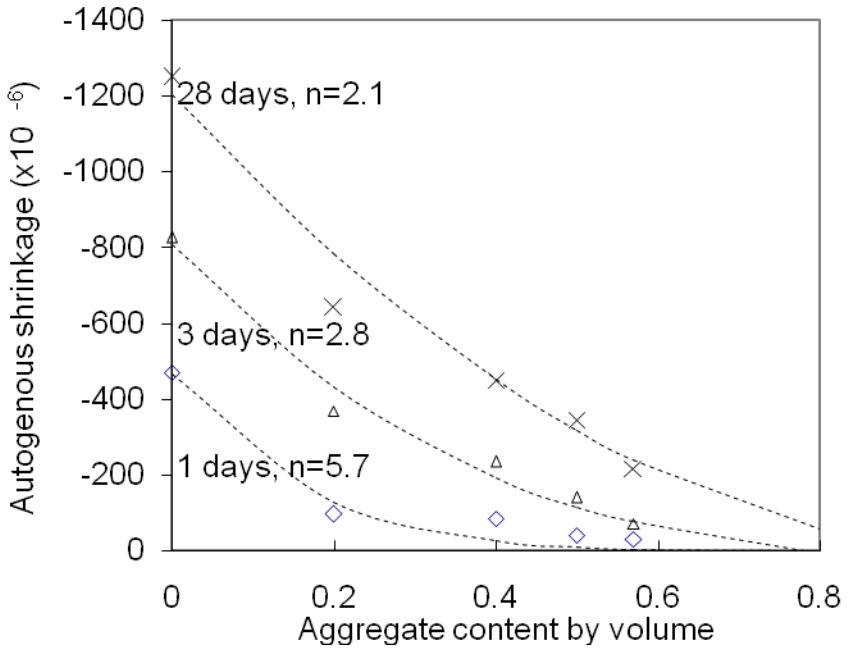

(a)

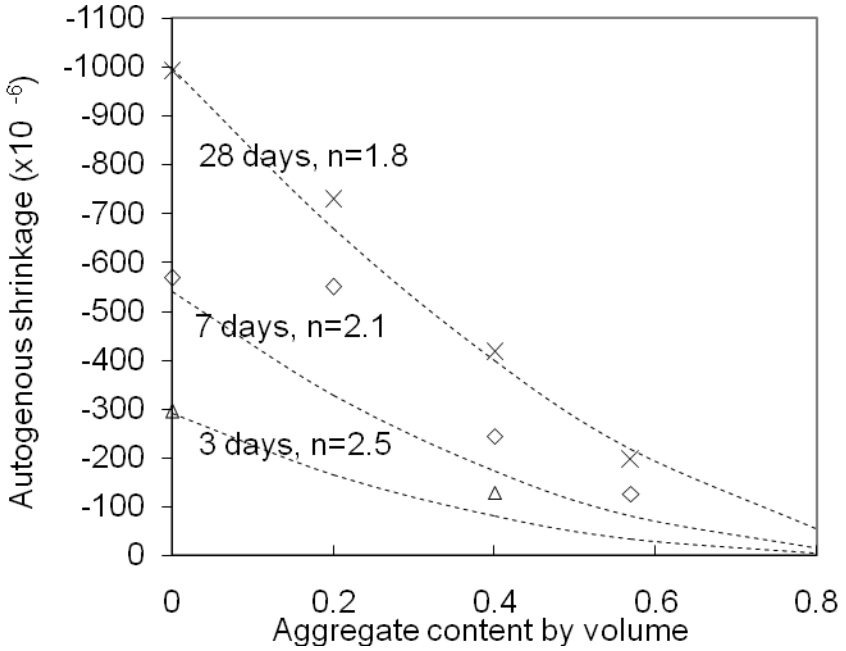

(b)

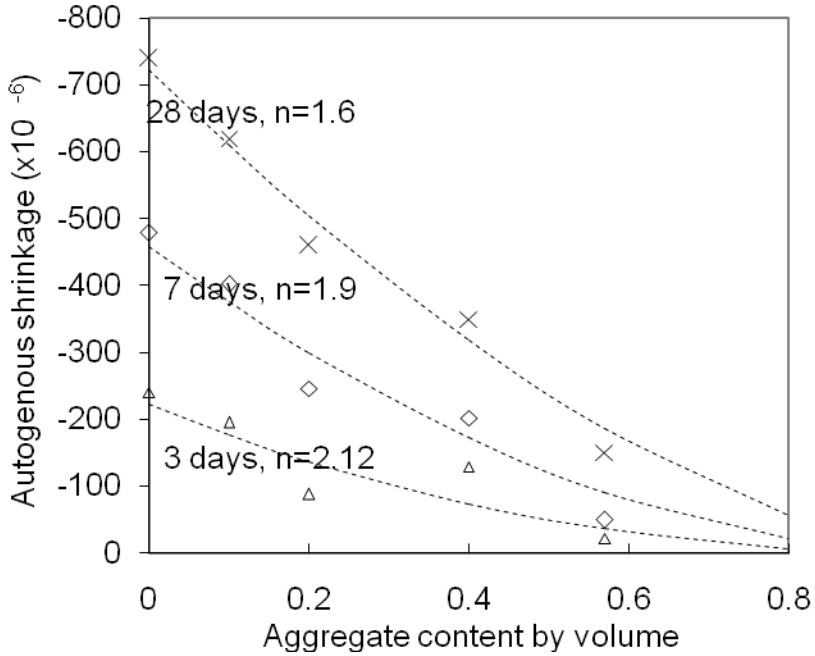

(c)

Figure 5.20 Relationship between aggregate content and autogenous shrinkage of concrete at different ages for (a) *w/cm*=0.35; (b) *w/cm*=0.4; and (c) *w/cm*=0.45

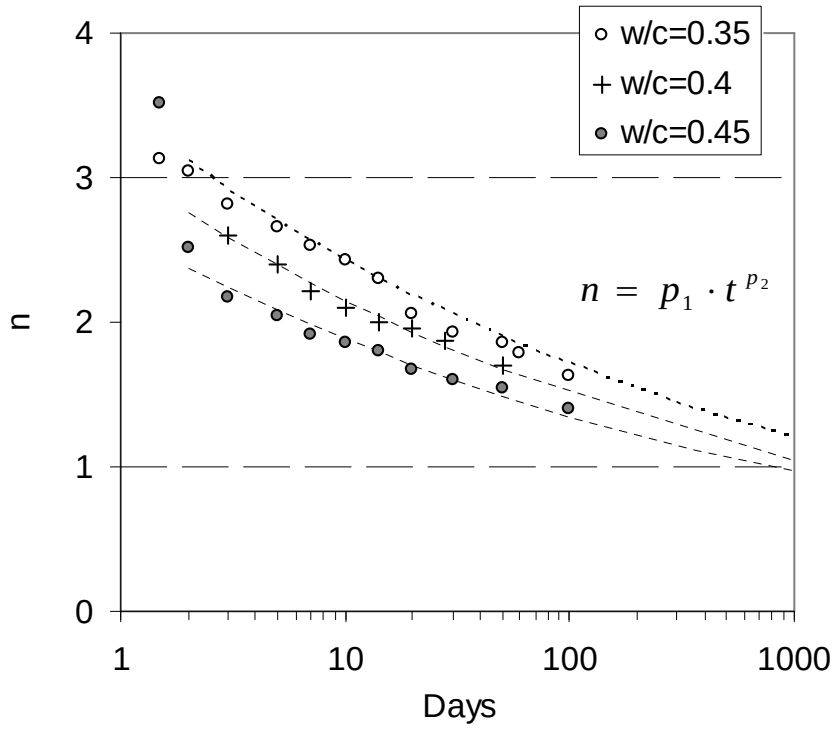

Figure 5.21 Predicted *n* values in modified Pickett's model

As shown in **Figure 5.21**, n can be expressed as a function of time for different *w/cm* systems:

$$n = p_1 \cdot t^{p_2} \qquad \text{Eq. 5.35}$$

where, p_1 and p_2 are parameters. As indicated in **Figure 5.22**, they are functions of *w/cm*. Thus, Eq. 5.35 can be further expressed as:

$$n = (q_1 + q_2 \cdot (w/c)) \cdot t^{q_3 + q_4 \cdot (w/c)} \qquad \text{Eq. 5.36}$$

Knowing paste autogenous shrinkage and the n values, the corresponding concrete autogenous shrinkage can be predicted using Eq. 5.34, which is the modified Pickett's model developed in this study. This modified Pickett's model is verified by comparing the predicted and measured autogenous shrinkage for systems (*w/cm*=0.35, ϕ_A=57%; *w/cm*=0.4, ϕ_A=57%; *w/cm*=0.45, ϕ_A=57%) that were not used for determining n values.

As shown in **Figure 5.23**, the modified Pickett's model provides a much improved prediction as compared to the measured values. The predicted concrete autogenous shrinkage can be used for assessing early-age cracking risk.

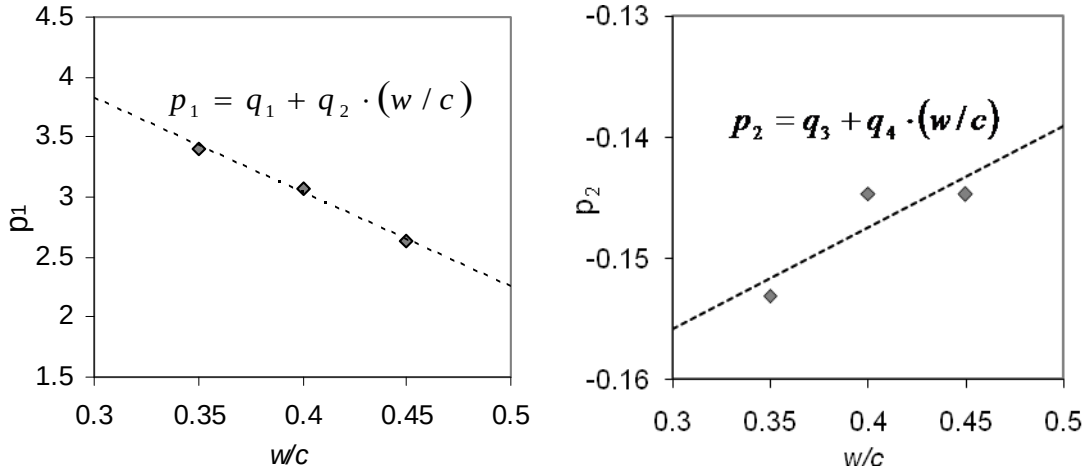

Figure 5.22 Parameters needed for prediction of n

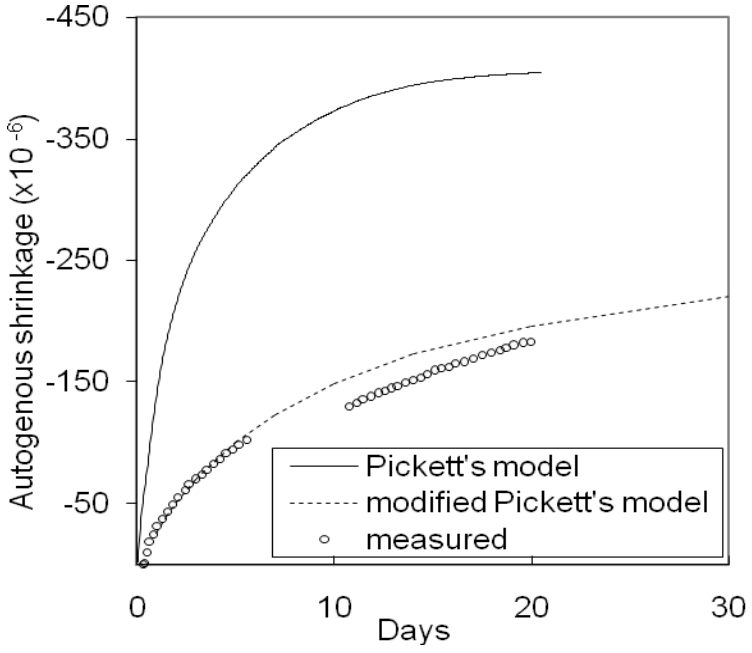

(a)

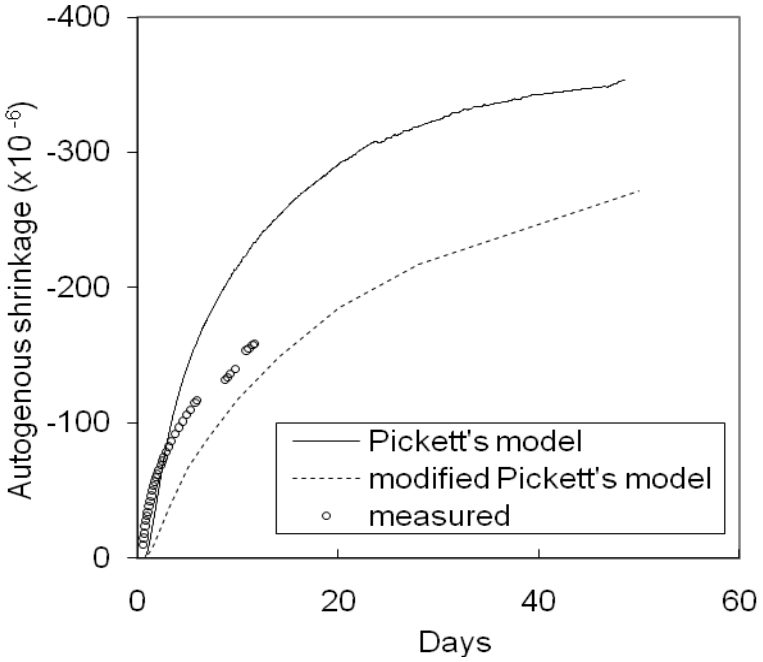

(b)

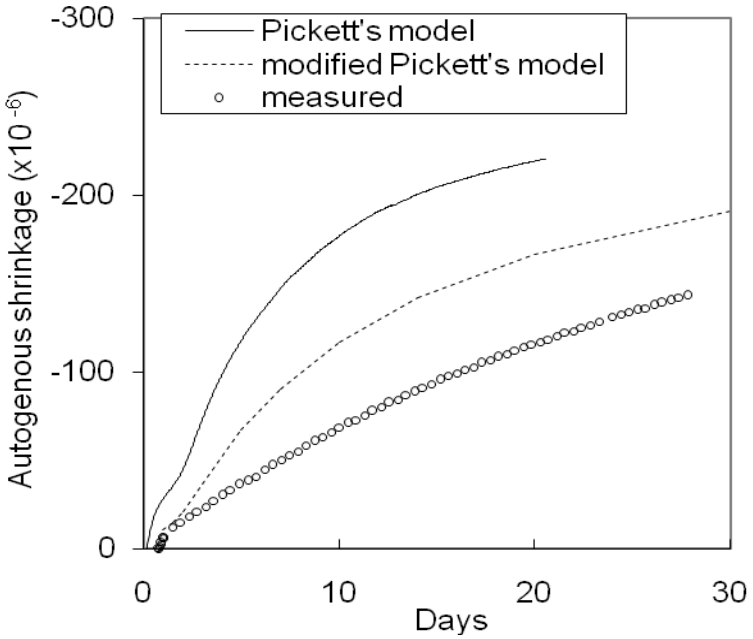

(c)

Figure 5.23 Comparison of Pickett's model and modified Pickett's model for autogenous shrinkage predictions (a) *w/cm*=0.35, ϕ_A=57%; (b) *w/cm*=0.4, ϕ_A=57%; (c) *w/cm*=0.45, ϕ_A=57%

5.4 ASSESSMENT OF EARLY-AGE CRACKING RISK DUE TO RESTRAINED AUTOGENOUS SHRINKAGE

When concrete hydrates, it shrinks. If concrete is prevented from shrinking freely, tensile stress develops [Weiss 1999]. The concrete can be expected to crack when the induced stress exceeds the materials strength.

Two major driving forces are responsible for early-age cracking: thermal contraction and moisture related shrinkage. Upon casting there is a temperature rise in concrete due to the initially accelerated cement hydration, which is followed by a temperature drop from the cooling down of the environmental temperature. Correspondingly, compressive and tensile stresses develop as illustrated in **Figure 5.24**. The zero-stress temperature, $T_{zero-stress}$, corresponds to the temperature when stress becomes from compression to tension. Any temperature below $T_{zero-stress}$ will cause construction and consequently tensile stress if the deformation is restrained.

Moisture related shrinkage, on the other hand, is the response of concrete to internal drying (autogenous shrinkage) from self-desiccation of pores and/or external drying (drying shrinkage) due to moisture exchange between concrete and environment. This study will focus on autogenous shrinkage as it mainly occurs during the early-age.

Calculation of the restrained tensile stress can be complicated, as it depends not only on the amount of the restrained shrinkage but also on the stress relaxation effect and the degree of restraint. The stress development in a hardening concrete structure with thermal and shrinkage being considered is written as:

$$\sigma_{restrained} = \left[\left(T - T_{zero-stress}\right) \cdot CTE + \varepsilon_{shrinkage}\right] \cdot E_{effective} \qquad \text{Eq. 5.37}$$

where,

$$E_{effective} = E_{elastic} \cdot \psi \cdot R \qquad \text{Eq. 5.38}$$

where, $T_{zero-stress}$ is zero-stress temperature; CTE is the coefficient of thermal expansion of concrete; $\varepsilon_{shrinkage}$ is shrinkage strain, and is commonly referred to drying shrinkage. In this study it is considered as autogenous shrinkage; $E_{elastic}$ is elastic modulus of concrete; ψ is relaxation coefficient; R is degree of restraint.

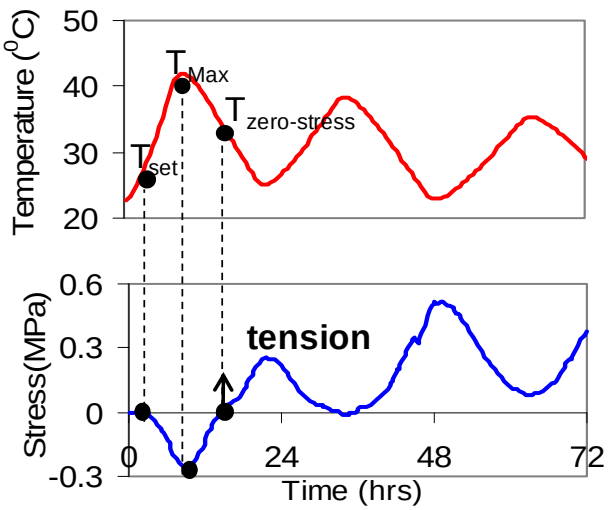

Figure 5.24 Development of temperature and stresses in a restrained concrete specimen

Autogenous shrinkage in concrete would not induce any detrimental effect if the material was homogenous and was allowed to deform freely. However, concrete is a heterogeneous material and usually restrained internally and externally. Restrained shrinkage in concrete can be categorized into three different scales: macroscopic, mesoscopic and microscopic [Bisschop 2002]. The macroscopic scale restraint often being referred to the external restraint is the confinement from the surrounding structures such as subgrade or adjacent structural components. The mesoscopic restraint is from the aggregates or self-restraint due to the moisture gradient. The microscopic restraint is due to the solid phase (for example, the anhydrous cement grains or calcium hydroxide crystals) in the cement paste. Both mesoscopic and microscopic level restraints are referred to as internal restraint in this study.

Figure 5.25 illustrates the generation of tensile stress from macroscopically restrained autogenous shrinkage. The self-induced stresses were measured using a temperature-stress-testing-machine (TSTM) as detailed in Chapter 3.

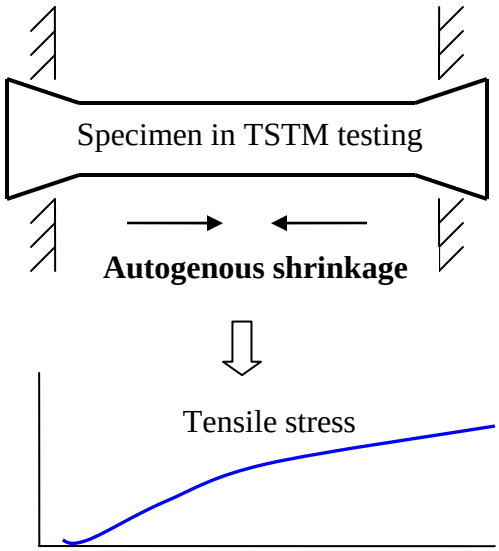

Figure 5.25 Schematic illustration of the generation of tensile stress from restrained autogenous shrinkage deformation

The tensile stresses from restrained autogenous shrinkage alone can be significant. **Figure 5.26** and **5.27** show the development of measured free autogenous deformation and the corresponding self-induced stresses of concretes with two *w/cm* rations, respectively. The concrete under sealed-cured conditions goes to shrinkage following the initial expansion within the first 1 to 2 days. This is consistent with the measured stress development which goes into compression and then tension. The self-induced tensile stresses from restrained autogenous shrinkage can account for 40% of the direct tensile strength after 25 days of sealed curing in concrete with *w/cm*=0.35 and ϕ_A=57%. The direct tensile strength was obtained by breaking TSTM specimens, which is about 70% - 80% of the split tensile strength measured on concrete cylinders. And thus, the restrained stresses from autogenous shrinkage should be considered in assessing early-age cracking, especially for low *w/cm* systems.

By plotting free shrinkage deformation vs. the self-induced stress, a linear constitutive relationship can be obtained as shown in **Figure 5.28**. The slope of the linear curve represents the effective modulus which lumps the effects of elastic modulus, creep effect, and degree of restraint together. This will allow engineers to easily estimate the tensile stress generated in concrete without going through complex calculation if the magnitude of the restrained shrinkage deformation is known. The effecitve modulus

determined in this study ranges from 15% to 20% of the elastic modulus. The effective modulus is small as compared to the elastic modulus. It should be noted that this effective modulus was determined from an direct tension test on concrete specimens. For this type of test, it is hypothesized in this work that the tension occurs mostly in paste phase rather than the aggregate phase because of its discontinuity and very high stiffness. And thus, a lower effective modulus results. For elasic modulus, however, it was measured on concrete cylinders through compression test (ASTM C496) when stiff aggregates greatly contribute to the entire stiffness of the concrete body. This phenomenon is demonstraed in **Figure 5.29**.

To test the hypothesis made here, self-induced stresses should be measured on concrete with different aggregate contents. The same effective modulus should be expected for concretes with different aggregate contents, as the effective modulus is mainly dependent on the flow of the paste phase rather than aggregates.

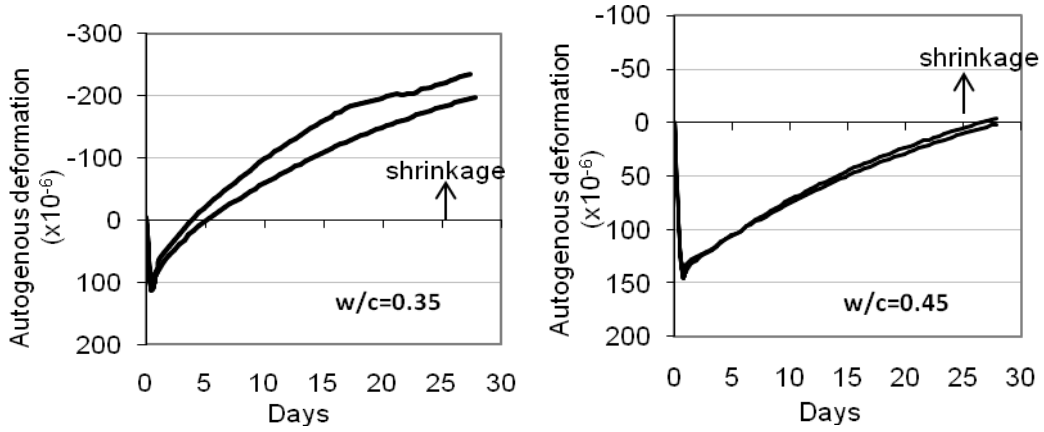

Figure 5.26 Measured free autogenous deformation for concrete with ϕ_A=57% (a) *w/cm*=0.35; (b) *w/cm*=0.45

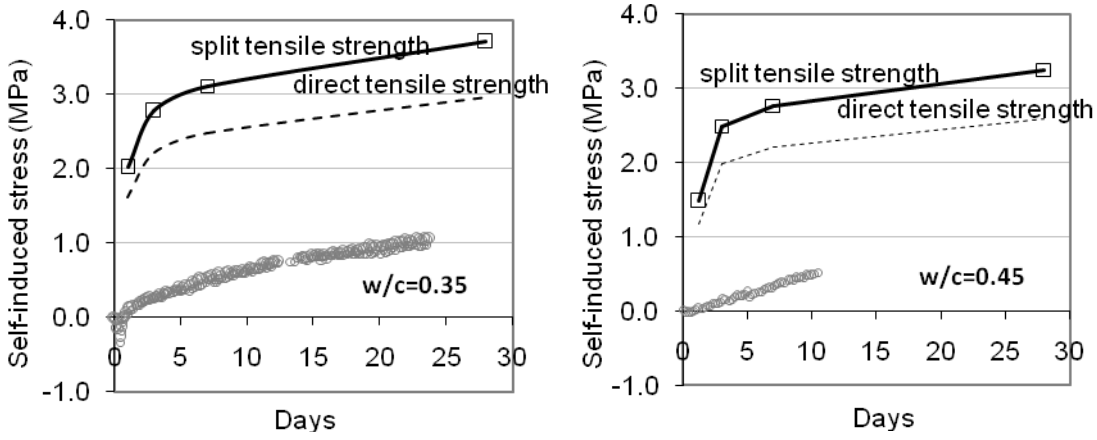

Figure 5.27 Measured stress from restrained autogenous deformation for concrete with ϕ_A=57% (a) *w/cm*=0.35; (b) *w/cm*=0.45

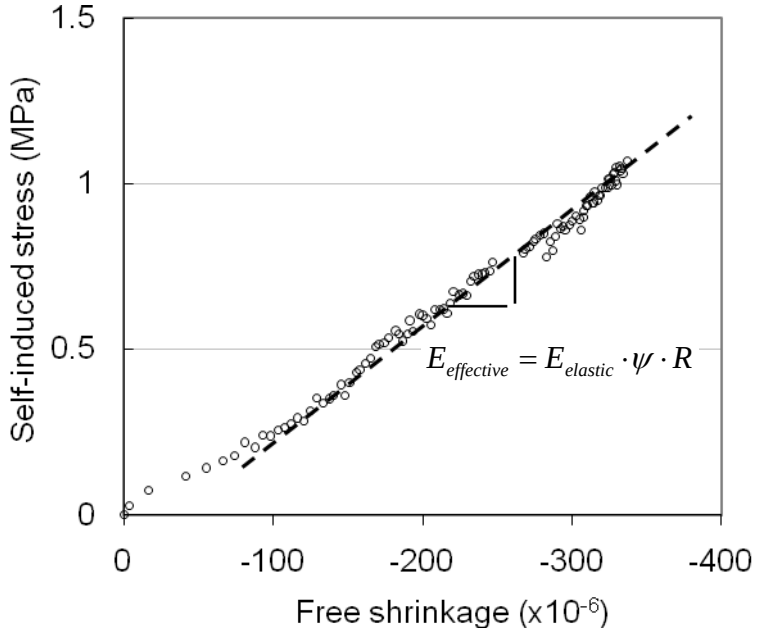

Figure 5.28 Relationship between free shrinkage and self-induced stress, *w/cm*=0.35, ϕ_A=57%

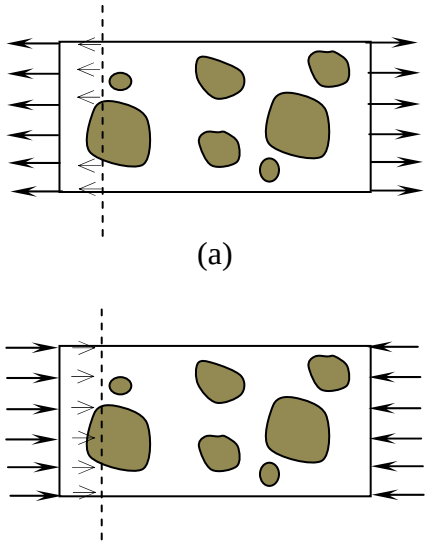

Figure 5.29 Illustration of the stress status in concrete when subjected to (a) tension; (b) compression

5.5 CONCLUSIONS

This chapter provides the experimental results and predictions of autogenous shrinkage of cement paste and concrete systems. The following conclusions can be drawn:

- The F-H model which was originally developed for predicting heat of hydration is found applicable to predict autogenous shrinkage of cement paste including the blended systems (with GGBFS). Chemically bound water may be used as a robustness indicator of autogenous shrinkage, especially for blended paste systems.
- The increase in aggregate volume dramatically reduces the overall autogenous shrinkage of a cementitious composite.
- Pickett's model is found adequate in determining concrete autogenous shrinkage though it was developed for drying shrinkage predictions. A modified Pickett's model is derived by incorporating a shrinkage-stress equilibrium model developed by Pickett with a time-domain model developed by Freiesleben-Hansen and Pedersen, where n is found to be a function of time and *w/cm*. A mathematic expression of n is provided. Thus, wide range of concrete with different *w/cm* ratios can be predicted.

CHAPTER 6

MOISTURE WARPING IN SLABS ON GRADE

6.1 INTRODUCTION

Observations and experiences tell us that when a floor slab or a highway pavement is exposed to water at the slab bottom while the top dries and shrinks, excessive warping deformation (5-6 mm at joint corner) can develop within months after construction [Hveem 1951, Leonards and Harr 1959]. How can this phenomenon be explained? It is well-known from work by Powers and Brownyard [1946] that self-desiccation of pores and consequently the autogenous shrinkage develops in the hydrating cement paste due to the chemical reactions and that this property is especially pronounced for concrete with water-cementitious ratios less than 0.40. This will affect the moisture transport properties of cement paste and thus the moisture deformations in a concrete structure such as slabs on grade.

The major objective of this chapter is to determine: (1) the influence of exposure to wetting at the slab bottom on the joint uplift of a slab; and (2) the cause for this uplift. Work presented here shows that exposure of slab bottom surface to wetting is a key factor. This condition can develop if the sub-surface drainage system is ineffective, leading to a saturated base/subbase condition and water contact with the slab bottom. Finally, a revised theory of moisture warping is provided based on the experimental and numerical studies.

6.2 FIELD INVESTIGATIONS

Curling and warping of a concrete slab, caused by differences in temperature and moisture, respectively, between the top and bottom slab surfaces, are deviations from its original shape. The slab's shape is constantly adapting to the thermal and moisture gradient changes within its cross section. This causes slabs to curl downward when the top surface is warmer than the bottom surface, while an upward curl results when the top of the slab is cooler/drier than the bottom.

The upward-curled slab condition will cause significant portions of the slab in the vicinity of joints unsupported. Joint loading under such conditions can increase the total stresses in the mid-slab region and adversely affect the long-term service life of a concrete pavement [Poblete et al. 1990, Darter et al. 1995, Khazanovich et al. 2000, and Hansen et al. 2002]. The magnitude and location of the maximum slab stresses change as a consequence of loss of slab support and truck axle loading position. The temperature and moisture conditions resulting in permanently upward-curled/warped slabs are most critical for Jointed Plain Concrete Pavement (JPCP). This condition can change the failure mode from bottom-up to top-down transverse cracking, which is typically mid-slab cracking caused by a loss of support at the joint and mid-slab stresses from multi-axle loading at the unsupported joints.

Premature top-down mid-slab transverse cracking has been found to develop rapidly for JPCP projects located in southeastern Michigan [Hansen et al. 2002], as shown in **Figure 6.1**. Surface elevation measurements of the uncracked slabs in these projects were conducted along the outer edge for west-bound (WB) I-96 on warm sunny days in June and July. Slabs were found to be in a permanent upward-curled condition with joint uplift varying from 2 to 4 mm (0.08 to 0.16 in.) as illustrated in **Figure 6.2 and 6.3**.

A total equivalent linear temperature difference (TELTD) between slab top and bottom was found to range from -28^{o}C to -47^{o}C (-50^{o}F to – 85^{o}F) as shown in **Figure 6.3 [**Wei et al. 2006]. These values were obtained by matching the edge uplift from surface profiles with the predicted uplift using ISLAB2000 [Khazanovich et al. 2000]. The concept of TELTD is described in detail by Rao and Roesler [2005].

Considering that field measurements were obtained on hot sunny days and this project was constructed during fall temperature conditions, these uplift results preclude daily curl and built-in curl from a temperature gradient. Thus, the most likely cause for the permanent uplift is moisture warping.

Field coring on these projects shows the presence of water at slab bottom. Dowel corrosion was observed in addition to dowel looseness. Dowels are corroded due to continuous presence of water around dowels, indicating there is retained water at the slab bottom as a result of ineffective drainage. The retained water at slab bottom is suspected to cause uplift in addition to that caused by regular drying shrinkage.

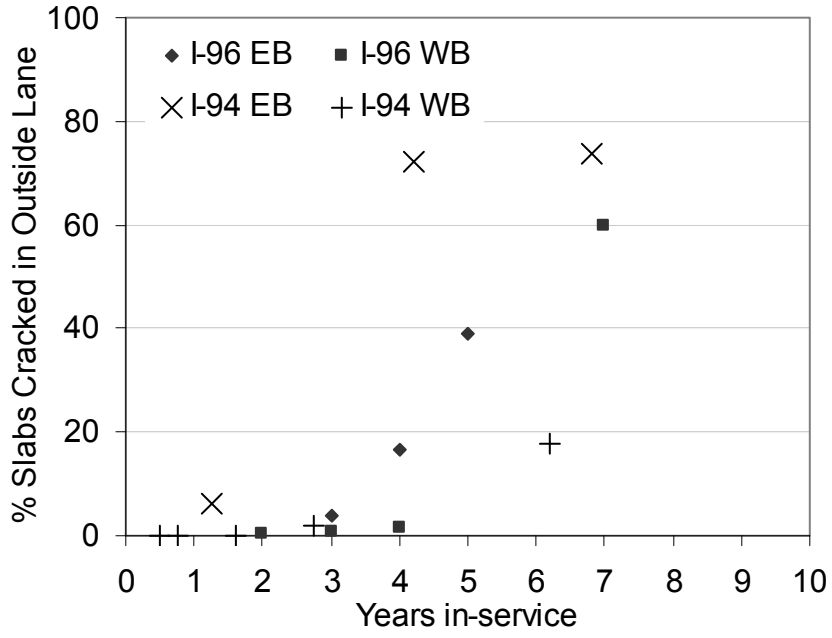

Figure 6.1 Development of pre-mature top-down transverse cracking in two JPCP projects

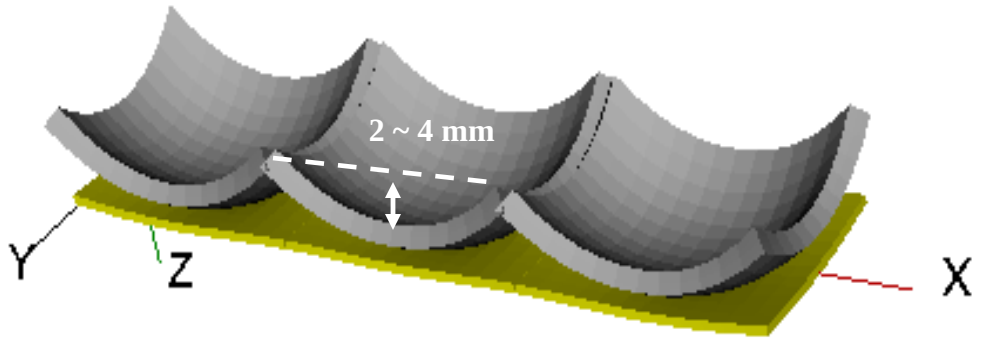

Figure 6.2 Finite element-based (EverFE) rendering of uplift for a JPCP project

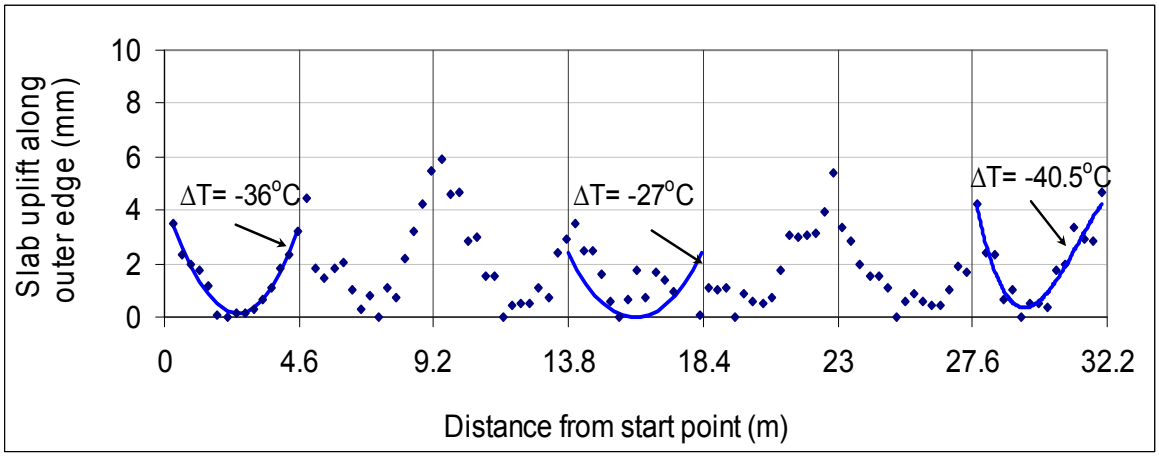

(a)

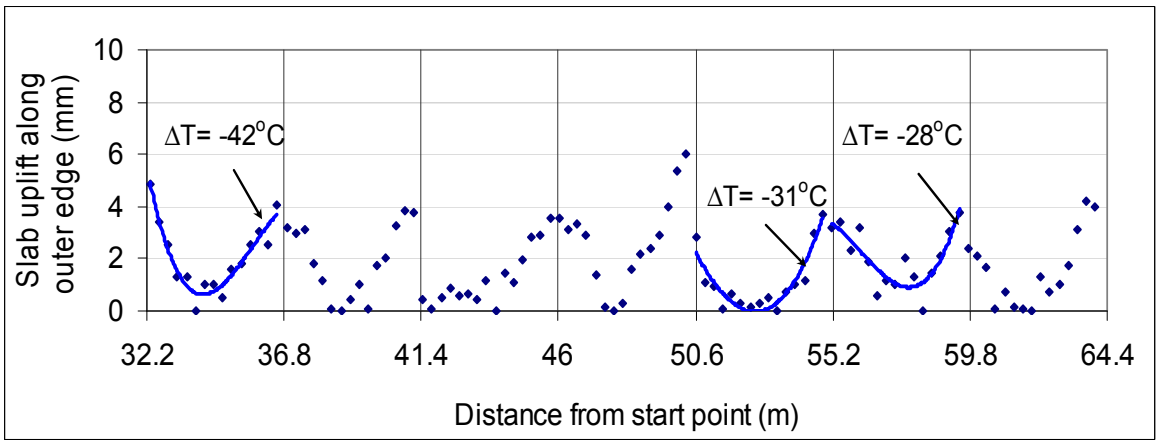

(b)

Figure 6.3 Surface elevation profiles for JPCPs in southeastern Michigan with matching TELTD values listed [Wei et al. 2006]

6.3 EXPERIMENTAL INVESTIGATIONS

It is generally believed that slab warping uplift in Jointed Plain Concrete Pavements (JPCP) is caused by drying shrinkage moisture gradients that develop within the top region of a slab cross section. However, field experiences have shown that excessive moisture warping uplift of joints can develop if a slab on grade is exposed simultaneously to drying at the top and moisture at the bottom surface.

For a better understanding of the mechanisms behind moisture warping, tests were conducted on concrete beams using a modified procedure based on the work by Springenschmid and Plannerer [2001]. The test can determine warping of a concrete beam from simultaneous drying at the top and wetting at the bottom.

In the warping test, the beam length was 2.3 m (7.5 ft) which is half of the JPCP slab length. The beam cross section was 0.2 m (8 in.) in thickness and 0.15 m (5.9 in.) in width. The thickness of concrete beams is comparable to the field slabs typically with thickness ranging from 0.2 m (8 in.) to 0.31 m (12 in.). One end of the beam was fixed to the supporting steel I-beam and the other end was free to lift up as shown in **Figure 6.4**. A dial-gauge was installed to record the amount of warping over time at the free end. To facilitate a through-thickness moisture gradient the top surface was exposured to the environment and the bottom surface was either in contact with water or sealed using water-proof paint dependent on the moisture conditions desired. All the other four sides were sealed.

A typical highway concrete with *w/cm*=0.45 was used throughout. The entire set up was placed in an environmental chamber maintained at constant relative humidity (50%) and temperature (23 ^{o}C/73 ^{o} F). Measurements were initiated after 7 days of sealed curing when the concrete beam has gained enough strength to lift up. Two beams were measured for each moisture conditions.

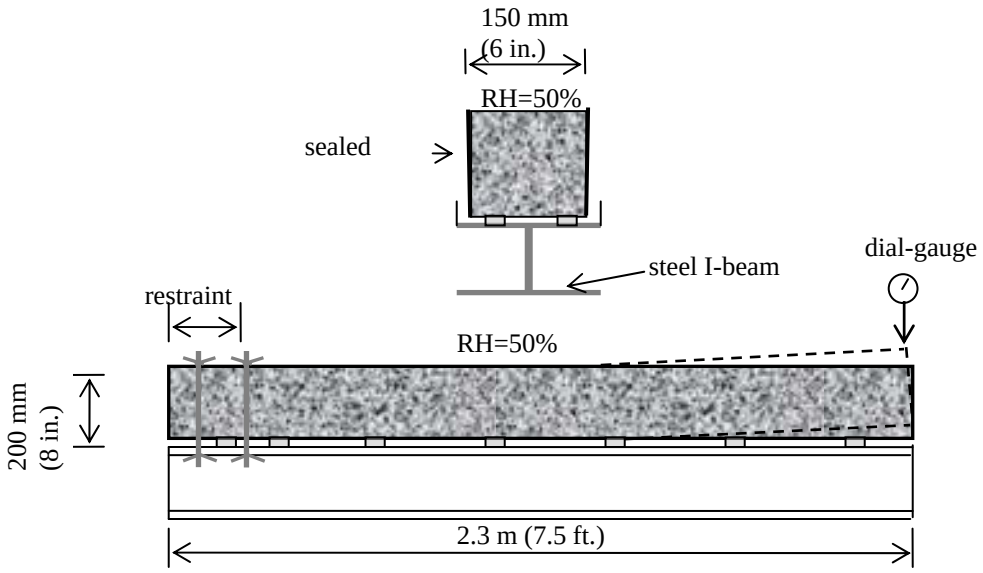

Figure 6.4 Laboratory moisture warping test

As discussed above, two components contribute to moisture warping of a concrete slab if water is present at the slab bottom: one is regular drying shrinkage as a result of moisture loss from external drying at the slab top; the other is water suction at slab bottom. These moisture conditions were simulated in the laboratory on concrete beams to quantify the amount of uplift. As shown in **Figure 6.5**, the first moisture condition is drying at beam top and water present at bottom, corresponding to the case of a field slab resting on a saturated base and drying occurring at the top. The second is drying at the top and the bottom is sealed, simulating moisture loss from the top surface only. The test results of these two moisture conditions will be compared.

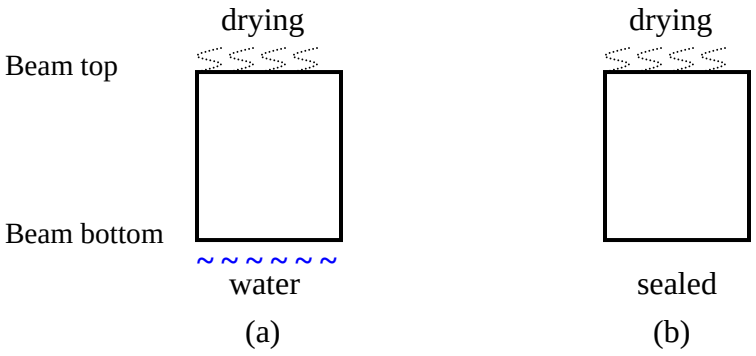

Figure 6.5 Moisture conditions simulated in beam warping test

The test results plotted in **Figure 6.6** show that warping of the concrete beam is the greatest when there is combined drying at the top and wetting at the bottom. The measured beam moisture warping increases with the exposure time and reaches a plateau after 55 days of exposure. A total amount of 2.3 mm (0.09 in.) moisture warping was observed. However, much less uplift was found for drying shrinkage from the top surface alone. The uplift was 0.4 mm (0.016 in.) after the top surface being exposed to a 50% relative humidity environment for 30 days, which is only 20 percent of the uplift induced by the simultaneous drying at the top and wetting at the bottom.

These experimental moisture warping results suggest that a field slab resting on a saturated base (water present at bottom) develop even greater corner uplift than the measured on concrete beams, because the amount of measured warping of concrete beam corresponds to the mid-joint uplift of a slab, which is less than the corner uplift.

The numerically modeling on moisture warping of a field slab is conducted. This gives the same conclusion as the experimental results that simultaneous drying at the top surface and moisture wetting at the bottom surface can result in a severe moisture warping uplift.

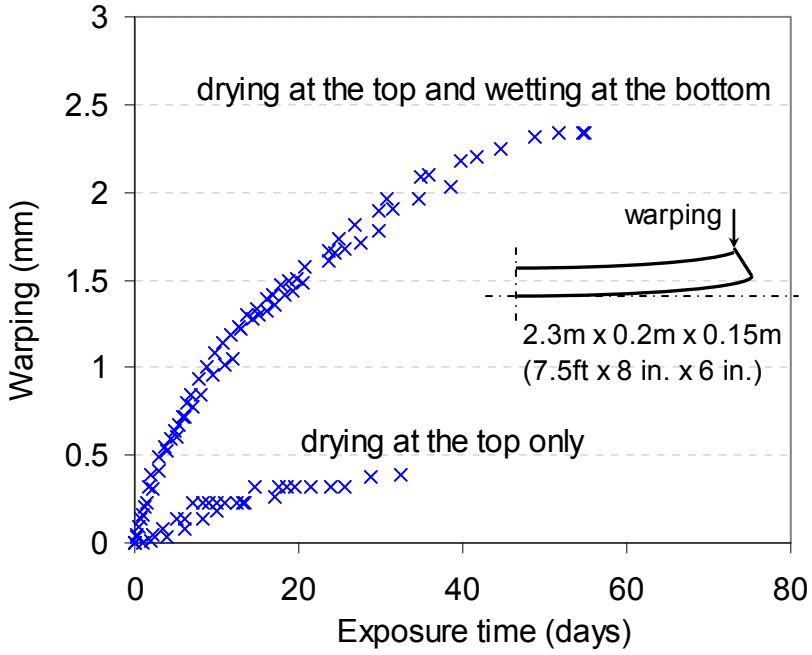

Figure 6.6 Measured beam warping results, *w/cm*=0.45

6.4 FINITE ELEMENT MODELING

6.4.1 Model in MLS and Its Calibration

MLS (Multi Layer Systems) [MLS 2003] is used in this study for numerical modeling on moisture warping of a slab under different hygral conditions. The detailed information on MLS can be found in Chapter 3. The physical and mechanical models that are used include: moisture transport properties, concrete maturity, heat of hydration, and viscoelasticity.

For accurately predicting slab's moisture warping, the physical (moisture transport property) and mechanical properties (creep and relaxation effects) and boundary conditions (surface transfer coefficient) that are used in the modeling are calibrated from beam warping test. This is done through matching the predicted beam warping to the measured results.

The concrete beam tested for moisture warping is modelled in MLS as shown in **Figure 6.7**. Similar to the experimental, the prescribed relative humidity of the external media was set at 50% for the top surface as the beam was exposured to an environment with 50% relative humidity. And the relative humidity was set as 100% for the bottom surface because it was exposed to moisture wetting. Same as the beam test, one end of the beam was fixed. The whole beam was rested on a series of linear springs with very high stiffness of 0.54 MPa/mm which is 10 times the stiffness of a regular base to simulate the very stiff supporting steel I-beam used in the test. These springs act in the downward direction only, which means the springs will not pull on the beam if it curls upward similar to the testing conditions.

Since warping can reduce over time due to the creep and relaxation effect from beam's self-weight, a Maxwell chain model was adopted to take into account this effect by specifying the number of units in the chain, and for each unit the elasticity and the relaxation.

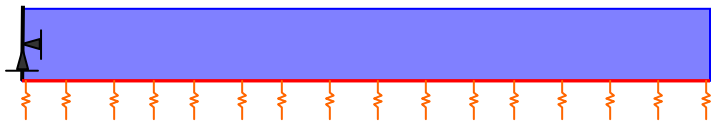

(a) Model in MLS

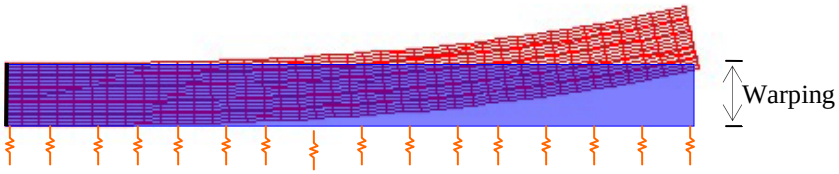

(b) Predicted beam warping

Figure 6.7 Finite element modeling of beam warping test

Modeling of moisture transport in porous materials such as concrete is rather complex due to the fact that water diffusion in concrete is highly non-liner. The diffusion coefficient is strongly dependent on pore humidity. In this study, Bazant's model is used in the modeling as it has proven to give consistent results in many practical cases. The mathematical description of the relation between diffusion coefficient and pore humidity is written as follow [Bazant and Najjar 1972]:

$$C(h) = C_1 \cdot \left(\alpha + \frac{1-\alpha}{1+\left(\frac{1-h}{1-h_t}\right)^{16}} \right) \qquad \text{Eq. 6.1}$$

where, h is pore humidity; $C(h)$ is diffusion coefficient; C_1 is diffusion coefficient for $h=1$; α is reduction factor for dry conditions; h_t is pore humidity at which the diffusion coefficient is equal to $C_1\left(\frac{1+\alpha}{2}\right)$. Among these parameters, C_1 has been found varying over a wide range of $5\text{x}10^{-7}$ to $10\text{x}10^{-6}$ m^2/h dependent on *w/cm*, the use of supplementary cementitious materials, and the binding capacity of cement paste [Bazant and Najjar 1972, Atkinson and Nikerson 1984, Byfors 1987, and Delagrave et al. 1998]. A faster rate of water diffusion with increasing *w/cm* should be used [Wong et al. 2001].

Another hygral property is the surface factor, also known as moisture transfer coefficient of the boundary which determines the moisture flux through the boundary as shown in Eq. 6.2:

$$q_D = f\left(H - H_e\right) \qquad \text{Eq. 6.2}$$

where, q_D is the moisture flux through boundary D (in m/s); f is surface factor for water evaporation (in m/s); H is relative humidity at boundary D; H_e is the environmental relative humidity.

Selecting appropriate hygral parameters as inputs in MLS is essential for determining reasonable moisture humidity profiles within a cross section. This is done by varying the hygral parameters to match the amount of predicted to the laboratory measured beam warping. As shown in **Figure 6.8** the predicted beam warping agrees well with the measured for the two moisture conditions if the following hygral parameters shown in **Table 6.1** were chosen. Therefore, hygral parameters in **Table 6.1** are used as input for predicting slab warping.

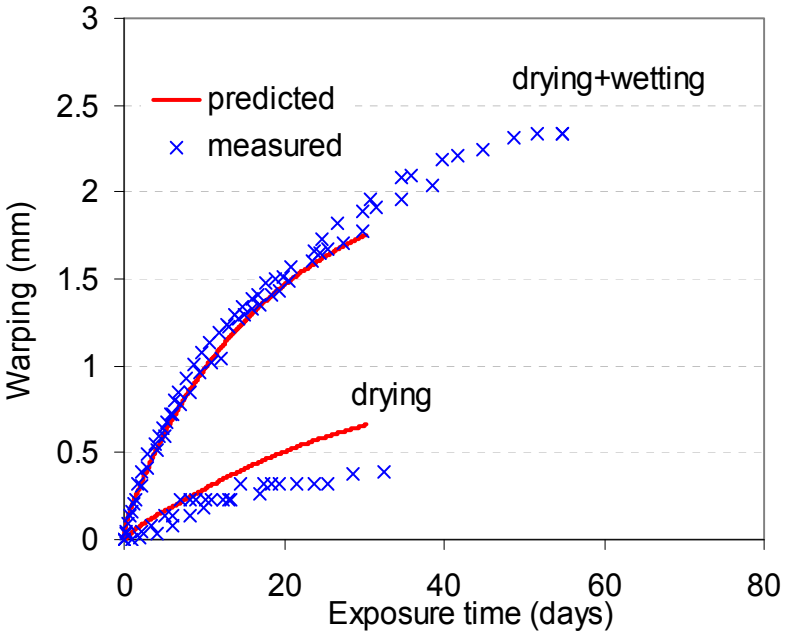

Figure 6.8 FE calibration results for beam warping test, *w/cm*=0.45

Table 6.1 Hygral parameters used in MLS

Diffusion coefficient C_1, m^2/h	$5x10^{-6}$
Surface factor at top surface f_{top}, m/s	$5x10^{-5}$
Surface factor at bottom surface f_{bottom}, m/s	$5x10^{-3}$

6.4.2 Prediction of Slab Warping

A field JPCP slab (4.6m in length, 3.7m in width and 250mm in thickness) is modelled in MLS. As shown in **Figure 6.9**, the slab is resting on an unbound base which is modelled as a series of linear compression springs with a total stiffness of 0.054MPa/mm. These springs act in the downward direction only and will not pull on the slab if it curls upward. This is to model the unbound base conditions where extensive warping has been found in this type of slab-base contact. Since MLS is a 2-D FE program, the predicted warping is actually located at the middle of the transverse joint.

Three moisture conditions are simulated. The first is sealed curing, meaning there is no moisture transport between the concrete and the environments. The second is drying at the top surface which is exposed to an environment with RH=50%. The third is the simultaneous drying at the top (RH=50%) and wetting at the bottom surface where the RH is 100%. The parameters shown in **Table 6.1** are used as inputs for moisture transport properties.

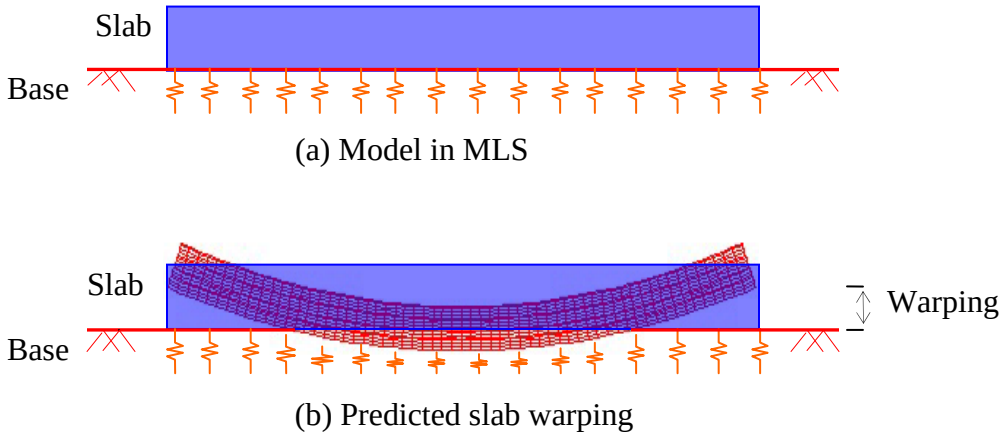

(a) Model in MLS

(b) Predicted slab warping

Figure 6.9 Slab model in MLS modeling

The simultaneous drying at slab top and wetting at slab bottom creates the most severe moisture warping as can be seen from **Figure 6.10**. In this case, the moisture warping reaches 1.7 mm after about 30 days of exposure, which could be higher for the slab corner uplift. The moisture warping is much reduced for the case of drying at slab top alone. There is no moisture warping that is predicted for the sealed curing. Results presented in **Figure 6.10** demonstrate that continued moisture contact at the slab bottom is the cause for excessive corner uplift in highway pavements and floors on grade.

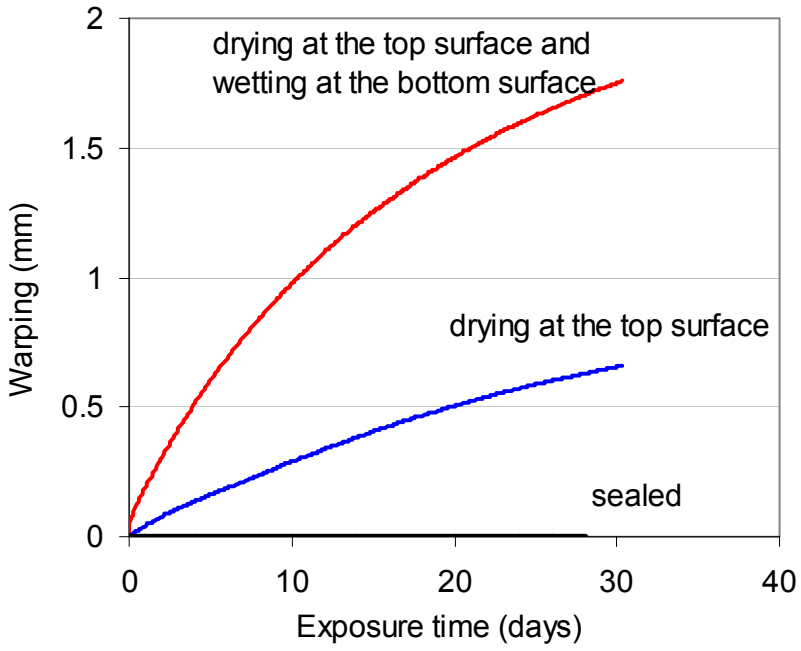

Figure 6.10 Predicted slab warping under three moisture conditions, *w/cm*=0.45

6.5 MECHANISM BEHIND MOISTURE WARPING

6.5.1 Theory of Depercolation of Capillary Pores

Using percolation/depercolation theory may help to develop a basic understanding of the microstructure-property relationships for moisture warping.

Percolation deals with the connectivity of one or more phases in a microstructure. In cementitious materials, such as cement paste, the cement particles are dispersed randomly in the system during the initial stage upon mixing. The free water is filled all

the spaces between these particles, which forms the original water-filled capillary pores. At this time all the capillary pores are connected and free water can transport across the entire section as shown in **Figure 6.11a**. No internal relative humidity reduction and humidity gradient result at this stage. As cement hydration continues, the original cement particles start to percolate into a load-bearing network because the individual cement particles are bonded one to another by the hydration product as shown in **Figure 6.11b**. This microstructural bridging is essential for strength development and mechanical properties. The setting of cement paste is a manifestation of this formation of a percolated solid.

Concurrently, the capillary pores (the original water-filled space) become disconnected (depercolated) as cement hydrates, because the percolated hydration products isolate capillary pores [Powers et al. 1959] as demonstrated in **Figure 6.11b**. The time required for capillary pores to become disconnected depends on *w/cm*. For example, it may take 7 days for *w/cm*=0.45 system to have disconnect pore structures (**Table 6.2**) [Powers et al. 1959]. According to the recent research [Bentz and Garboczi 1991, Geiker 1983, Bentz 1997], the capillary porosity in cement paste is found to become from connected to disconnected at a volume fraction of about 20 % porosity.

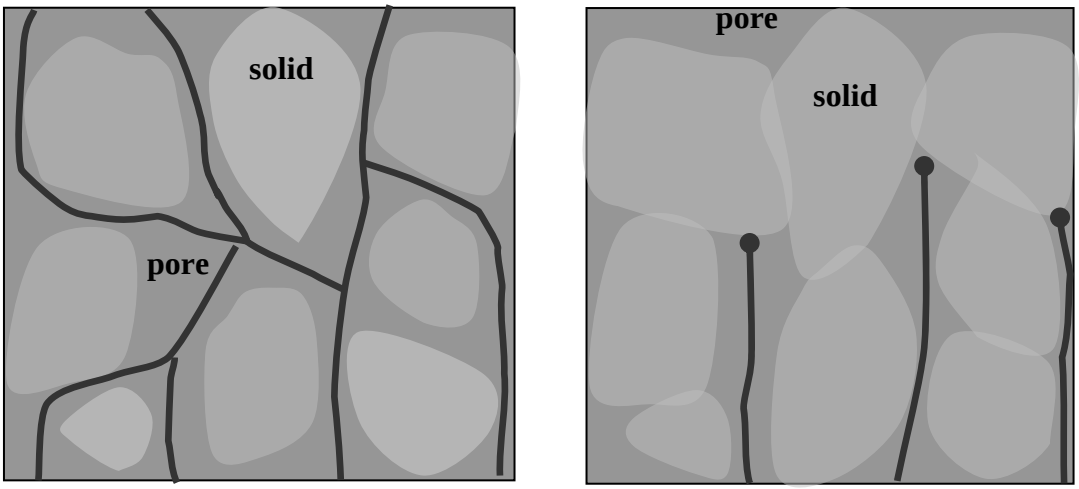

(a) (b)

Figure 6.11 (a) percolation and (b) depercolation of capillary pores in hydrating paste

Table 6.2 Approximate age for the capillary pores to become discontinuous [Powers et al. 1959]

Water-cementitious ratio	Time required
0.4	3 days
0.45	7 days
0.5	14 days
0.6	6 months
0.7	1 year
>0.7	impossible

The depercolation of capillary pores has many implications for the transport properties and durability of cement-based materials as it is limiting moisture transport. In the initial stage of cement hydration, the capillary pores are all connected and the cement paste has a high permeability. With cement hydration capillary pores decrease in volume and size and start to become disconnected. As a consequence, the permeability decreases. When the capillary pores reach a point where no connection exists, a significant and sudden reduction in permeability occurs.

Powers et al. [1959] first noted the significant (sudden) reduction in permeability. The permeability of a cement paste with a depercolated pore structure can be more than a factor of 1000 less than an equivalent age paste with higher *w/cm* and pore structure that remains percolated [Powers et al. 1959]. In most cement pastes (with *w/cm* less than 0.5), after 28 days or so, the permeability would be sufficiently low that any water vapor formed at elevated temperatures would have difficulties in escaping from the system.

Ye [2005] has compared permeability values by different authors as shown in **Figure 6.12**. Though the water permeability of cement paste reported shows significant variations, a significant drop does exist for all the mixes. Ye concluded that the variations are largely dependent on a series of factors, i.e., type of media (O2, N2, water or other liquid solutions) used in permeability tests, sample preparation, influence of

curing conditions (sealed or saturated) and age of the sample and the pressure used in the permeability tests.

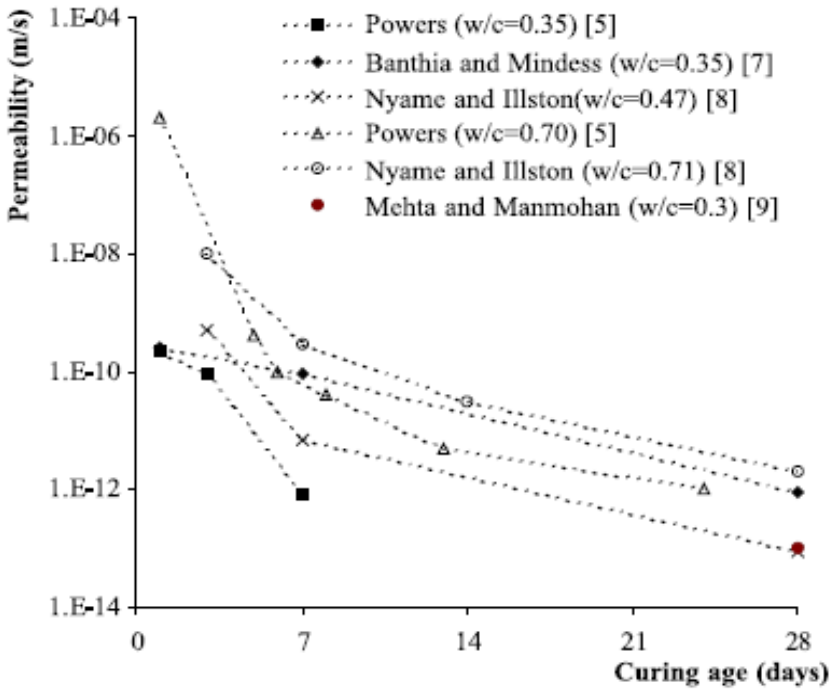

Figure 6.12 Measured permeability changes over time by different authors

6.5.2 Understanding Moisture Warping

The theory of pore depercolation can be used to explain the extensive moisture warping found in JPCPs.

Both experimental and numerical analysis demonstrate that simultaneous drying at the top surface and moisture wetting at the bottom surface results in a much higher moisture warping than caused by drying at the top surface alone. There is no warping in a sealed-cured slab. To help explain these phenomena, the relative humidity profiles within slab's cross section are predicted for each moisture conditions by using MLS (see **Figure 6.13**).

Predictions of relative humidity within the slab cross section are consistent with the predicted moisture warping under different moisture conditions. For the sealed curing, the humidity profile is uniform along slab depth, because it is caused by self-

desiccation which occurs wherever cement hydration exists. As shown in **Figure 6.13a**, the uniform humidity profiles reduce over time and the reduction is rapid at early ages due to the intensive cement hydration. These uniform moisture profiles will not result in moisture warping.

Drying shrinkage uplift develops if the top surface is exposured to drying. As shown in **Figure 6.13b**, the slab is sealed cured for 28 days and then exposured to drying (environment RH=50%) at the top surface for 28 days. The moisture content is reduced in a region near the slab top surface from drying. As drying shrinkage is a diffusion-controlled very slow process, its affecting depth is limited to a small portion near the top surface. Therefore, the warping caused by drying shrinkage alone is considered less severe.

The largest uplift is associated with simultaneous drying shrinkage at the top and moisture wetting at the bottom. According to the predicted humidity profiles (**Figure 6.13c**), the moisture wetting at slab bottom increases the entire humidity gradient within slab cross section as compared to the profiles of drying at slab top alone. This increased humidity gradient will not diminish as moisture transport is hindered within the slab bottom portion and there is not much moisture being transported to the top portion. These findings are consistent with both field observations and experimental investigations.

Beddoe and Springenschmid [1999] also point out that the excessive warping can be found in slab with its bottom surface in contact with water because moisture transport in concrete is limited to a region of less than about 80 mm (3.2 in.) in depth from the exposure surface.

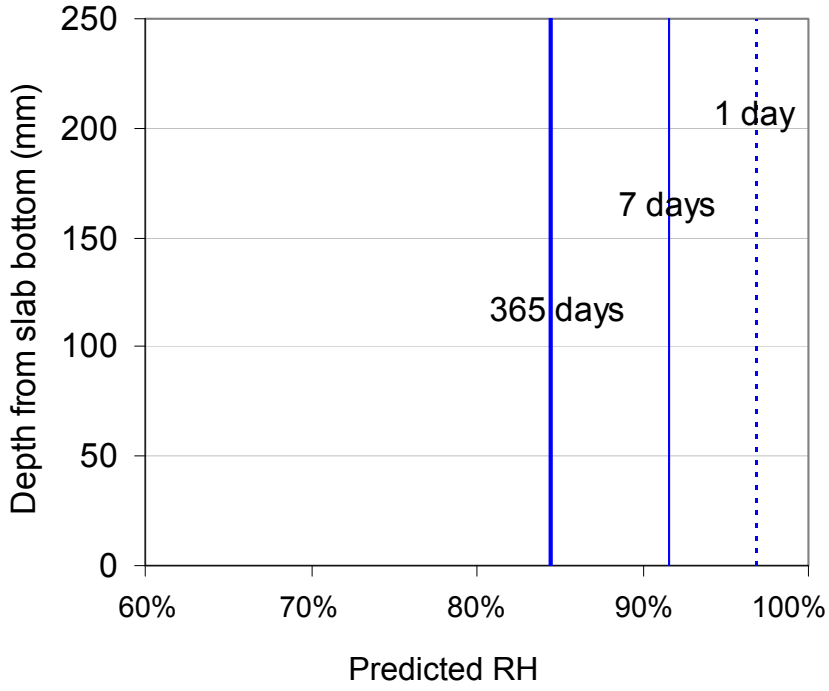
250
200
150
100
50
0
Depth from slab bottom (mm)
1 day
7 days
365 days
60%
70%
80%
90%
100%
Predicted RH

(a)

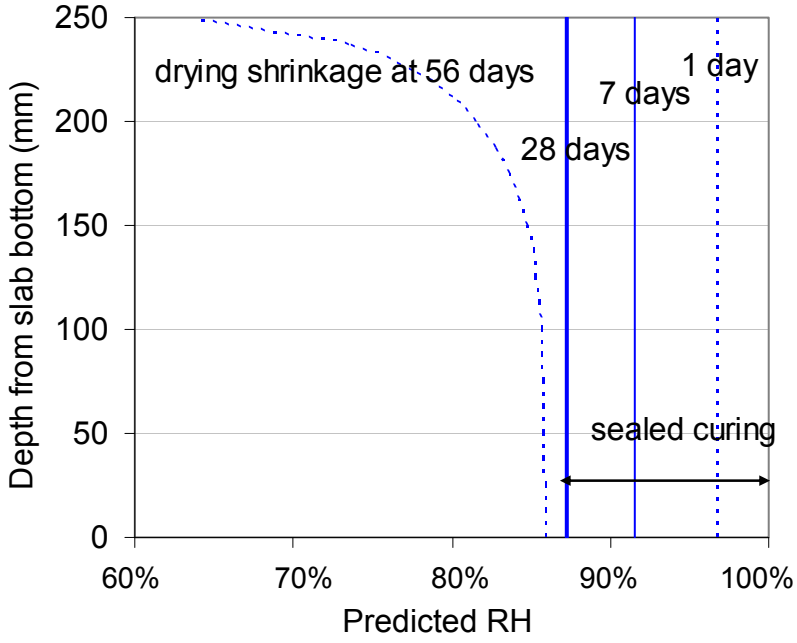
250
200
150
100
50
0
Depth from slab bottom (mm)
drying shrinkage at 56 days
1 day
7 days
28 days
sealed curing
60%
70%
80%
90%
100%
Predicted RH

(b)

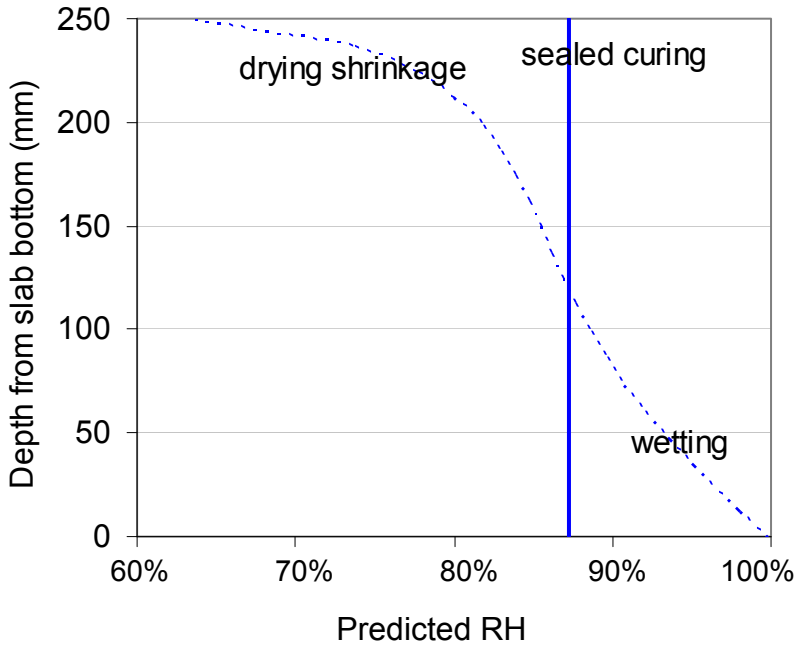

(c)

Figure 6.13 Predicted (a) uniform moisture gradient from sealed curing; (b) non-uniform moisture gradient after 28 days of exposure to drying at slab top following 28 days of sealed curing; (c) combined moisture gradient after 28 days of exposure to drying at top and moisture wetting at slab bottom following 28 days of sealed curing, *w/cm*=0.45

6.6 REVISED MOISTURE WARPING THEORY

Work presented here shows that exposing the slab bottom surface to wetting is a key factor resulting in severe slab moisture warping. This condition can develop if the sub-surface drainage system is ineffective, leaving a saturated base/subbase condition and water contact with the slab bottom. These findings lead to the revised warping theory.

The influence of self-desiccation on water transport seems particularly important, as cement pastes hydrate to depercolate the capillary pore structures. The added warping from continued exposure to moisture at the bottom surface is likely a result of differential autogenous moisture gradient. During cement hydration a volumetric reduction occurs in cement paste, which is proportional to the degree of cement hydration. This phenomenon is known as autogenous shrinkage. As long as the concrete surfaces are sealed during hydration, autogenous shrinkage is uniform and thus no warping develops. Capillary discontinuity is another fundamental factor associated with hydration [Powers et al.

1959]. Once capillary discontinuity has developed, any slab thicker than about 80 mm is subject to nonlinear moisture gradient if one of the free surfaces is exposed to moisture. This is what causes a differential autogenous shrinkage strain. **Figure 6.14** illustrates both phenomena.

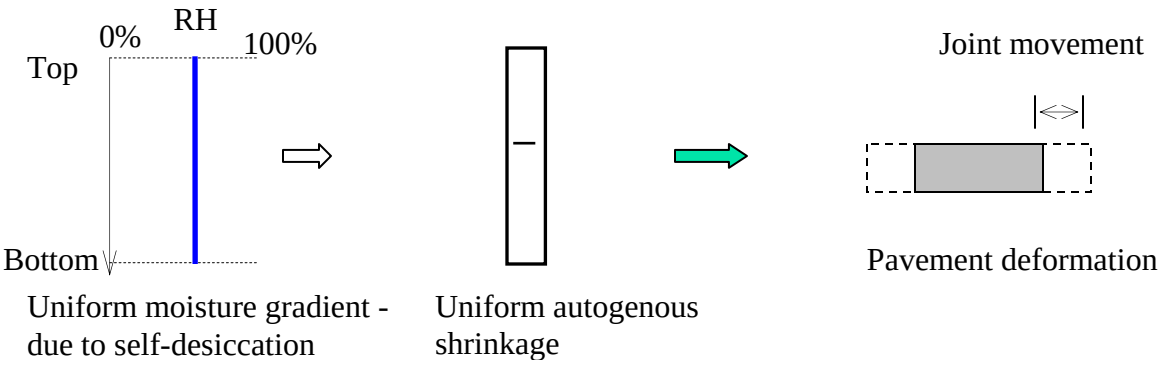

(a)

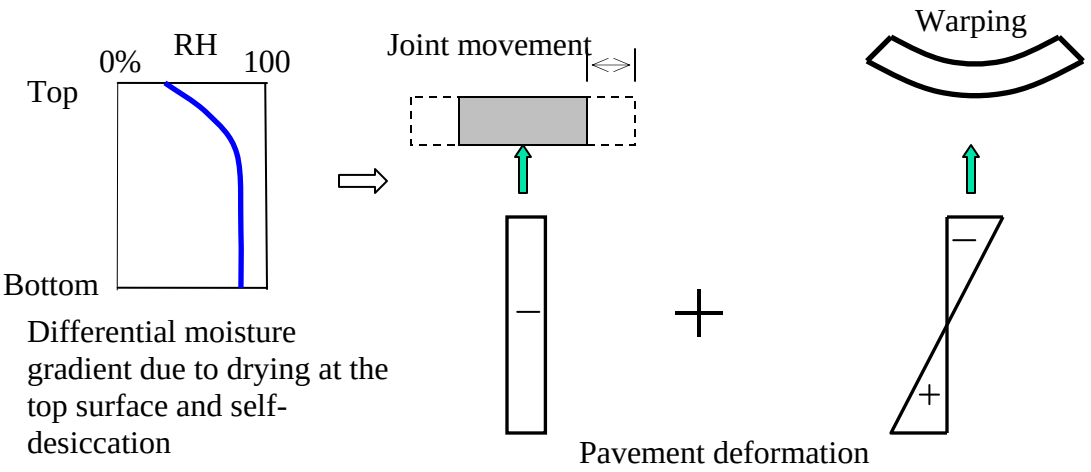

(b)

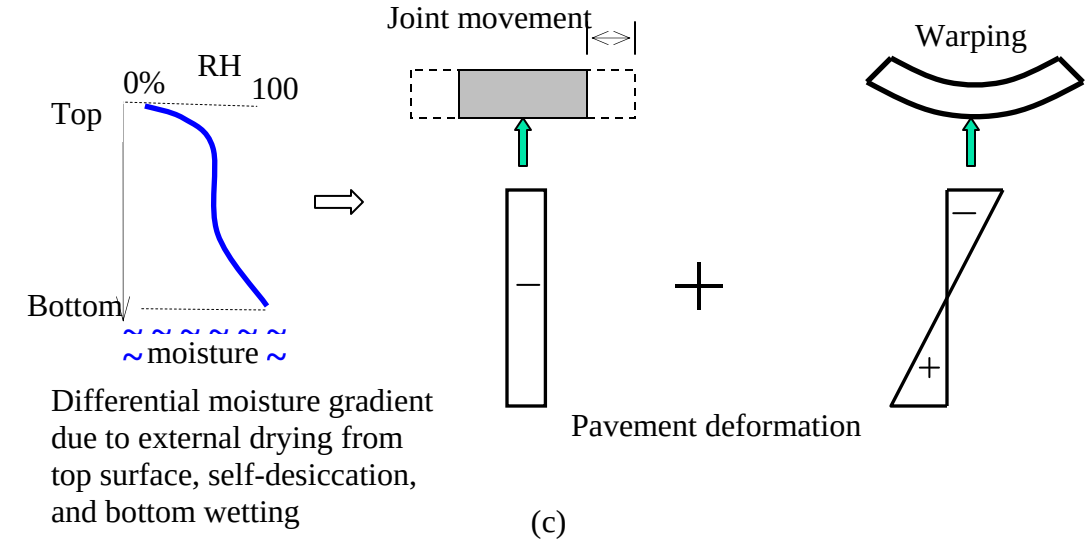

(c)

Figure 6.14 Sketch of slab deformations under different moisture gradients

6.7 CONCLUSIONS

The major conclusions of this chapter are:

- Laboratory moisture warping measurements on concrete beams show that moisture warping uplift from combined drying at top and wetting at bottom is dominant (80% of total), while the uplift from drying shrinkage at 50% RH is only 20% of the total.
- Numerical modeling of hygral effects (i.e. moisture gradient and moisture warping uplift) in concrete slabs on grade explains why combined drying at slab top and exposure to water at the slab bottom cause larger slab uplift than from drying shrinkage gradient alone. Sealed curing alone causes no uplift. However, the decrease in pore humidity as a result of cement hydration renders concrete slabs on grade prone to moisture warping uplift if exposed to water at the bottom from an impermeable subbase.
- Differential autogenous deformation is a major factor in warping of floor slabs on a stiff grade and highway pavement whenever the subbase becomes saturated for an extended period of time. Design specifications and construction practices must address these factors to assure that the expected long-term performance of concrete pavement will occur.

CHAPTER 7

PRE-SOAKED LIGHTWEIGHT FINE AGGREGATE AS ADDITIVES FOR INTERNAL CURING IN CONCRETE

7.1 INTRODUCTION

Field studies have shown that low *w/cm* (less than 0.40) bridge-deck or overlay concretes often develop shrinkage-related cracking, as autogenous shrinkage is higher in these low *w/cm* mixtures. External curing of the concrete usually does not mitigate autogenous shrinkage because the curing moisture has difficulties to penetrate into the concrete due to the discontinuity of the pore structure.

If autogenous shrinkage can be mitigated through internal curing procedures, the advantages of using low *w/cm* concrete can be better realized. This chapter explores the concept of internal curing using pre-soaked lightweight fine aggregate (LWFA) as the partial replacement of sand for mitigating autogenous shrinkage and moisture warping. New experimental results and test methods have been presented for quantifying the effectiveness of internal curing in mitigating shrinkage and associated tensile stresses. Concretes with *w/cm* of 0.35 and 0.45 and total aggregate content by volume (ϕ_A) of 57% were investigated. The LWFA to sand ratios of 20% and 40% by volume were used.

7.2 REVIEW OF INTERNAL CURING TECHNIQUES

7.2.1 Lightweight Aggregate

Internal curing implies the introduction of a component into the concrete mixtures that serves as a curing agent. Though the lightweight aggregate has been used in concrete for many years on bridges and buildings, the original purpose of using it is to reduce the structure's dead load and improve the fire resistance performance. It was until early

1990's that the lightweight fine aggregate started to draw attention as a curing agent [Philleo 1991].

The porous lightweight aggregate has vast network of internal pores which act as internal reservoirs providing an internal source of water necessary to replace that consumed by chemical shrinkage during hydration and thus minimize the development of self-desiccation and consequently the autogenous shrinkage and help avoiding early-age cracking. The water absorption capacity of lightweight aggregate (LWA) can range from 5 to 25% in 24 hours [Hoff 2002].

The individual pores in the lightweight aggregate are much larger than the typical sizes of the capillary pores in the hydrating cement paste. And thus, the capillary forces within the cement paste are large enough to transport water from the LWA internal reservoirs to the drying/hydrating cement paste, where continuing hydration can then occur [Weber and Reinhardt 2003]. The remaining anhydrous cement particles now have more free water available for hydration, as the capillary pores within the cement paste remain saturated. As new hydration products form, the capillary pores will be further reduced in size, and thus further increasing the capillary suction and drawing more water from the internal reservoirs of LWA. Water movement from the LWA to the hydrating paste will stop only when all the cement is hydrated or when the relative humidity within the LWA internal reservoir is equivalent to that in the hydrating cement paste [Weber and Reinhardt 2003].

Scanning electron microscope images of mortar mixtures show the concentrated pores and voids within the lightweight fine aggregate particles as the dark areas shown in **Figure 7.1** [Lam 2005].

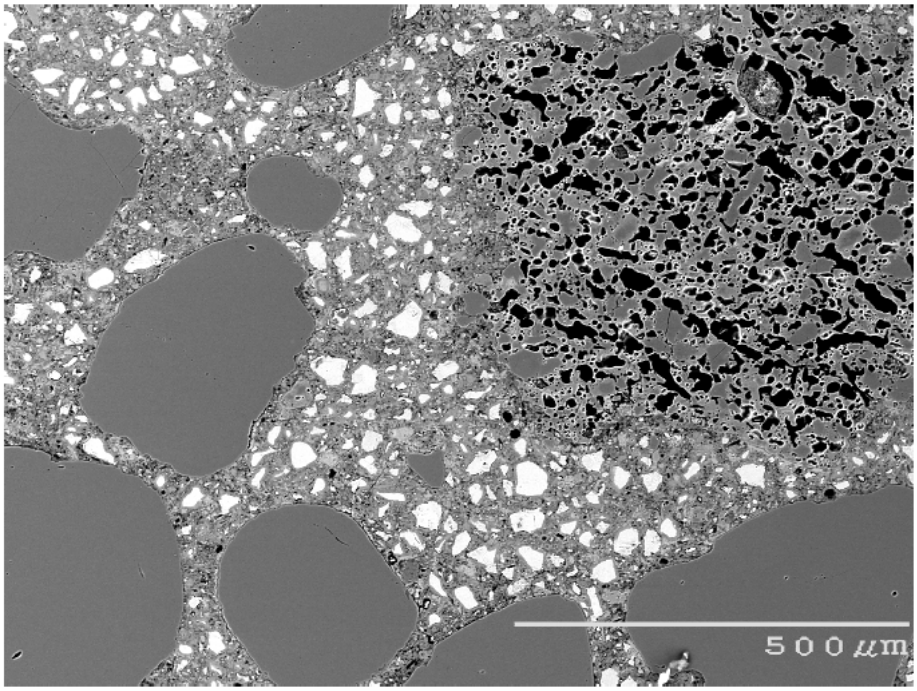

Figure 7.1 Scanning electron image of mortar containing lightweight sand [Lam 2005]

On the other hand, the drawback of using lightweight aggregate as an internal curing agent can be the reduction in the freezing and thawing resistance, strength, and stiffness of the concrete as the lightweight aggregate usually has lower strength than the normal aggregate.

7.2.2 Superabsorbent Polymer

Superabsorbent polymers (SAP) are primarily used in personal care products as a medium for liquid storage such as diapers and feminine hygiene products. Most of today's SAPs are from partially neutralized, lightly crosslinked poly (acrylic acid) [Buchholz and Graham 1998]. Upon in contact with water, the SAP will swell into a gel-like substance until it has reached its threshold for absorption. After absorbing the water, the weight of SAP can vary from 20 times to 2000 times its original weight [Jensen and Hansen 2001].

According to the first publication on the use of SAP by Jensen and Hansen [2001], the entrained SAP was able to mitigate autogenous deformation and maintain a high relative humidity within the bulk cement pastes.

7.3 EXPERIMENTAL

Experimental tests including free and restrained autogenous deformation, moisture warping, and drying shrinkage test were conducted for assessing the effectiveness of internal curing technique by using LWFA on mitigating shrinkage, restrained stress and warping deformations. The detailed experimental information can be found in Chapter 3 and Chapter 6.

7.4 RESULTS AND DISCUSSIONS

7.4.1 Mitigation of Autogenous Shrinkage

The results shown in **Figure 7.2** demonstrate that pre-soaked LWFA is highly effective in reducing autogenous shrinkage, and that a smaller amount of LWFA is needed for higher *w/cm* concrete [Wei and Hansen 2007]. Autogenous shrinkage during the first 28 days of sealed curing can be completely eliminated for the *w/cm* of 0.35 concrete if 40% of the sand is replaced by LWFA. For a mix with *w/cm*=0.45, 20% LWFA is sufficient in preventing autogenous shrinkage.

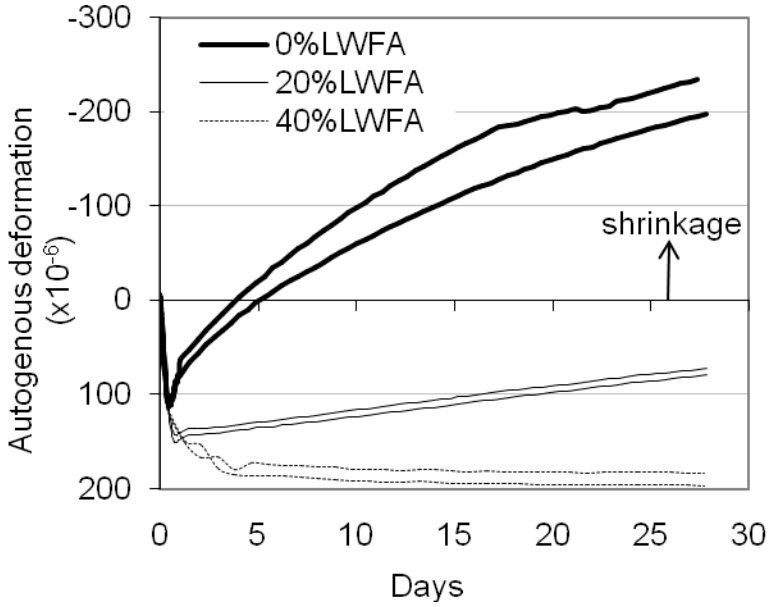

(a)

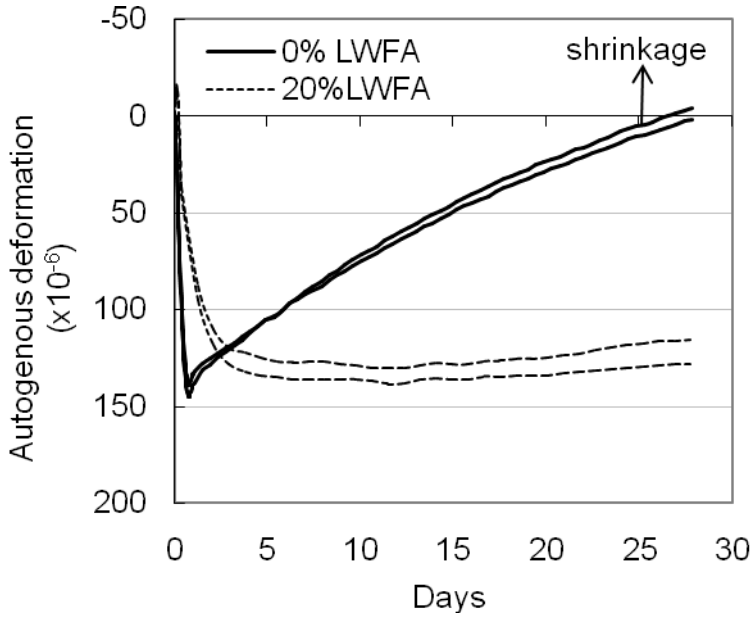

(b)

Figure 7.2 Measured autogenous deformation (internal curing vs. no internal curing) for concretes with ϕ_A=57% and (a) *w/cm*=0.35; (b) *w/cm*=0.45

7.4.2 Mitigation of Self-induced Stress

The internal curing using pre-soaked lightweight fine aggregate can mitigate self-induced stress from restrained autogenous shrinkage. The measured development of self-induced stress is plotted in **Figure 7.3** for mixtures with and without internal curing at *w/cm*=0.35 and 0.45. According to the results, the self-induced tensile stress is completely eliminated in concretes with 40% LWFA at *w/cm*=0.35 and 20% LWFA at *w/cm*=0.45, which is consistent with the free deformation results. For the control mix with *w/cm*=0.35, tensile stresses develop over time and reach 40% of the direct tensile strength after 25 days of sealed curing, suggesting that tensile stress induced from restrained autogenous shrinkage can significantly reduce the tensile capacity of the early-age concrete. And thus, autogenous shrinkage, especially in lower *w/cm* concrete, should be considered an important factor in assessing early-age cracking risk. The direct tensile strength was obtained by breaking TSTM specimens, which is about 70% to 80% of the split tensile strength of concrete cylinders.

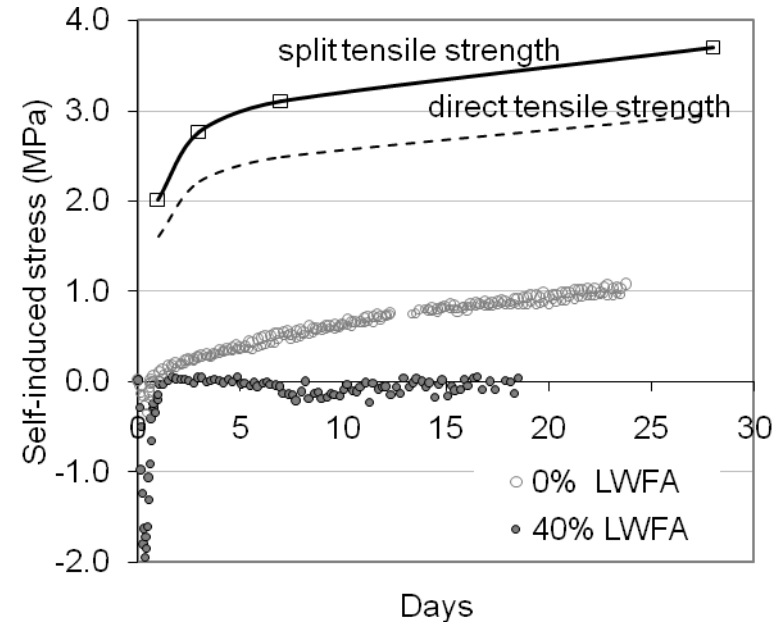

(a)

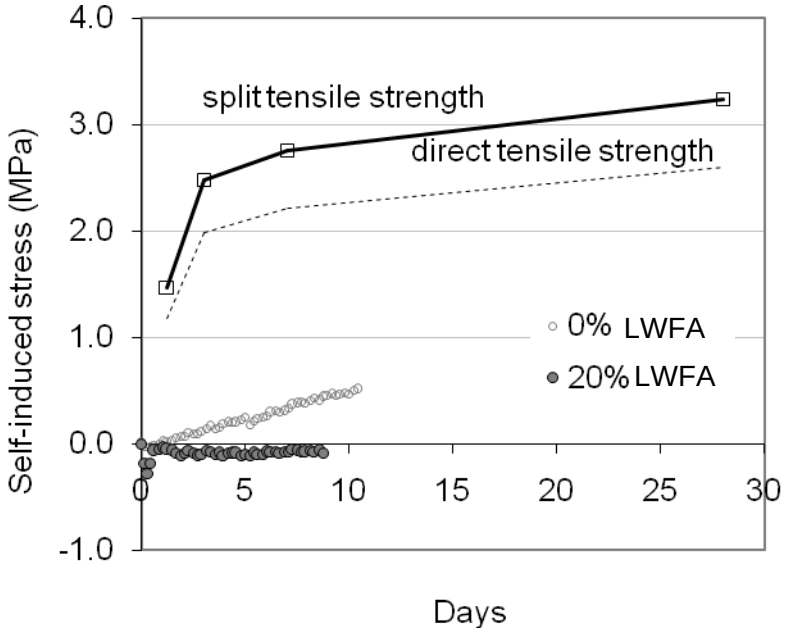

(b)

Figure 7.3 Measured self-induced stress (internal curing vs. no internal curing) for concretes with ϕ_A=57% and (a) *w/cm*=0.35; (b) *w/cm*=0.45

7.4.3 Mitigation of Moisture Warping

Within days after pouring, the hydrating cement paste develops capillary discontinuity [Powers et al. 1959, Bentz 2006]. This has been found to hinder moisture

transport in cross sections greater than about 80 mm (3.2 in.) [Beddoe and Springenschmid 1999]. Once this happens a moisture gradient can develop within the cross section any time the concrete is exposed to water at the free surfaces. Consequently, moisture gradients from drying at the top surface and water suction at the bottom surface work together to cause uplift at joints and free edges of a slab. Severe warping deformation occurs. If poor base-drainage conditions exist a permanent moisture gradient (warping) uplift can result in slabs [Springenschmid and Plannerer 2001, Hansen and Wei 2008].

According to the experimental results on autogenous shrinkage, 20% pre-soaked LWFA replacement is capable of completely eliminating autogenous shrinkage in concrete with *w/cm* of 0.45. To investigate if LWFA is also effective in reducing moisture warping, the same replacement level of LWFA and *w/cm* concrete were used for moisture warping measurements.

It was found that LWFA in a pre-soaked condition is effective in reducing moisture warping in addition to eliminating autogenous shrinkage [Wei and Hansen 2007]. As shown in **Figure 7.4**, about 80% of moisture warping is reduced at the exposure time of 16 days. The substantial reduction in moisture warping suggests that using LWFA decreases the moisture gradient along beam depth. Since the beam's bottom is in contact with water, RH at that portion is high with or without LWFA. However, the top portion of the beam with LWFA will have higher RH possibly due to (1) the release of water from LWFA upon drying; and (2) faster consumption of water released from LWFA and higher degree of hydration than that in the interior of the concrete leaving a dense layer of concrete at the top portion which helps reduce the evaporation rate and consequently the moisture gradient along the beam depth. Water movement from LWFA to the hydrating cement paste will stop when the relative humidity in the pores of LWFA is equivalent to that in cement paste [Weber and Reinhardt 1995], this may reduce the effectiveness of LWFA on reducing the moisture gradient if the slab top surface is exposed to drying for a longer period of time.

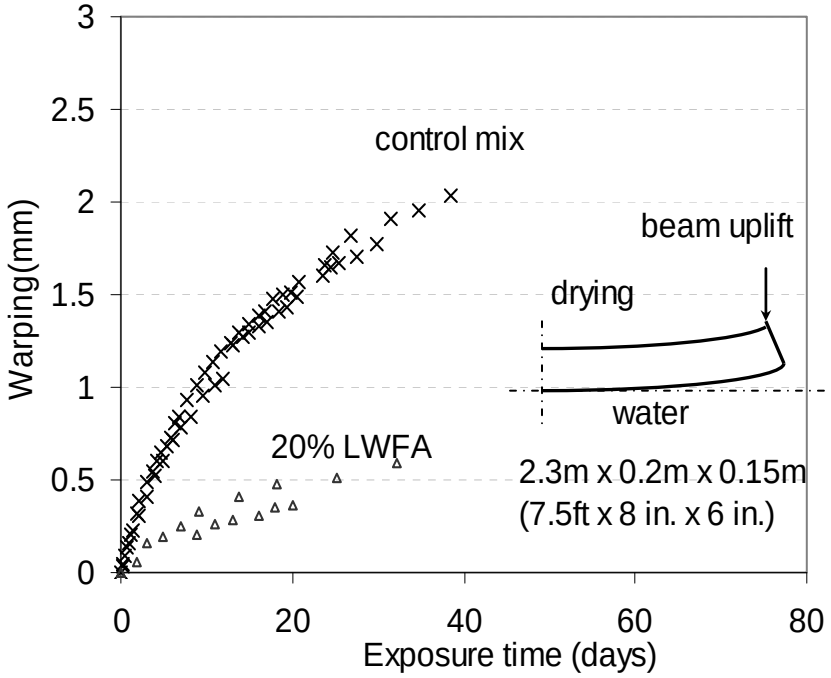

Figure 7.4 Measured development of beam warping (internal curing vs. no internal curing) for *w/cm*=0.45 concrete

7.4.4 Mitigation of Drying Shrinkage

LWFA is not found effective in reducing the external drying shrinkage as demonstrated in **Figure 7.5** for the uniform drying shrinkage results of mortar bars with and without internal curing. The mortar bars were kept in the same environmental chamber where the concrete beams for moisture warping tests were kept. The relative humidity of that chamber was kept at 50%. It can be seen that there is no significant difference in measured uniform drying shrinkage between bars with 20% LWFA and no LWFA. The disagreement on the results of using LWFA to reduce moisture warping and uniform drying shrinkage is as expected. Unlike autogenous shrinkage, drying shrinkage is an external drying process and the free water provided by LWFA is drawn to the environment rather than to the capillary pores in cement paste. And thus, there is no much help in reducing drying shrinkage by using LWFA. Be aware that, the measured uniform drying shrinkage actually includes autogenous shrinkage portion. From **Figure 7.5**, the LWFA mix shows even slightly higher shrinkage (drying shrinkage plus

autogenous shrinkage) than the control mix which may suggest that even more drying shrinkage occur in LWFA mix.

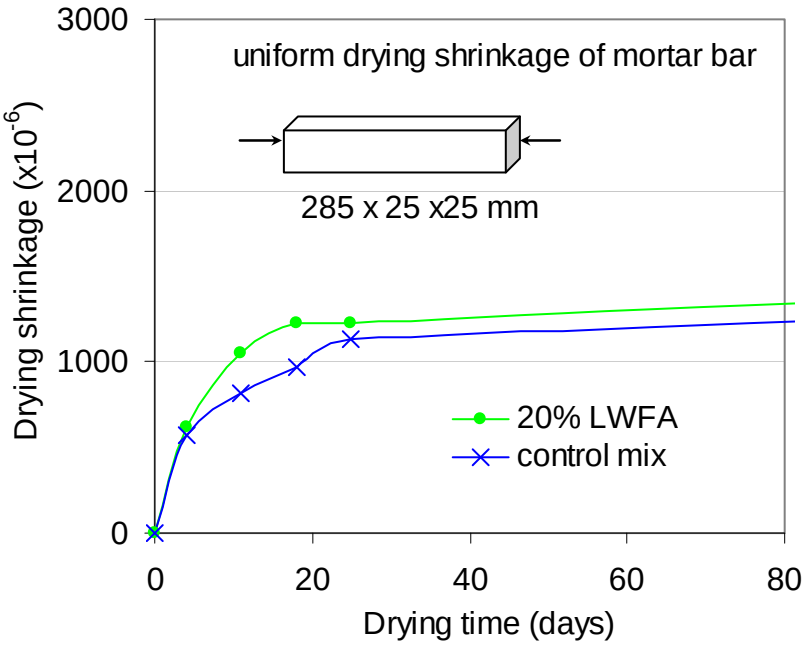

Figure 7.5 Measured development of drying shrinkage (internal curing vs. no internal curing) for *w/cm*=0.45 concrete with ϕ_A=57%

7.5 CONCLUSIONS

In this chapter the use of water-soaked lightweight fine aggregate (LWFA) as additives for internal curing in concrete is explored:

- LWFA was used as partial replacement of regular sand by volume percentage ranging from 20% to 40%. These aggregates are effective in providing a source for internal curing by acting as internal reservoirs during the hydration of the cement.
- Pre-soaked lightweight fine aggregate (LWFA) is found to be effective in reducing and even eliminating autogenous shrinkage in concretes with *w/cm* ranging from 0.45 to 0.35. Internal curing is effective in eliminating self-induced tensile stresses from restrained autogenous shrinkage as well.

- Using LWFA can reduce slab warping from combined drying at the top surface region and continued wetting at the bottom surface from the saturated base, a condition encountered if inadequate base drainage exists.

CHAPTER 8

CONCLUSIONS

8.1 THESIS SUMMARY

In recent years, cracking caused by shrinkage has been observed in highway pavements, bridge decks, parking structures, airport pavements, and industrial floors soon after construction. Cracks accelerate the ingression of water and corrosive agents and thus reduce the overall durability and increase the maintenance cost.

Autogenous shrinkage, as the major source of early-age concrete shrinkage, is a consequence of the chemical volume reduction from cement hydration. Internal pore-humidity drops and capillary stresses develop as the hydration progresses. Pore-drying and thus autogenous shrinkage increases with extent of hydration (or time) and is especially pronounced in low water-cementitious ratio concrete. Quantifying the autogenous shrinkage of cementitious systems, especially given the increasing and widespread utilization of high-performance concrete containing supplementary cementitious materials, becomes important in order to understand and control premature cracking in concrete structures.

Numerous researchers have investigated on the extent of the influence factors toward better understanding the underlying process of autogenous shrinkage. However, lack of data on this property due to testing challenges has hampered the fully capture of the mechanism and the development of sound prediction models for this property.

The thesis focus has been on the measurement and subsequent modeling of the autogenous deformation in cementitious systems containing various amounts of ground granulated blast-furnace slag (GGBFS). An improved methodology is presented for accurate measurement of this property on various mixture compositions to characterize the role of the constituent materials on autogenous shrinkage development. Autogenous shrinkage in hydrating cement paste is explained with emphasis on the evolution of microstructures and hydration products. New prediction models are developed for both cement paste and concrete shrinkage. The improved elastic-theory-based composite model is capable of predicting concrete autogenous shrinkage irrespective of aggregate content. Finally, the cause of extensive moisture warping found in Jointed Plain Concrete Pavements is explained through combining drying shrinkage and autogenous moisture predictions. A revised warping theory is provided.

8.2 PRIMARY CONCLUSIONS

The general conclusions with regards to the main objectives of this research are gathered from all chapters and given below:

- Refined Test Procedure on Autogenous Shrinkage Measurement
  As a free self-induced deformation measurement, the main difficulties are capturing autogenous shrinkage of concrete, minimizing friction between the specimen and the rig, preventing moisture exchange with the external, and keeping the curing temperature constant. This research overcomes these difficulties and obtains good reproducibility by doing the following: (1) using concretes with different aggregate content (less than the normal range of aggregate content) and the maximum aggregate size of 12.5 mm (0.5 in.) are used to adapt the capability of the measuring rig and to reduce possible friction from the large-size aggregates; (2) two layers of removable Neoprene sheets are placed between the rig and the specimen to avoid wall friction; (3) specimen is wrapped and sealed tightly during testing; (4) constant-temperature water is circulated through the double-walled stainless steel rig to maintain curing temperature.

- Clear Understanding of GGBFS Effect on Autogenous Shrinkage
  Autogenous shrinkage of cement paste is a result of the porous hydration products (PHP), majority of which is calcium silicate hydrate (C-S-H) gel combined with a reduction in pore humidity within these porous hydration products. The autogenous shrinkage of cementitious blends of portland cement and GGBFS follows the same mechanism as neat paste. Initially lower autogenous shrinkage develops, proportional to the reduction in portland cement, while later-age pozzolanic reactions cause increase in porous hydration products and associated pore-drying. Ultimate autogenous shrinkage may or may not increase.

- Improved Elastic-based Composite Modeling on Autogenous Shrinkage
  Concrete autogenous shrinkage is effectively modeled using the improved composite model as a function of paste shrinkage and aggregate concentration through incorporating a uniform shrinkage-stress equilibrium model developed by Pickett with a time-domain function developed by Freiesleben-Hansen and Pedersen. This elastic-based model does not have to rely on the incorporation of the viscoelastic properties which are difficult to determine.

- A Revised Warping Theory
  Numerical modeling and experimental investigation show that the cause of extensive moisture warping found in slabs consists of three components: (1) uniform relative humidity reduction due to cement hydration. Though it causes no uplift, the decrease in pore humidity and the depercolation of pore structure as a result of cement hydration render concrete slabs on grade prone to moisture warping if exposed to water at the bottom; (2) drying shrinkage from the top surface, which should be considered minor; and (3) wetting at bottom through water uptake if the pore structures have been disconnected from cement hydration.

- Internal Curing Using LWFA for Mitigating Autogenous Shrinkage

Using pre-soaked lightweight fine aggregate (LWFA) is effective in mitigating or reducing autogenous shrinkage, self-induced stresses, and moisture warping in slabs.

8.3 RECOMMENDATIONS FOR FUTURE WORK

Based on the work conducted in this thesis, several aspects on the experimental and modeling of cementitious materials are recommended for further research:

- Exploring Microstructure and Transport Properties of Porous Hydration Products

  Further research on autogenous shrinkage must be based on physical, chemical and thermodynamic examinations to establish relationship between hydration, pore structure evolution, self-desiccation and transport properties such as diffusion and sorption properties of cement-based materials.

- General Modeling of Autogenous Shrinkage

  Expand upon current models to develop a more general procedure capable of predicting autogenous shrinkage of wide-range cementitious materials containing GGBFS, and fly ash at different *w/cm* ratios.

- Assessing Early-age Cracking Risk

  The improved measurement on autogenous shrinkage could be implemented for experimentally assessing the risk of self-induced cracking by incorporating a horizontal restraint stress test. This experimental investigation is intended for developing a model for computational assessment of the cracking sensitivity of concrete with respect to the effects of curing ages, material compositions, and structural restraint.

REFERENCES

Aldea, C.M., Shah, S.P. and Karr, A., (1999) "Permeability of cracked concrete", *Materials and Structures*, Vol. 32 No. 219, pp. 370-366.

Alexander, M.G., (1996) "Aggregates and the Deformation Properties of Concrete", *ACI Materials Journal*, 93/6, pp. 569-577.

Atkinson, A., and Nikerson, A.K., (1984) *J. Mater. Sci.,* 9, pp.3068–3078.

Bangham, D.H., and Fackhoury, N., (1931) "The Swelling of Charcoal", Proceedings of Royal Society of London, Series A, 130, pp. 81–89.

Baroghel-Bouny, V., (1996) "Texture and Moisture Properties of Ordinary and High-performance Cementitious Materials", Proceedings of Séminaire RILEM.

Baroghel-Bouny, V., Godin, J., and Gawsewitch, J., (1996) "Microstructure and Moisture Properties of High Performance Concrete", Fourth International Symposium on the Utilization of High Strength/High Performance Concrete, pp. 451-461.

Baroghel-Bouny, V., and Mounanga, P., (2005) "Effects of Self-desiccation on Autogenous Deformations, Microstructure and Long-term Hygral Behavior", *Self-desiccation and its Importance in Concrete Technology*, Proceedings of the Fourth International Research Seminar, Gaithersburg, USA, June, pp.1-20.

Battagin, A.F., (1992) "Influence of Degree of Hydration of Slag on Slag Cements", Proceedings of the 9th ICCC, National Council for Cement and Building Materials, vol. III. New Delhi, India, pp. 166– 172.

Bazant, Z.P., and Najjar, L.J., (1972) "Nonlinear water diffusion in nonsaturated concrete", *Mater. Struct*., 5, pp. 1-18.

Beaudoin, J.J., Ramachandran, V.S., and Feldman, R.F., (1991) "Identification of Hydration Reactions through Stress Induced by Volume Change – Part I: C_3A System", *Cem. Concr. Res*., Vol 21, No. 5, pp. 809-818.

Beaudoin, J.J., Ramachandran, V.S., and Feldman, R.F., (1992) "Identification of Hydration Reactions through Stress Induced by Volume Change – Part I: C_4AF System", *Cem. Concr. Res*., Vol 22, No. 1, pp. 27-34.

Beckemeyer, C. A., Khazanovich, L., Yu, H. T., (2002) "Determining Amount of Built-in Curling in Jointed Plain Concrete Pavement: Case Study of Pennsylnania I-80", *Transportation Research Record 1809*, 85-92.

Beltzung, F., and Wittmann, F., (2002) "Influence of Cement Composition on Endogenous Shrinkage", *Self-desiccation and its Importance in Concrete Technology*, Proceedings of the Third International Research Seminar, Lund, Sweden, June, pp.113-126.

Bentz, D.P., and Garboczi, E.J, (1991) "Percolation of Phases in a Three-dimensional Cement Paste Microstructural Model", *Cement and Concrete Research*, Vol. 21, pp. 324-44.

Bentz, D.P., (1997) "Three-dimensional Computer Simulation of Portland Cement Hydration and Microstructure Development", *Journal of the American Ceramic Society*, Vol. 80, No. 1, pp. 3-21.

Bentz, D.P., Garboczi, E.J., and Quenard, D.A., (1998) "Modeling Drying Shrinkage in Reconstructed Porous Materials: Application to Porous Vycor Glass", *Modeling Simul. Mater. Sci. Eng*. Vol. 6, pp. 211-236.

Bentz, D.P., (2006) "Capillary Porosity Depercolation/Repercolation in Hydrating Cement Pastes via Low-Temperature Calorimetry Measurements and CEMHYD3D Modeling", *J. Am. Ceram. Soc.*, 89 (8), pp. 2606–2611.

Bernander, S., (1982) "Temperature Stresses in Early-age Concrete due to Hydration", Proceedings of International Conference on Concrete at Early Ages, RILEM, Paris, Vol. II, pp. 218-221.

Bijen, J., (1996), "Benefits of slag and fly ash" *Construction and Building Materials,* Vol. 10 (5), pp. 309-314.

Bisschop J., (2002) "Drying Shrinkage Microcracking in Cement-Based Materials", Delft University Press, Netherlands.

Bjontegaard, Ø., (1999) "Thermal Dilation and Autogenous Deformation as Driving Forces to Self-induced Stress in High Performance Concrete, The Norwegian University of Science and Technology, PhD thesis.

Beddoe, R., and Springenschmid, R., (1999) "Moisture Transport through Concrete Structural Components", (In German), Beton-und Stahlbetonbau, 94 (4), pp.158-166.

Buchholz, F.L., and Graham, A.T., (1998) "Modern Superabsorbent Polymer Technology", John Wiley & Sons Inc, New York.

Byfors, K., (1987) “Influence of Silica Fume and Fly Ash on Chloride Diffusion and Ph Values in Cement Paste”, *Cem. Concr. Res.,* 17, pp.115–130.

Carlson, R.W., (1937) “Drying Shrinkage of Large Concrete Members”, *Journal of the American Concrete Institute*, Jan.~Feb, pp. 327-336.

Copeland, L.E., and Bragg, R.H., (1995) “Self-desiccation in Portland Cement Pastes”, *ASTM Bull.*, No. 204, pp 1-11.

Darter, M.I., Hall, K.T., and Kuo, C.M., (1995) “Support under Portland Cement Concrete Pavements”, NCHRP Report 372, pp. 1-50.

Delagrave, A., Marchand, J., and Pigeon, M., (1998) “Influence of Microstructure on the Tritiated Water Diffusivity of Mortars”, *Advn. Cem. Bas. Mat*, 7, pp. 60–65.

EI-Jazairi, B.EI, and Illston. J.M., (1980) “The Hydration of Cement Paste using the Semi-isothermal Method of Derivative Thermogravimetry”, *Cem. Concr. Res.*, Vol. 10 (3), pp. 361-366.

Escalantea, J.I., Go´meza, L.Y., Johal, K.K., Mendoza, G., Mancha, H., and Me´ndez, J., (2001) “Reactivity of Blast-furnace Slag in Portland Cement Blends Hydrated under Different Conditions”, *Cement and Concrete Research*, Vol. 31, pp. 1403–1409.

Ferraris, C., and Wittmann, F.H., (1987) “Shrinkage Mechanisms of Hardened Cement Paste”, *Cem Concr Res*, 17(3), pp. 453-464.

Geiker, M., (1983) “Studies of Portland Cement Hydration: Measurements of Chemical Shrinkage and a Systematic Evaluation of Hydration Curves by Means of the Dispersion Model”, Ph. D. Thesis, Technical University of Denmark.

Grasely, Z.C., Lange, D.A., Brinks, A.J., and D’Ambrosia, (2005) “Modeling of Autogenous Shrinkage of Concrete Accounting for Creep Caused by Aggregate Restraint”, *Self-desiccation and its Importance in Concrete Technology*, Proceedings of the Fourth International Research Seminar, Gaithersburg, USA, June, pp.1-20.

Grasley, Z.C., (2006) “Measuring and Modeling the Time-Dependent Response of Cementitious Materials to Internal Stresses”, Ph.D. Thesis, 216pp.

Hammer, T.A., Bjøntegaard, Ø., and Sellevold, E.J., (2002) “Internal Curing – Role of Absorbed Water in Aggregates”, Presented at ACI Fall 2002 Convention, Session High-Performance Structural Lightweight Concrete, Phoenix, AZ.

Hanehara, S., Hirao, H., and Uchikawa, H., (1999) “Relationship between Autogenous Shrinkage and the Microstructure and Humidity Changes at Inner Part of

Hardened Cement Pastes at Early Ages", Proc. Int. Workshop Autoshrink'98, ed. E.-I. Tazawa, Hiroshima, Japan, E & FN SPON, London, pp. 89-100.

Hansen, T.C., and Nielsen, K.E.C., (1965) "Influence of Aggregate Properties on Concrete Shrinkage", *Journal of the American Concrete Institute*, July, pp. 783-794.

Hansen, P. and Pedersen, E., (1977) "Maleinstrument til Kontrol of Betons Haerdning," *Nordisk Betong* (1), 21pp.

Hansen, W., (1987) "Drying Shrinkage Mechanisms in Portland Cement Paste", *J. Am. Ceram. Soc.* 70, pp. 323-328.

Hansen, W., Smiley, D., Peng, Y., and Jensen, E.A., (2002) "Validating Top-down Premature Transverse Slab Cracking in Jointed Plain Concrete Pavement (JPCP)", *Transportation Research Record 1809*, Transportation Research Board, Washington, D.C..

Hansen, W. and Wei, Y., (2008) "PCC Pavement Acceptance Criteria for New Construction When Built-In Curling Exists", Research Report RC-1481.

Hansen, W., Wei, Y., and Schlangen, E., (2008) "Modeling Moisture Warping in Concrete Pavement", CONMOD08 RILEM International Conference, May 26-28, Delft University, The Netherlands.

Hiller, K.H., (1964) "Strength Reduction and Length Changes in Porous Glass caused by Vapor Adsorption", *J App Phys*, Vol. 35, pp. 1622–1628.

Hinrichs, W., Odler, I., (1989) "Investigation of the Hydration of Portland Blast Furnace Slag Cement: Hydration Kinetics", Adv. Cem. Res., Vol. 2, pp. 9 – 13.

Hveem, F.N., (1951) "Slab Warping Affects Pavement Joint Performance," *Journal of the American Concrete Institute*, June, pp. 797-809.

Hobbs, D.W., (1969) "Bulk Modulus Shrinkage and Thermal Expansion of a Two Phase Material", Nature 222, pp 849-851.

Hoff G.C., (2002) "The Use of Lightweight Fines for the Internal Curing of Concrete", Prepared for Northeast Solite Corporation.

Holt, E., (2002) "Very Early Age Autogenous Shrinkage: Governed by Chemical Shrinkage or Self-desiccation", in the Proceedings of the Third International Research Seminary in Lund, pp1-26.

Hua C., Acker P. & Ehrlacher A., (1995) "Analyses and Modeling of the Autogenous Shrinkage of Hardening Cement Paste – I. Modeling at Macroscopic Scale", *Cement and Concrete Research*, Vol. 25, No. 7, pp. 1457-1468.

Janssen, D.J., (1987) "Moisture in Portland Cement Concrete", *Transportation Research Record 1121*, Transportation Research Board, Washington, D.C.

Japan Concrete Institute Committee on Autogenous Shrinkage, (1999) "Report on Autogenous Shrinkage of Concrete", Proc. Int. Workshop Autogenous Shrinkage, ed. E.-I. Tazawa, Hiroshima, Japan, E & FN SPON, London, pp. 1-67.

Jennings, H.M., Dagleish, B.J., and Pratt, P.L., (1981) "Morphological Development of Hydrating Tricalcium Silicate as Examined by Electron Microscopy Techniques", J Am Ceram Soc 64 567–572.

Jennings, H.M., (2004) "Colloid model of C-S-H and implications to the problem of creep and shrinkage", *Materials and Structure*.

Jensen, O.M., (1995) "Thermodynamic limitation of self-desiccation", *Cem Concr Res*, 25(1), pp.157-164.

Jensen, O.M, and Hansen, P.F., (1995) "A Dilatometer for Measuring Autogenous Deformation in Hardening Portland Cement", *Material and Structure*s, Vol. 28, pp 406-409.

Jensen, O.M., and Hansen, P.F., (1996) "Autogenous Deformation and Change of the Relative Humidity in Silica Fume-Modified Cement Paste", *ACI Mat. J.*, Nov. – Dec.

Jensen, O.M., and Hansen, P.F., (2001) "Autogenous Deformation and RH-change in Perspective", *Cement and Concrete Research*, Vo. 31, pp 1859-1865.

Jensen, O.M., and Hansen, P.F., (2001), "Water-Entrained Cement-Based Materials: I. Principle and Theoretical Background", *Cement and Concrete Research*, Vol. 31 (4), pp. 647-654.

Jonasson, J.-E., Groth, P., and Hedlund, H., (1998) "Modeling of Temperature and Moisture Field in Concrete to Study Early Age Movements as a Basis for Stress Analysis", RILEM Proceedings 25 of Thermal Cracking in Concrete at Early Ages, pp. 45-54.

Justnes, H., Gemert, A.V., Verboven, F., and Sellevold, E., (1996) "Total and External Chemical Shrinkage of Low w/c Ratio Cement Pastes", *Adv. Cem. Res.*, Vol. 8 (31), pp 121-126.

Khazanovich, L., Yu, H. T., and Beckemeyer, C, A., (2000) "Application of ISLAB2000 for Forensic Studies", 2nd Int. Symp., 3D Finite Element for Pavement Analysis, Design & Research, Charleston, Virginia.

Koenders, E.A.B., (1997) "Simulation of Volume Changes in Hardening Cement-Based Materials", Delft University of Technology, Ph.D. thesis, Delft, The Netherlands.

Kovler, K., (1994) "Testing System for Determining the Mechanical Behavior of Early-Age Concrete under Restrained and& Free Shrinkage", *Materials & Structures*, 27, pp. 324-330.

Kovler, K., Zhutovsky, S., (2006) "Overview and Future Trends of Shrinkage Research", *Materials and Structures*, Vol. 39, pp. 827–847.

Lachowski, E.E. and Diamond, S., (1983) "Investigation of the composition and morphology of individual particles of Portland cement paste: 1. C-S-H gel and calcium hydroxide particles", *Cement and Concrete Research*, vol. 13 (2) pp. 177-185.

Lam, H., (2005) "Effects of Internal Curing Methods on Restrained Shrinkage and Permeability", PCA R&D Serial No. 2620.

Lee, K.M., Lee, H.K., Lee, S.H., and Kim, G.Y., (2006) "Autogenous Shrinkage of Concrete Containing Granulated Blast-Furnace Slag", *Cement and Concrete Research*, 36, pp. 1279-1285.

Leonards, G.A., and Harr, M.E., (1959) "Analysis of Concrete Slabs on Ground," *Journal of the Soil Mechanics and Foundation Division*, Proceedings of the American Society of Civil Engineers, June, pp. 35-58.

L'Hermite R, (1960) "Volume Changes of Concrete", Proceedings of fourth international symposium on the chemistry of cement, Washington, DC, pp 659–694.

Locher, F.W., Richartz, W. and Sprung, S., (1976) "Erstarren von Zement" (in German), Zement Kalk Gips, Vol. 29 (10), pp. 435-442.

Lumley, J.S., Gallop, R.S., Moir, G.K., and Taylor, H.F.W., (1996) "Degrees of Reaction of the Slag in Some Blends with Portland Cements", *Cem. Concr. Res.*, Vol. 26, pp. 139–151.

Lura, P., (2003) "Autogenous Deformation and Internal Curing of Concrete", Delft, The Netherlands, Delft University.

Lura, P., and Jensen, O.M., (2005) "Volumetric Measurement in Water Bath – an Inappropriate Method to Measure Autogenous Strain of Cement Paste", PCA R&D Serial No. 2925.

Mackenzie, R., (1970) “Differential Thermal Analysis”, Volume 1, Fundamental Aspects, Academic Press, pp.775.

Marsh, B.K., and Day, R.L., (1988) “Pozzolanic and Cementitious Reactions of Fly Ash in Blended Cement Pastes”, *Cement and Concrete Research*, Vol. 8, pp. 301-310.

Mehta, K., (1983) “Pozzolanic and Cementitious Byproducts as Mineral Admixtures for Concrete – A Critical Review”, Fly Ash, Silica Fume, Slag and Other Mineral By-Products in Concrete, SP – 79, American Concrete Institute, Detroit, pp. 1-46.

Melo Neto, A.A., Cincotto M.A., and Repette, W., (2008) “Drying and Autogenous Shrinkage of Pastes and Mortars with Activated Slag Cement”, *Cement and Concrete Research*, Vol. 38, pp. 565–574.

Midgley, H.G., (1979) “The Determination of Calcium Hydroxide in Set Portland Cements”, *Cem. Concr. Res*., Vol. 9 (1), pp. 77–82.

Mindess, S., Young, J.F., Concrete, (1981) Prentice-Hall, Inc., 671pp.

Miyazawa, S., and , Tazawa, E., (2005) “Prediction Model for Autogenous Shrinkage of Concrete with Different Type of Cement”, *Self-desiccation and its Importance in Concrete Technology*, Proceedings of the Fourth International Research Seminar, Gaithersburg, USA, June, pp.125-138.

Mizobuchi, T., Yokozeki, K. and Nobuta, Y., (2000) “Experimental Estimation of Thermal Cracking using the Modified Temperature-stress Testing Machine”, in Control of Cracking in Early Age Concrete, pp. 153-162.

MLS, (2003) “Computer Program for the Analysis of the Thermal and Mechanical Behavior of Hardening Concrete”, User Manual.

Moon, J.H., Rajabipour, F., Pease, B., and Weiss, J., (2005) “Autogenous Shrinkage, Residual Stress, and Cracking in Cementitious Composites: the Influence of Internal and External Restraint”, *Self-desiccation and its Importance in Concrete Technology*, Proceedings of the Fourth International Research Seminar, Gaithersburg, USA, June, pp.1-20.

Nasvik J., (2002) “Reducing Curling of Concrete Floor and Slabs”, *Concrete Construction*, September, pp. 21-25.

Neville, A.M., (1964) “Creep of Concrete as Function of its Cement Paste Content”, *Magazine of Concrete Research*, 16/46, pp. 21-30.

Neville, A.M., and Dilger, W., (1970) “Creep of Concrete: Plain, Reinforced, Prestressed”, Amsterdam: North-Holland.

Neville, A. M., (1996) "Suggestions of Research Areas Likely to Improve Concrete", *Concrete International*, 18(5), pp. 44–49

Odler, I., (1998) "Hydration, Setting, and Hardening of Portland Cement", in Lea's Chemistry of Cement and Concrete, 4th ed. Edited by P. C. Hewlett. Arnold, London, U.K., pp. 241.

Paillbre, A.M., Buil, M., and Serrano, J.J., (1990) "Effect of Fiber Addition on the Autogenous Shrinkage of Silica Fume Concrete", *AC1 Materials Journal*, pp. 82.

Pane, I., (2001) "Hydration Kinetics and Thermomechanics of Blended Cement Systems", Thesis Dissertation, University of Michigan.

Pane, I., Hansen, W., (2005) "Investigation of Blended Cement Hydration by Isothermal Calorimetry and Thermal Analysis", *Cement and Concrete Research*, Vol. 35, pp. 1155– 1164.

Papadakis, V., Fardis, M.N., and Vayenas, C., (1992) "Hydration and Carbonation of Pozzolanic Cements", *ACI Mat. J.*, Vol. 89 (2), pp 119-127.

Philleo, R.E., (1991) "Concrete Science and Reality", in Materials Science of Concrete II, Eds. J. Skalny and S. Mindess, American Ceramic Society, Westerville, OH, pp. 1-8.

Pickett, G., (1956) "Effect of Aggregate on Shrinkage of Concrete and Hypothesis Concerning Shrinkage", *Journal of the American Concrete Institute*, Vol. 56, pp. 581-90.

Poblete, M. Garcia, A., David, J., Ceza, P., and Espinosa, R., (1990) "Moisture Effects on the Behavior of PCC Pavements", Proceedings, *2nd International Workshop on the Design and the Evaluation of Concrete Pavements*, Siguenza, Spain.

Powers, T.C., (1947) "A Discussion of Cement Hydration in Relation to the curing of concrete", Proceedings, Highway Research Board, Vol. 27, pp. 178.

Powers, T.C., and Brownyard, T.L., (1947) "Studies of the Physical Properties of Hardened Portland Cement Paste", Proceedings, ACI, Vol. 43, pp. 971.

Powers, T.C., and Brownyard, T.L., (1948) "Studies of the Physical Properties of Hardened Portland Cement Paste", *J Amer Concr Inst,* Vol. 43, Bulletin 22, Research Laboratories of the Portland Cement Association, Chicago.

Powers, T.C., Copeland, L.E., and Mann, H.M., (1959) "Capillary Continuity or Discontinuity in Cement Pastes", PCA Bulletin, vol. 1 (110), pp. 2-12.

Powers, T.C., (1968) "Session I: The Thermodynamics of Volume Change and Creep," *Materiaux et Constructions* 1, pp. 487-507.

Rao, S, and Roesler, J.R., (2005) "Characterizing Effective Built-In Curling from Concrete Pavement Field Measurements", *Journal of Transportation Engineering*, ASCE, April , pp. 320-327.

Reinhardt H.W. and Jooss, M., (2003) "Permeability and Self-healing of Cracked Concrete as a Function of Temperature and Crack Width", *Cement and Concrete Research*, Vol. 33, pp. 981-985.

Roy, D.M., and Idorn, G.M., (1982) "Hydration, Structure and Properties of Blast Furnace Slag Cements, Mortars, and Concrete", *ACI Journal*, Vol., 79(6), pp. 444-457.

Roy, D.M., (1999) "Alkali-Activated Cements: Opportunities and Challenges", *Cem. Concr. Res.*, Vol. 29 (2), pp. 249–254.

Schieβl, P. and Raupach, M., (1997) "Laboratory Studies and Calculations on the Influence of Crack width on chloride-induced corrosion of steel in concrete, *ACI Materials Journal*, Vol. 94, No. 1, pp. 56-62.

Schleibinger, (2007) "Manual of Schleibinger Shrinkage-Cone and Shrinkage-Drain, Bending-Drain and Thin-Layer-Shrinkage-System", 37 pp.

Schmitt, T.R., and Darwin, D., (1999) "Effect of Material Properties on Cracking in Bridge Decks", *Journal of Bridge Engineering*, Vol. 4, No. 1, pp.8-13.

Sellevold, E., Bjontegaard, Ø., Justens, H. and Dahl. P.A., (1994) "High Performance Concrete: Early Volume Change and Cracking Tendency", Thermal Cracking in Concrete at Early Ages, E&FN SPON London, Munchen.

Sersale, R., (1983) "Aspects of the Chemistry of Addiitons", Advances in Cement Technology, S. N. Ghosh, Editor, Pergamon Press, New York, pp. 537-567.

Sharma, R.L., Pandey, S.P., (1999) "Influence of Mineral Additives on the Hydration Characteristics of Ordinary Portland Cement", *Cement and Concrete Research*, Vol. 29, pp. 1525–1529.

Shi, C., (1998) "Pozzolanic Reaction and Microstructure of Chemical Activated Lime-Fly Ash Pastes", *ACI Mater. J.*, Vol. 95 (5), pp. 537– 544.

Soroka, I., (1979) Portland Cement Paste and Concrete. The Macmillan Press Ltd., London.

Springenschmidt, R., Gierlinger, E., and Kernozycki, W., (1985) "Thermal Stress in

Mass Concrete: A New Testing Method and the Influence of Different Cements", Proceedings of the 15th International Congress For Large Dams, Lausanne, R4, pp. 57-72

Springenschmid, R., Plannerer, M, (2001) "Experimental Research on the Test Methods for Surface Cracking of Concrete, Institute for Building Materials", Technical University Munich, Germany.

Stutzman, P.E. (2001) "Scanning Electron Microscopy in Concrete Petrography", Proc. Materials Science of Concrete Special Volume: Calcium Hydroxide in Concrete, The American Ceramic Society. November 1-3, 2000, Anna Maria Island, Florida, pp. 59-72.

Suprenant, B. A., (2002) "Why Slabs Curl-Part II: Factors Affecting the Amount of Curling", *Concrete International*, American Concrete Institute, April.

Taylor, H.F.W., (1997) "Cement Chemistry", 2nd Edition, Thomas Telford, New York, 459 pp.

Tazawa, E., and Miyazawa, S., (1995) "Influence of Cement and Admixture on Autogenous Shrinkage of Cement Paste", *Cement and Concrete Research*, Vol 25, No. 2, pp. 281-287.

Tazawa, E., Miyazawa, S., and Kasai T., (1995) "Chemical Shrinkage and Autogenous Shrinkage of Hydrating Cement Paste", *Cement and Concrete Research*, Vol. 25 (2), pp. 288-292.

Tazawa, E., Sato, R., Sakai, E., and Miyazawa, S., (2000) "Work of JCI Committee on Autogenous Shrinkage", Int. RILEM Workshop on Shrinkage of Concrete, Paris, pp. 21-40.

Timoshenko, S., and Goodier, J.N., 1951, "Theory of Elasticity", 2nd Edition, McGraw-Hill Book Co., Inc., New York, 359pp.

Toma, G., Pigeon M., Marchand J., Bissonnette B. and Barcelo L., (1999) "Early Age Restrained Shrinkage: Stress Build Up and Relaxation", International Research Seminar: Self-desiccation and Its Importance in Concrete Technology, Lund, Sweden, June 18., pp. 61-71.

Van Breugel, K., (1991) "Simulation of Hydration and Formation of Structure in Hardening Cement-Based Materials", PhD thesis, Delft University of Technology, Delft.

Weber, S., and Reinhardt, H.W., (2003) "Modeling the Internal Curing of High Strength Concrete Using Lightweight Aggregates", Theodore Bremner Symposium on High Performance Lightweight Concrete, Eds. J.P. Ries and T.A. Holm, Sixth

CANMET/ACI International Conference on Durability, Thessalonika, Greece, pp. 45-64.

Wei, Y., Hansen, W., Smiley, D.L., and Jensen, E.A., (2006) "Analysis of Total Effective Linear Temperature Difference from Concrete Pavement Field Measurements", Proceedings of International Conference on Long-life Concrete Pavements, Chicago, pp. 201-216.

Wei, Y., Hansen, W., (2007) "Pre-soaked Lightweight Fine Aggregate as Additives for Internal Curing in Concrete", ACI-SP on Internal Curing of High-Performance Concretes: Laboratory and Field Experiences, ACI Fall Convention, October 14-18, Puerto Rico, in press.

Wei, Y., Hansen, W., and Schlangen, E, (2008) "Moisture Warping in Slabs on Grade", Sixth RILEM International Conference on Cracking in Pavements, June 16-18, Chicago, Illinois.

Wei, Y., Hansen, W., and J.J., Biernacki, 2008 "Autogenous Shrinkage of Hydrating Cement – Effects of Water-cementitious Ratio and Ground Granulated Blast-Furnace Slag Content", *ACI Materials Journal*, Submitted.

Weiss, J., (1999) "Prediction of Early-age Shrinkage Cracking in Concrete", Ph.D thesis, 268 pp.

Wittmann F.H., (1968) "Surface Tension, Shrinkage and Strength of Hardened Cement Paste", *Materials & Structures*, 1(6), pp. 547–552.

Wittmann, F.H., (1982) "Creep and Shrinkage Mechanisms", in "Creep and Shrinkage in Concrete Structures", Baˇzant, Z.P., Wittmann, F.H., John Wiley & Sons, pp 129–163.

Wong, S.F., Wee, T.H., Swaddiwudhipong, S., and Lee, S.L., (2001) "Study of Water Movement in Concrete", *Magazine of Concrete Research*, Vol. 53(3), pp. 205-220.

Ye, G., (2003) "Experimental Study and Numerical Simulation of the Development of the Microstructure and Permeability of Cementitious Materials", Ph.D thesis.

Ye, G., (2005) "Percolation of Capillary Pores in Hardening Cement Pastes", *Cement and Concrete Research*, Vol. 35, pp. 167– 176.

Ytterberg, R. F., (1987) "Shrinkage and Curling of Slabs on Grade Part III-Additional Suggestions", *Concrete International*, June, vol. 9, pp.72-81.

Zhang, T, Qin, W, (2006) "Tensile Creep due to Restraining Stresses in High-strength Concrete at Early Ages", *Cement and Concrete Research,* 36, pp. 584 – 591.